VRIJE UNIVERSITEIT

# Liquid-phase cavity ring-down spectroscopy for improved analytical detection sensitivity

ACADEMISCH PROEFSCHRIFT

door

Sibbelina Maria Frederika van der Sneppen

geboren te Terneuzen

promotoren:     prof.dr. W.M.G. Ubachs
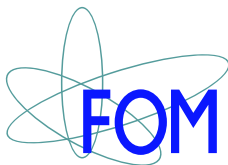                prof.dr. C. Gooijer
copromotor:     dr. F. Ariese

leescommissie:
Prof.dr.ir. M. C. M. van de Sanden
Prof.dr. H. Irth
Prof.dr. H. V. J. Linnartz
Prof.dr. M. L. Groot

1

# preface and scope of this thesis

Cavity ring-down spectroscopy (CRDS) is a well-established absorption spectroscopic technique for gas-phase samples. Briefly, the exponential decay of light intensity behind a high-finesse cavity after abrupt termination of excitation is being measured. The rate of decay of this light intensity (or the fitted 1/e time, denoted as the ring-down time) is dependent on the mirror reflectivities. If there is an absorber present in the cavity, additional intensity will be lost due to light absorption, a shorter ring-down time will be measured. The two most important advantages of CRDS are its immunity to intensity fluctuations, so that pulsed lasers can be used, and the extremely long path-lengths that are achieved due to the multipass nature of the technique.

The subject of this thesis is *liquid-phase* CRDS, which is currently in its early development stage. Complications include the introduction of a liquid or liquid flow in an optically stable cavity and the additional scattering in the liquid phase leading to short ring-down times. Absorption spectroscopy is attractive since it is almost universally applicable; it is often the detection method of choice in analytical chemistry. Conventional absorption spectroscopy suffers from an inherently low sensitivity, and improvement of absorption detection performance in analytical chemistry remains a relevant challenge. Therefore, the implementation of CRDS as an absorption detector in liquid chromatography (LC) has recently gained interest.

Another rapidly developing field is that of evanescent-wave (EW) CRDS for surface-specific absorption detection in liquid flow systems. In EW-CRDS, one of the reflections in the cavity is a total internal reflection event. Only the exponentially decaying EW is being used to probe the sample, thus combining the excellent sensitivity of CRDS with surface specificity.

The scope of this thesis will be the development of CRDS as an absorbance detection technique in various analytical liquid flow systems. An introduction of CRDS focussing on measurement principles as well as recent developments in liquid-phase and evanescent-wave CRDS will be given in **chapter 1**.

CRDS absorbance detection in liquid chromatography is performed using different wavelengths (from the visible, **chapters 2 and 3** to the ultraviolet, **chapter 4**) as well as two different geometries **chapter 5**. Whereas at present the performance of liquid chromatography with CRDS detection at ultraviolet wavelengths is limited due to insufficient reflectivities of currently available mirrors, in the visible and near-UV range CRDS is shown to strongly improve the sensitivity in absorption detection as compared to conventional chromatography absorption detectors.

The feasibility of using EW-CRDS in such a way that the fused silica surface of a prism at which total internal reflection occurs can be used for repeated analyzes, is demonstrated in **chapter 6**. Furthermore, it has been shown in **chapter 7** that surface characteristics can be modified by covalent attachment of a self-assembled monolayer on the internally reflecting face of the prism, without destroying the EW-CRDS ring-down times. Thus, a

sound basis is obtained to develop EW-CRDS as a useful tool in bio-sensing.

Finally, some conclusions regarding the research described in this thesis, as well as the importance of our developments in the field of liquid-phase and evanescent-wave CRDS will be presented in **chapter 8**.

# Contents

# Chapter 1

# Cavity ring-down spectroscopy in chemistry

## 1.1 Introduction

Absorption spectroscopy in the UV, visible and IR range of the electromagnetic spectrum is a basic technique in chemistry. It is almost universally applicable both in the gaseous and the liquid phase and to both atoms and molecules. Electronic or vibrational transitions may be involved. Whereas in e.g. fluorescence spectroscopy or REMPI (resonantly enhanced multi-photon ionization) the molecule should be fluorescent or ionizable, an absorption spectrum can be measured for virtually any molecule. As will become obvious below, conventional absorption spectroscopy suffers from a serious drawback: its limited sensitivity. A lot of effort has been and still is being spent on developing alternative detection modes. CRDS (cavity ring-down spectroscopy) is an example of such an approach. While it is becoming a mature technique in gas-phase studies, the implementation of CRDS in liquid-phase studies is a recent and rapidly developing research field.

Recording an absorption spectrum involves the measurement of the decrease in intensity of a light beam impinging on the sample. The attenuation of radiation can be described quantitatively by the so-called Lambert-Beer law. In liquid-phase studies the following form is used:

$$-\log \frac{I_l}{I_0} = \epsilon C l \tag{1.1}$$

where $\epsilon$ is the molar extinction coefficient, $I_l$ is the intensity of light as measured after travelling a distance $l$ through a sample with a concentration $C$ of absorbing molecules and $I_0$ is the intensity of light before it impinges upon the sample. An alternative equation is frequently used in the gas-phase literature:

$$-\ln \frac{I_l}{I_0} = \alpha l = N \sigma l \tag{1.2}$$

where $\alpha$ is the absorption coefficient, $\sigma$ is the molecular absorption cross section and $N$ is the number density of the molecules. These equations immediately show that the measurement is based on the attenuation of a light beam. Its sensitivity depends on the accuracy with which a small decrease on a large signal can be determined and thus on the stability of the light source used. Absorption spectroscopy is therefore inherently less sensitive than zero-background spectroscopic techniques such as fluorescence or phosphorescence spectroscopy. It is readily understood that the detection of one photon in a dark

environment is easier than the detection of a decrease of 1 photon on a signal of 1000 photons. Nevertheless, due to its universality and simplicity absorption spectroscopy is often the detection method of choice. Several alternative methods have been developed to overcome the lack of sensitivity. In this chapter one of these alternatives, cavity ring-down spectroscopy or CRDS, is described in detail.

### 1.1.1 Increasing the sensitivity of absorption spectroscopy

Deriving the Lambert-Beer law is quite straightforward: when considering an infinitesimally thin layer $dx$, the intensity reduction due to the absorption of light by molecules (that is, $dI_x$) depends linearly on the ability of the molecules in this layer to absorb the light and on the number of molecules ($\alpha = N\sigma$) and the amount of light present. Thus,

$$dI_x = -\alpha I_x dx \tag{1.3}$$

or

$$\frac{dI_x}{I_x} = -\alpha dx \tag{1.4}$$

For a layer of thickness $l$, the total decrease of the light intensity is obtained by integration of Eq. (1.4) which leads to

$$\frac{I_l}{I_0} = e^{-\alpha l} \tag{1.5}$$

or alternatively:

$$\frac{I_l}{I_0} = 10^{-\epsilon Cl} = 10^{-(\alpha/2.303)l} \tag{1.6}$$

The output (the absorbance) of a conventional absorption spectrometer will be $-\log \frac{I_l}{I_0}$ or $\epsilon Cl$ in so-called absorbance units (the measured quantity is unit-less). The path length $l$ depends on the cuvette used, for standard cuvettes for liquid solutions it is one cm, $\epsilon$ is usually given in $M^{-1}cm^{-1}$. In order to determine $-\log \frac{I_l}{I_0}$ more accurately, most benchtop absorption spectrometers have a double-beam configuration. The reference beam is by-passed around the sample, and the ratio between the two beams is measured.

Increasing the sensitivity of absorption spectroscopy remains a relevant challenge, especially if the cell dimensions are limited as in miniaturized systems. An obvious way to do this, as is immediately apparent from the Lambert-Beer law, is to increase the path length. Without changing the cuvette dimensions, this can be done by using multipass configurations such as the so-called Herriot-type and White-type multi-pass cells, which make use of mirrors with small apertures [1, 2]. Injection and detection of light occurs through the apertures in the entrance and the exit mirror, respectively. The light can undergo several tens or hundreds of reflections inside the absorption cell before exiting through the aperture in the exit mirror, thus creating a long path length. However, due to instability problems these configurations have not found widespread use in analytical chemistry.

Alternatively, a specially designed detector cell such as an LCW (liquid-core waveguide) can be used in liquid-phase absorption detection. Here, a hollow-core fiber is filled with liquid. The refractive index of the cladding (i.e. the wall of the fiber) is lower than that of the liquid core, and the LCW acts as a conventional optical fiber: light is confined in the core by means of TIR (total internal reflection). This way, even for microliter-sized flow cells, optical path lengths of 0.5 to 1 m can be achieved [3,4]. The requirement to use

such small detector cell volumes (or even much smaller ones) applies for instance to on-line detection systems for FIA (flow injection analysis) or LC (liquid chromatography). Care should be taken that the detection cell volume will not cause significant band-broadening.

Other modes of absorption spectroscopy that are compatible with FIA and LC have also been developed. An overview of non-fluorescence detection techniques for LC has been given in [5]. In thermal lensing spectroscopy (TLS), one makes use of the heating up of the solution molecules when the analyte molecules in the solution absorb light and dissipate the excess energy via non-radiative energy transfer. This heating up causes a change in the refractive index and the formation of a negative lens in the solution. This negative lens defocuses the excitation beam. When a pin-hole is placed in front of the detector which will block any defocused excitation light, the measured decrease in light intensity due to light absorption will be larger than expected from the Lambert-Beer law. TLS has successfully been implemented as a detector in analytical flow systems [6, 7].

An appealing zero-background detection scheme is photo-acoustic spectroscopy (PAS) [8,9]. Here, the shockwave that is induced by the heat-up of solution after light absorption and energy dissipation is measured using a piezo-electric transducer (PZT) or sensitive microphone. The improvement in sensitivity and detection limits is limited in the liquid phase [8], but excellent limits of detection can be obtained in the gas phase [9]. PAS is particularly useful in the case of scattering samples that hamper conventional transmission measurements.

Another zero-background alternative for detection of temperature increase after light absorption is degenerate four-wave mixing (D4WM) [10, 11]. In a D4WM measurement, two pump beams are overlapped, the constructive and destructive interference of the beams causes a light-intensity pattern where the beams cross. In the planes where the light intensity is high, analytes can absorb light and dissipate the energy and a temperature pattern is formed. A third beam is used to probe the light-intensity pattern, and will be reflected off this pattern only when a temperature pattern exists as well (if there are molecules that absorb the light). The fourth beam that is generated in this way is as directional as a laser beam. When coupled to a separation system, a slight improvement in performance is obtained compared to conventional absorbance detection [11].

Whereas TLS is based on the regular measurement principle of absorbance spectroscopy (the measurement of $\Delta I/I_0$), a baseline noise reduction with two orders of magnitude compared to the best available conventional absorbance detector has been shown to be feasible [7]. TLS can only be applied to the liquid phase. Unfortunately, the sensitivity of the TLS depends on a favorable dn/dT, and the sensitivity of PAS depends on a favorable temperature expansion coefficient. Both values are five times worse for water than for organic solvents, making both techniques less sensitive when using pure water or aqueous buffer, as is the case for capillary electrophoresis (CE) separations. In D4WM the situation is more dramatic: not only the dn/dT ratio, but also the thermal conductivity of the solvent plays an important role, making D4WM 300 times more effective in acetonitrile than in water.

A major draw-back of all the above-mentioned thermo-optical techniques is that gradient elutions, in which the solvent and its refractive index is continually changing, can not be used. Especially in LC, gradient separations are widely used and the applicability of the above-mentioned measurement schemes is severely limited.

In this chapter we will demonstrate that CRDS is a promising method for improving absorption detection sensitivity, and can be used both in the gas and the liquid phase, and even for solid samples.
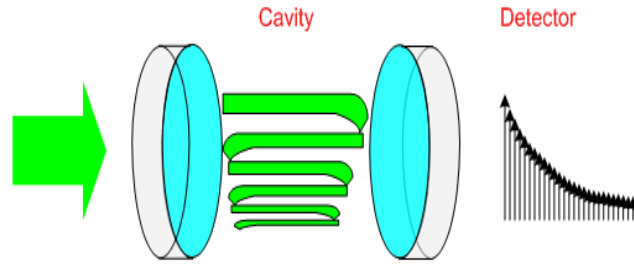
Figure 1.1: Schematics of the principle of CRDS. After abrupt termination of the excitation, the light stored in the cavity will decay exponentially as it bounces back and forth between the mirrors losing a small portion at each reflection. The decay rate of this light can be measured behind the cavity.

### 1.1.2 Cavity ring-down spectroscopy

CRDS is based on the measurement of the decay rate of light behind a high-finesse cavity (see Fig. 1.1). The cavity is made of high-quality mirrors, reflectivities being on the order of 99.9% or 99.99%. This means that only 0.1 to 0.01 % of the excitation light will enter the cavity, and the leakage from the cavity is also 0.1 to 0.01 % per round-trip. After abrupt termination of the excitation, the rate of decay of the light is measured behind the cavity and fitted to an exponential:

$$I_t = I_0 e^{-t/\tau} \tag{1.7}$$

where $I_t$ is the measured intensity and $t$ is the time. The ring-down time $\tau$ of this exponential is directly related to the reflectivity $R$ of the mirrors, scatter losses $\beta_{scatt}$ and the absorption coefficient $\alpha$ of the absorber between the mirrors:

$$\tau = \frac{(n_{avg}L)/c}{(1-R) + (\alpha l) + \beta_{scatt}} \tag{1.8}$$

$L$ is the cavity length and $l$ the effective path length through the sample (in most cases, $L = l$) while $n$ is the refractive index of the medium surrounding the sample. $c$ is the speed of light and $n_{avg}$ is the weighted refractive index of the cavity if it contains more than a single medium. Absorbance units ($\varepsilon Cl$) can be derived from the ring-down times via:

$$\varepsilon Cl = \frac{\alpha l}{2.303} = \frac{n_{avg}L}{2.303c} \left[ \frac{1}{\tau} - \frac{1}{\tau_0} \right] \tag{1.9}$$

where $\tau$ and $\tau_0$ are the ring-down times in presence or absence of analyte. Subtraction of the baseline loss $\tau_0$ is necessary to account for the background (reflection and scatter) losses, as well as impurities in the blank solvent.

CRDS is a multi-pass technique that elegantly circumvents the need for a stable light source. The decay rate will not depend on the amount of light initially brought in the cavity, and light sources that are less stable (such as pulsed lasers) can be used. Equations (1.5) and (1.7) both exhibit a mono-exponential decay, and this is the basis for relating the ring-down time $\tau$ directly to the absorbance quantity $\alpha l$. Ring-down times are on the order of nanoseconds for small cavities to micro- or even milliseconds for long cavities. Effective path lengths are usually on the order of meters (for mm-sized cavities) to kilometers, which

makes CRDS a very sensitive absorption detection method. Sensitivities as low as $10^{-6}$ to $10^{-9}$ cm$^{-1}$ can be obtained and applications of CRDS range from the measurement of forbidden transitions in the gas phase to increasing the detection sensitivity in LC.

Besides the advantage of high sensitivity most variants of the CRDS technique have a second major advantage for absorbance measurements. CRDS is calibration-free or it has an intrinsic calibration of the absorbance, under the assumption that the entire cavity is filled with homogeneously distributed sample: in Eq. (1.9) the length of the probe volume $l$ then equals the cell length $L$. For a gas phase experiment it can be easily shown, in analogy to Eq. (1.9), that the material property of $N\sigma$ (the product of the density and the cross section) can be derived straightforwardly from measurement of ring-down transients only:

$$N\sigma = \left[\frac{1}{\tau} - \frac{1}{\tau_0}\right] \frac{n}{c} \qquad (1.10)$$

Hence it is not necessary to determine the path length over which the absorption takes place. In the terminology of absorbance in the liquid phase the material property of the $\epsilon C$ product can directly be determined in an intrinsically calibrated fashion. Of course these relationships do not hold in cases where e.g. an absorption cell is inserted inside the optical resonator or when the CRDS mirror-configuration is built around a flame in a combustion analysis experiment (in those cases $L \neq l$).

This chapter will begin with an overview of gas-phase CRDS without trying to cover the whole field. For a more complete overview of gas-phase CRDS studies, the reader is referred to one of the many reviews on this subject [12–18]. The main focus here will be on new developments in condensed media.

Since many implementations of the technique have first been demonstrated in the gas phase and were adapted for measurements in condensed media more than a decade later, it seems natural that general considerations and several different applications of CRDS are discussed in the following section "CRDS in gas phase measurements". The section "Condensed media CRDS" will mainly describe the recent extension of CRDS into the liquid phase. Another recent and rapidly evolving field is described in the section "Evanescent-wave CRDS", a technique that combines surface specificity with the excellent sensitivity that is feasible with CRDS.

## 1.2  CRDS in gas phase measurements

CRDS was originally developed for a purpose very different from absorption spectroscopy. When in the 1970's and 1980's ion beam sputtering and vapor deposition techniques were developed as well as techniques for superpolishing (in which chemical and mechanical treatments are combined), the quality of high-reflectivity mirrors increased considerably. Dielectric mirrors were being produced by stacking multiple layers of two transparent optical materials with a slightly different refractive index on superpolished high-quality substrates. Dielectric mirrors are usually Bragg mirrors, where the layers are exactly a quarter of a wavelength thick. Despite the fact that the interfaces between the layers are not very reflective, the reflections from many interfaces will constructively interfere with each other and the overall reflectivity will be very high.

The improvement in mirror quality led to a demand for equipment to measure the exact reflectivity, and reflectometers based on the principle of CRDS were developed [19, 20]. It was noted that since the measured reflectivity depends on the ambient air quality, the cells used in the reflectometers should be evacuated [20]. The full potential of these

reflectometers in absorption spectroscopic studies was first realized by O'Keefe and Deacon [21], who measured a weak transition band of molecular oxygen. This seminal paper is considered to be the first CRDS study.

Mirrors that are commonly used in CRDS have reflectivities of 99.9% or even higher than 99.99%. Since the reflective interfaces between the different layers should be spaced a quarter of a wavelength apart, high-quality CRDS mirrors are quite narrow-banded. As a rule of thumb they are useable to within 5 or 10 % of the center wavelength. Furthermore, one can imagine that as the wavelength becomes shorter, it becomes increasingly difficult to make the dielectric layers of the correct thickness and with the required purity. Whereas some deep-UV CRDS studies have been published (for example, [22]), to date the use of CRDS in the UV remains a challenge.

### 1.2.1  Pulsed-laser CRDS

In a first-order derivation it was shown that the ring-down from a cavity exhibits a decay behavior that can be described with a single exponential (see Eq. (1.7)). Because this exponential decay follows a similar functional behavior as the Lambert-Beer law of Eq. (1.5) the temporal decay can be interpreted in terms of the absorption coefficient.

However, this treatment fully ignores some of the characteristic features of an optical resonator: interference and a resulting mode structure. Indeed, an optical resonator is known as a Fabry-Perot interferometer or etalon, where interference between propagating and reflected light beams makes that the transmission of the resonator is strongly wavelength dependent. In an etalon, light will be transmitted when the reflected beams in the etalon are in phase or when the length of the etalon is a multiple of the wavelength. In other words, different longitudinal modes in the resonator can be excited.

A first prerequisite of using an optical resonator in a ring-down experiment is that the stability criterion of a cavity must be fulfilled [23]:

$$0 < (1 - \frac{L}{R_c})^2 < 1 \tag{1.11}$$

with $R_c$ being the radius of curvature of the mirrors. A similar criterion of stability holds if the radii of curvature of the two mirrors building the cavity are different. Eq. (1.2.1) entails that stable cavities must have a length $0 < L < 2R_c$, a consideration that follows from geometric as well as Gaussian optics [23].

If interference is taken into account the transmission spectrum of the cavity becomes the familiar etalon pattern with transmission peaks equally spaced by the so-called Free Spectral Range or FSR (see Fig. 1.2):

$$\delta\nu = \frac{c}{2nL} \tag{1.12}$$

In general, a cavity has a mode pattern with resonant frequencies

$$\nu = \frac{c}{2L}[q + (m + n + 1)(\frac{1}{2} + \frac{2}{\pi} \arctan \frac{L - R_c}{L + R_c})] \tag{1.13}$$

with $q$ the longitudinal mode number and $m$ and $n$ referring to the transversal modes. If an etalon is aligned under exactly confocal conditions ($L = R_c$, the focus of one mirror is exactly at the other mirror) destructive interference may cause half of the longitudinal modes to disappear, yielding a FSR of $c/4nL$. Under non-confocal conditions it is easy to excite some of the transverse modes of the cavity; their resonance frequencies shift in frequency space to the extent that they may fill up the entire space between the transmission modes of Fig. 1.2. Meijer and co-workers have experimentally demonstrated this
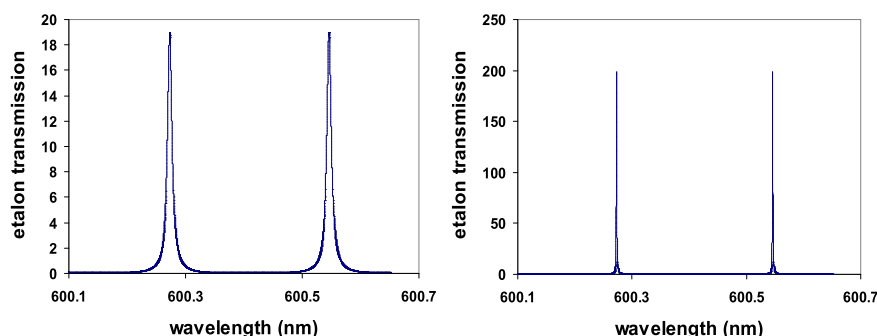
Figure 1.2: The transmission pattern of an etalon or cavity illustrating the FSR (free spectral range). The left panel shows the transmission spectrum as simulated using 90% reflectivity mirrors. The right panel shows the same simulation, but the reflectivity was set to 99%.

"filling of frequency space" by shifting away from a confocal geometry [24]. This filling in by transverse modes can go as far as making the ring-down cavity into a white-light transmitter [25], which is the desired response function for pulsed CRDS. The white-light condition is usually fulfilled if the length of the cavity deviates at least 25% or more from the confocal condition $L = R_c$.

Another effect of transverse modes is in the spatial distribution of the light intensity over the propagating wave-front (see Fig. 1.3). In principle, if multiple modes inside the cavity are excited to the same extent, the different modes will have different path lengths through the cavity. The higher order modes will experience more diffraction losses (not all modes are covered by the mirrors, which have a finite size). Both effects may give rise to a multi-exponential decay. However, it has been shown that if a sufficient number of modes is excited and the cavity can be considered "white", the non-exponentiality of the ring-down transient can be neglected [25]. Under such conditions the single exponential decay of Eq. (1.7) holds.

The onset of coherence effects and the effect on the ring-down decay function was experimentally demonstrated by Martin *et al.* [26]. If a laser pulse with a coherence length larger than the length of the cavity is used, an oscillating behavior becomes superimposed on the decay transients. This phenomenon can be described by beating effects (so-called mode-beating) involving different transverse modes of the optical resonator. This is for most CRDS applications an undesired condition.

Mode-beating can readily be seen when using a detector that is smaller than the cavity output spot. Ripples superimposed on the exponential decay are observed, the pattern of which changes when the detector is moved. Such ripples of course influence the fitting of the exponent through the measured transient and the standard deviation of the ring-down times will become larger than the usual 1%. An extreme case of mode-beating is shown in Fig. 1.4. The left panel of Fig. 1.4 shows ring-down transients as taken using a laser with a short coherence length; the cavity will always be excited since the laser pulse is broader than the FSR of the cavity. The ring-down traces to the right shows the undesired condition: as the cavity length is affected by temperature fluctuations, the laser might or might not be able to excite the cavity. Whereas more than 100 traces are overlapped, only a few of the laser shots yielded a useable ring-down trace. It is therefore easier to use lasers with a short coherence length (the bandwidth should be larger than the FSR of the
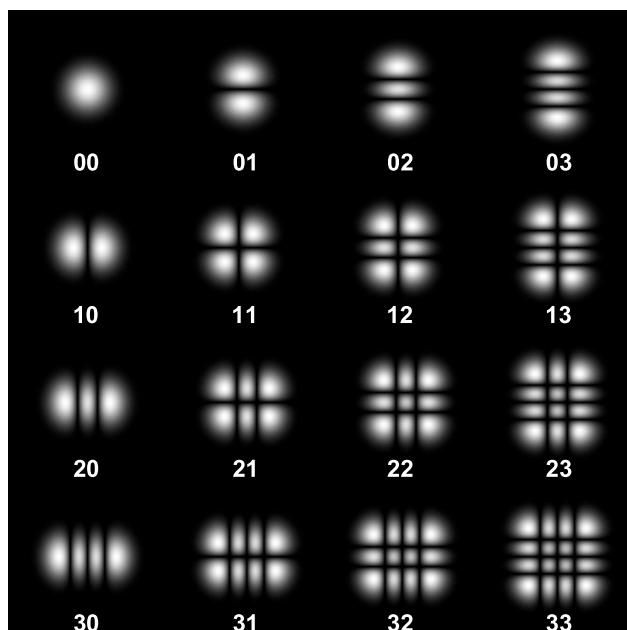
Figure 1.3: Rectangular transverse mode patterns. Photons that are in higher-order modes trace out another path inside the cavity, the path length will be longer.

cavity).

Proper alignment of the cavity is commonly tested by checking the standard deviation of a series of ring-down times of the empty cavity to confirm the absence of mode-beating and non-exponential behavior. Furthermore, when using a small-sized detector such as a photodiode, care should be taken to focus all the light on the diode. Larger detectors such as PMTs (photomultiplier tubes) should be used, and placed as close to the exit mirror as possible. However, some residual non-exponential behavior cannot be prevented.

The most common ring-down application is pulsed CRDS, where excitation occurs for instance using a Nd:YAG laser combined with an OPO (optical Parametric Oscillator) or dye laser where wavelength tunability or bandwidth broadening is required. Usually the speed of data transfer combined with the speed of online fitting routines limits the repetition rates of the lasers to a range of 10 Hz to 1 kHz. Different excitation approaches (multi-mode and single-mode) can be used, requiring different experimental conditions.

**Multi-mode excitation**

In multi-mode excitation, the bandwidth of the laser pulse is much larger than the free spectral range of the cavity. This condition corresponds to the coherence length of the laser pulse being much shorter than the length of the cavity and is usually satisfied when using a non-single mode OPO or a dye laser. The shot-to-shot noise of the obtained ring-down times is typically 1% or better.

The calibration-free condition of CRDS holds in particular for the generic pulsed CRDS method; it will be discussed later that it does not hold for some of the cavity-enhanced detection methods. It should be realized, however, that no disturbing effects of frequency-selectivity or of mode-selectivity by the cavity, nor any line-shape effects should occur that cause the decay of the CRDS transient to deviate significantly from a mono-exponential. Such phenomena prevent a straightforward quantitative interpretation of the decay tran-

Figure 1.4: Ring-down curves as taken under pulsed multi-mode conditions are shown to the left. Each laser shot is able to excite many modes in the cavity, this is the desired situation. An instrumental response func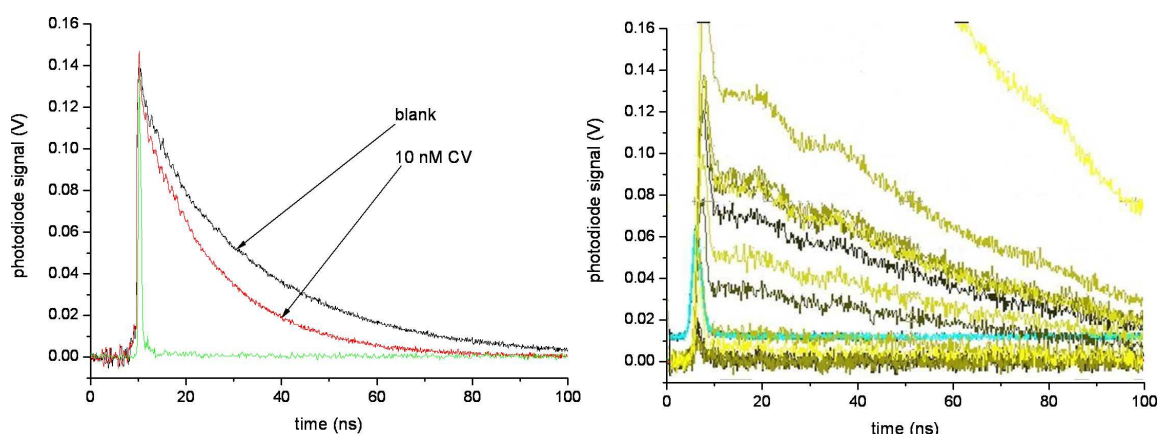tion is shown together with a ring-down curve of a methanol-filled cavity and one with absorber (10 nM Crystal Violet). The cavity was a 2-mm liquid-only cavity; the complete experiment is described in chapter 2 [27]. Since the 2-mm cavity has a large FSR, mode-beating effects can readily be observed for narrow-band lasers (to the right, the experiment is the same except for the use of a Fourier-transform limited laser). As the length of the cavity fluctuates due to ambient temperature drifts, the laser might or might not excite the cavity and one might or might not observe a ring-down.

sient into an absorbance. One well-known example in gas-phase CRDS is the molecular line shape effect in case when the bandwidth of the excitation laser is larger than a molecular line shape (either Doppler, naturally or collisionally broadened). In such case the bandwidth of the laser source may be decomposed in its frequency components $d\nu$, and each of these will probe a different part of the spectral line and hence exhibit a different absorbance. Hence the decay time of each frequency component will be different, resulting in a different decay time $\tau_{d\nu}$ for each frequency interval $d\nu$. This causes the overall experimentally measurable ring-down transient to be multi-exponential. This should be avoided for an experimental determination of $N\sigma$ since the mathematical deconvolution of a multi-exponential decay is painstakingly difficult. A first attempt was performed by approximative methods by Jongma *et al.* [28], but it has remained an issue in the literature. A more thorough analysis of this problem was presented by Hodges *et al.* [29].

In cases where the molecular cross section is constant over the bandwidth of the excitation laser, e.g. the inherently broad liquid-phase absorbance spectra, this problem is avoided. As was shown in studies on very broad collisionally-induced absorptions in oxygen such multi-exponential decays do not occur and a cross section could be determined [30]. Also, it was demonstrated that absolute Rayleigh scattering cross sections could be determined from CRDS [31]. Note that in the latter experiments an extinction due to scattering is measured rather than an absorption feature.

**Single-mode excitation**

Single-mode CRDS is possible by locking one of the modes of the cavity to the narrow bandwidth output of a laser; passive locking is performed by temperature stabilization to within the mK-range, active locking requires a feedback loop, for a 1-MHz frequency stability the cavity length should be varied by 0.25-nm steps [32]. Other tricks for single-mode excitation are using a confocal cavity and mode-matching. For mode-matching of

the laser to the $TEM_{00}$ mode of the cavity, the combination of the lens and the concave mirrors should focus the laser light in the middle of the cavity.

The laser should also have a narrow bandwidth; that is why the authors of [32] used an injection-seeded OPO with a bandwidth of 115 MHz. This way, the locking of the CRDS cavity resulted in a shot-to-shot noise of the ring-down times on the order of $10^{-4}$. The noise of the system is now mainly determined by the shot noise, and the sensitivity as well as the spectral resolution of the system is much better than in multi-mode excitation. Unfortunately, the system is also more complex.

### 1.2.2 Continuous-wave CRDS

In CW (continuous-wave) CRDS a CW laser is used to excite the cavity and the ring-down is measured after switching off the laser, for example using an acousto-optic modulator or AOM. An AOM consists of a material such as glass to which a PZT (piezo-electric transducer) is attached, the PZT creates a sound-wave in the glass that is used to periodically diffract the light off the formed refractive-index grating. One of the first demonstrations of using the decay time of an optical cavity for measuring the mirror reflectivity was actually based on a CW laser [20]. The advantage of these systems is that the duty cycle can easily be increased (with the current speed of data transfer and fitting algorithms, the repetition rate can be on the order of kHz) and averaging will increase the S/N (signal-to-noise) ratio thus improving the sensitivity. Furthermore, since the excitation time can be much longer than in case of pulsed CRDS, more light can be brought inside the cavity (similar to a ring-down, a cavity will have a ring-up as well). CW lasers have a narrower band-width than pulsed lasers and analoguously to single-mode CRDS, the cavity length should therefore be such that the laser frequency coincides with one of the cavity modes in order to achieve excitation.

CW-CRDS for absorption spectroscopy studies has been developed by Romanini et al [33–35]. Rather than locking the cavity to the laser, which would complicate the set-up somewhat, the cavity length was swept across one free spectral range of the cavity using a piezo-electric transducer so that the laser line was in resonance once per sweep. A direct comparison with photo-acoustic spectroscopic measurements on acetylene [36] shows that CW-CRDS is as sensitive as PAS or even better [33]. Other applications of CW-CRDS include the measurement of $NO_2$ as well as $CHF_3$ spectra using diode lasers [34, 35] and the measurement of a high-resolution spectrum of $N_2O$ and $CHCl_3$ [37]; in this study the cavity was actively locked to the laser. Another quite straightforward method is to use a fixed cavity with a relatively low FSR (the use of a 2-m cavity results in a FSR of 150 MHz) and only measure at the different longitudinal modes of the cavity; each data-point in the spectrum corresponds with 150 MHz or 0.005 $cm^{-1}$ [38]. Of course, this approach works well when the absorption features of interest are much broader. The authors measured a water vapor line with a FWHM of 0.15 $cm^{-1}$.

Interestingly, single-mode CW-CRDS can also be applied in laser medicine. CW-CRDS was used for the development of non-invasive breath analysers for the detection of exhaled ethane (a marker for oxidative damage in tissue, which plays a role in diseases like cancer, artherosclerosis and others) [39, 40]. CW-CRDS was also used for the measurement of the $^{12}C/^{13}C$ ratio in exhaled $CO_2$ after the patient had been given $^{13}C$-enriched urea (a marker for bacteria causing stomach ulcers) [41]. In both studies, the approach of Romanini *et al.* [33] was followed: a single-mode CW laser is used to excite the cavity which is being swept over one FSR, the excitation is switched off using an AOM when the $TEM_{00}$ mode is excited and the subsequent intensity decay is fitted to an exponential.
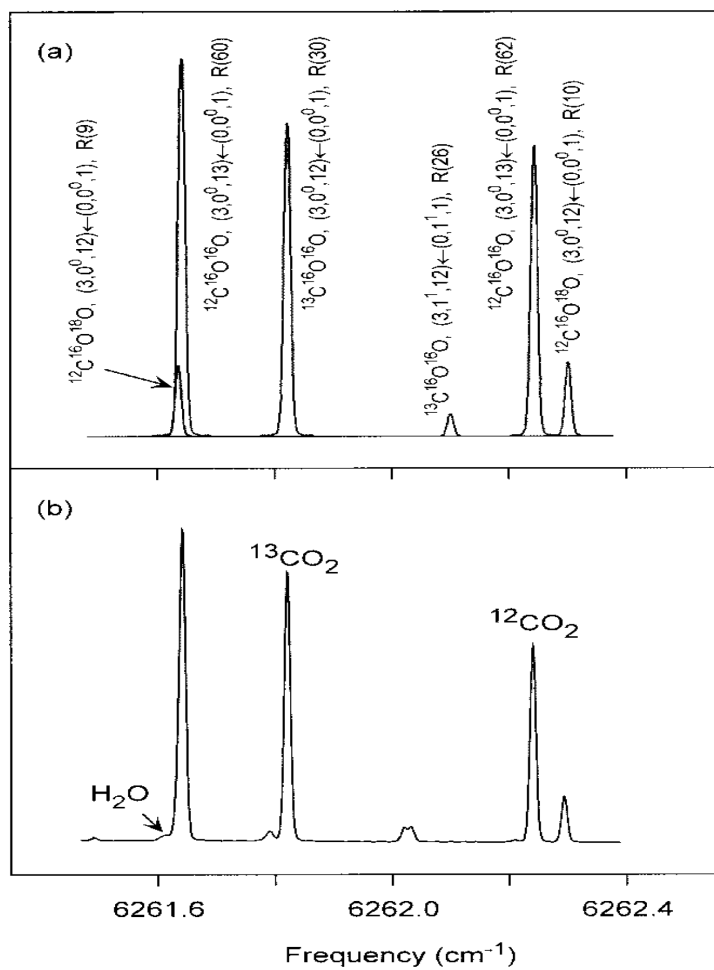
Figure 1.5: A simulated absorption spectrum using the HITRAN database (upper panel) together with a CRDS absorption spectrum of 5 Torr of $CO_2$ obtained using the breath analyzer (Reproduced with permission from [41]. Copyright 2002 American Chemical Society.).

The measurement principle of the breath analyzer of Crosson *et al.* is based on the differences in the $CO_2$ absorption spectra of the two carbon-isotopes. The relative area of appropriately chosen peaks in the spectrum reflect the $^{12}C/^{13}C$ ratio (see Fig. 1.5). Even at low partial $CO_2$-pressures, the signal-to-noise ratio of the measurement was sufficient for analysis. The obtained results were comparable with those obtained by IRMS (isotope ratio mass spectrometry), the current technique for the detection of bacteria associated with stomach ulcers using the $^{12}C/^{13}C$ ratio [41]. In IRMS, breath is injected (after a tedious pre-concentration) into a mass spectrometer; the $^{12}C/^{13}C$ isotope ratio follows directly from the obtained mass spectrum.

PAS has also been used in the development of an ethene breath analyzer (ethene is a marker for skin damage) [42]. The sensitivity levels of PAS and CRDS analyzers are comparable, but an advantage of the CRDS analyzers could be a better selectivity: since PAS has to be carried out at ambient conditions rather than at low pressures, the spectral lines are pressure-broadened and might prove more difficult to resolve.

As mentioned earlier, matching the cavity modes to a single mode of the laser or to a narrow-bandwidth continuous-wave laser is not straightforward. An elegant way to circumvent the need for locking the laser output to a cavity mode is the use of an off-axis alignment [43]. In fact, large-diameter (0.75 inch) CRDS mirrors are aligned in a fashion similar to the previously mentioned Herriot-cell [1]. In the case of off-axis CRDS, there are no entrance and exit holes for the injection of light. The light which will start to ring back and forth between the mirrors will trace out an ellipse on the back mirror, or even a Lissajous pattern when some astigmatism is induced in the mirrors by tightening the set screws of the mirror holders. When the pattern becomes reentrant, the light will have bounced back and forth more than 500 times, thus decreasing the FSR by a factor of 500. The FSR of the cavity is significantly narrower than the laser bandwidth and the transmission of the cavity will not change when scanning the laser [43].

The off-axis technique is most promising in combination with cavity-enhanced absorption techniques denoted as CEAS [43] as will be outlined in the next section. Using this CEAS technique, several studies have been performed; for example, kinetic studies on the nitrate radical, produced by the reaction of F atoms with $HNO_3$ molecules and a microwave discharge [44]. Also, the absolute density of singlet oxygen in an inductively coupled plasma has been measured [45]. However, since a rather large optical lay-out is required, the method is not well suited for detection of small liquid-phase samples such as in LC.

### 1.2.3   Cavity-enhanced techniques: CEAS or ICOS

The above-mentioned cavity-enhanced techniques share the common feature that a decay rate is measured after termination of the excitation of a high-finesse optical cavity. Another approach is to determine the absorption by integrating the total signal transmitted through an optical cavity [46–49]. This technique has been dubbed ICOS (integrated cavity output spectroscopy) by the group of O'Keefe, but it is also known as CEAS (cavity-enhanced absorption spectroscopy). Its sensitivity stems from the long effective optical pathlength, but since the measurement principle is similar to that of conventional absorption spectroscopy (i.e. $\Delta I/I_0$ is measured), the obtainable sensitivity is dependent on light source stability and the accuracy with which a small $\Delta I/I_0$ can be measured.

A direct comparison of the sensitivity of pulsed CRDS and pulsed ICOS showed that the latter is quite promising [46]: whereas in absence of absorber the total amount of light measured at one side of the cavity is of course 0.5 times the initial amount of light, an

absorption of $10^{-6}$ per pass already results in a decrease of 1% of this value when using 99.99% mirrors. Measurement of a weak absorption band of molecular oxygen showed that the obtained sensitivity in ICOS is comparable to that of conventional CRDS using the same set-up. Measurements of vibrational combination bands of $CO_2$ and $H_2O$ in the 1300 nm region using continuous-wave ICOS also yielded a similar sensitivity level [47]. In this study, both the frequency of the input light source and the optical cavity were dithered to avoid problems with the frequency mode spacing of the cavity: 5 - 10 cavity modes were covered. No correction was made for the laser output instability which was 1% or less.

The major drawback of the ICOS scheme (the dependence of the measurement on the light source stability) can be corrected for by dividing the integrated output by the initial intensity (the first data point of the integrated ring-down transient) [46]. Another drawback is that the measurements are not absolute i.e. $N\sigma$ does not follow directly from the measured quantity. At higher concentrations, the effective path length decreases. This causes deviations from linearity, but on the other hand it results in a larger dynamic range [50].

Gherman *et al.* used a broad-band approach for measuring the spectrum of acetylene in a cavity that was actively locked to a mode-locked femtosecond Ti:Sapphire laser. The output of the cavity was dispersed by a spectrograph, no scanning of the laser was needed to obtain a spectrum spanning more than 4 nm [48]. In a follow-up study, acetylene was measured using a more cumbersome set-up employing a mode-locked DP-VECSEL (diode-pumped vertical external-cavity surface-emitting laser) [49].

### 1.2.4 Special applications of CRDS

Many variations of CRDS such as phase-shift CRDS, broad-band CEAS and polarization-dependent CRDS and different applications which combine CRDS with one or more other techniques have been described in the literature. A few examples are listed below to illustrate their potential. Some of these approaches have been applied to CRDS measurements in the liquid phase as well, as will be discussed in section 3.

**Phase-shift CRDS**

Phase-shift CRDS is related to CEAS since the total light transmittance of a cavity is being measured. In phase-shift CRDS, however, the intensity of a tunable CW laser is modulated. Rather than the total integrated light, the phase shift of this modulated light after passing through the cavity is being used to extract an absorption spectrum from the data. This way, the measurement is independent from random light source fluctuations. This approach was already used in one of the first CRDS studies in 1980 [19]. The aim of that study was to develop a measurement technique for reflectance measurements of high-reflectivity mirrors and other optics, but the authors repeatedly stated that the same measurement technique could be used for high-sensitivity absorption spectroscopy as well.

However, it took 16 years for the first spectrum to be published [51]. In phase-shift CRDS, the excitation laser is sinusoidally intensity-modulated in time. The phase shift that the modulated light will experience upon passing through a cavity is related to the cavity ring-down time and thus the absorbance. When a stable linear cavity that is not locked to the laser or temperature-stabilized is used for CRDS measurements, one observes that from time to time the cavity is excited when the length of the cavity happens to match exactly a multiple of half a wavelength. This coincidental mode-matching caused by random cavity length variations was used and laser excitation happened several times per microsecond [51]. In addition the phase shift caused by the ring-down cavity could be

detected by lock-in amplification thus enhancing the sensitivity. The laser was scanned several tens of times making sure that at each wavelength a sufficient number of data points was available for the construction of an absorption spectrum. The detection sensitivity compared favorably to the detection sensitivity as obtained for conventional pulsed multi-mode CRDS performed on the same set-up, probably due to the higher duty cycle of the laser [51].

In another study [52], the performance of ICL-PAS (intra-cavity laser photo-acoustic spectroscopy) and pulsed multi-mode CRDS was compared to previously obtained phase-shift CRDS measurements of the fifth overtone of saturated hydrocarbons [53]. The precision of pulsed CRDS was ten times better than that of ICL-PAS due to an internal calibrant added to the sample. The baseline noise and thus the sensitivity of the systems were comparable [52, 53]. Whereas the cross-sections as obtained by pulsed CRDS and ICL-PAS were similar, the values obtained by phase-shift CRDS were 35% higher, which according to the authors might be ascribed to a systematical error introduced by the measurement technique. Nevertheless, it has been demonstrated that phase-shift cavity ring-down spectroscopy can be used for the determination of absolute line intensities [54]. Since the ASE (amplified stimulated emission) of the diode laser used experiences a phase shift different from the phase shift of the laser light, a correction for this ASE should be made.

**CRDS using broad-band light sources**

The use of BB (broad-band) sources allowing for multiplexing in CRDS measurements was already pioneered in 1996 [55], but the full potential of BB-CRDS (i.e. using an IBB (incoherent broad-band) light source) was not further explored until recently.

In the first CRDS study using an IBB source (a xenon arc lamp) rather than a laser, a combination of Fourier transform spectroscopy and phase-shift CRDS was used for measuring a spin-forbidden transition of oxygen in an open-air cavity [56]. Since incoherent broad-band light sources are usually less intense than laser sources, it is better to use mirrors that are less highly-reflective in order to get sufficient light in the cavity. Another advantage of mirrors of lower quality is the fact that they exhibit a larger wavelength coverage so that a larger range of the IBB source can be utilized. By putting a bandpass filter in front of the detector, it is possible to select only the light that has made many round-trips through the cavity [56]. The baseline noise of this system is higher when compared to "conventional" phase-shift spectroscopy as discussed in the previous section (about $3 \cdot 10^{-6}$ cm$^{-1}$ [56] compared to $0.5 \cdot 10^{-6}$ cm$^{-1}$ [51] or $0.05 \cdot 10^{-6}$ cm$^{-1}$) [53].

In CEAS, continuous light sources can be used, and the experimental configuration is more straightforward than in CRDS. This makes IBB-CEAS quite attractive. The first CEAS set-up using IBB light (dubbed IBBCEAS) was quite similar to a conventional absorption spectrometer geometry [57]. The absorption spectrum of an azulene jet was measured over a spectral range of 493 to 578 nm. Part of this spectrum was compared to earlier measurements using conventional pulsed CRDS over a range of 602 to 616 nm [58] (see Fig. 1.6). The observed spectral resolution of 4 cm$^{-1}$ for IBBCEAS was related to the resolving power of the classical spectrometer used. In the pulsed CRDS study, the spectral resolution was determined by the 0.16 cm$^{-1}$ width of the laser. The sensitivity as obtained after 100-s exposure time of Fig. 1.6 compared well with conventional pulsed CRDS.

An actual absorption spectrometer was converted to an IBBCEAS apparatus by putting mirrors around the cuvette and rearranging the cuvette holder to permit alignment of the
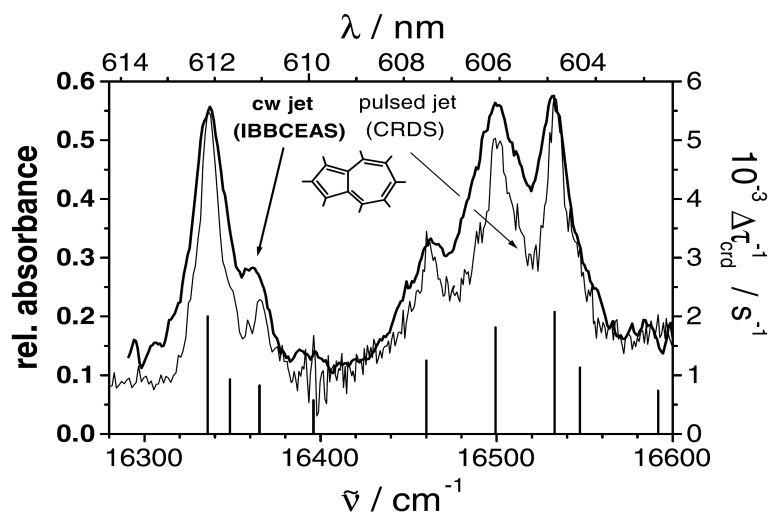
Figure 1.6: Comparison of part of the IBBCEAS spectrum and the pulsed CRDS spectrum of an azulene jet (Reproduced with permission from [57]. Copyright 2003 Elsevier). The left axis in the figure is the absorbance as measured with IBBCEAS, the right axis is derived from the decrease in ring-down time as measured with pulsed CRDS; this value is directly proportional to the actual absorbance according to equation 1.9.

cuvette [59]. This configuration permits liquid-phase measurements and these developments will be discussed in section 3.3. Other interesting gas-phase IBBCEAS applications are the *in situ* detection of atmospheric trace gases [60], the development of an FT-IBBCEAS set-up [61] and the use of LEDs (light emitting diodes) as light source [62], both for the measurement of oxygen and water vapor.

**Polarization-dependent CRDS**

Some attention has been devoted to the development of CRDS for polarization studies. A paramagnetic substance such as molecular oxygen can be made optically active by putting a magnetic field perpendicular (the Voigt configuration) or parallel (the Faraday configuration) to the cavity axis. This way, the three M spatial quantization components of a transition line in oxygen have been measured [63]. One should, however, realize that many multi-layer reflection coatings are optically active; that is why the authors carefully chose mirrors that would not deteriorate the degree of polarization of the light inside the cavity. Without polarization selection in the detection step, the three $\Delta$M transitions can already be observed in the Voigt configuration by rotating the polarization of the incoming field. The simultaneous detection of the decay of light perpendicular and parallel to the incoming field yields a difference spectrum with information on polarization-dependent absorptions. With the Faraday configuration, it was possible to determine the absolute value for $[n_+(\nu) - n_-(\nu)]$ or the optical rotation.

To date, a disadvantage of CRDS is that it is not easily applicable in the UV region (where most analytes absorb), since UV dielectric mirrors are of significantly lower quality as compared to visible and IR mirrors. Furthermore only a limited wavelength range can be probed so that recording of an absorption spectrum is complicated. Switching to another wavelength involves the re-alignment of the cavity using a different mirror set. Such complications do not apply to polarimetry (the measurement of rotation of polarized light, at a wavelength at which a molecule should not be absorbing), so that optical

rotation measurements in CRDS mode in principle have great potential. A set-up using visible light can be used almost universally.

A cavity polarimeter, sensitive enough to measure the low optical activities of chiral (optically active) gases, has been developed [64]. The CRDS (or rather CEAS) cell was a mode-matched confocal cavity used in CW single-mode operation (the cavity length was locked to the laser frequency using a feedback loop). The light source was a He-Ne laser with a wavelength ($\lambda = 633$ nm) far removed from the electronic transitions of the terpenes that were studied. Two anti-reflection coated quarter-wave plates (which will make the linearly polarized light circularly polarized and vice versa) were inserted in the cavity, and a polarizer was used behind the cavity to reject one polarization (this rejected light was used in the feedback loop). The total transmitted intensity depends on the angle of the two quarter-wave plates and the optical activity of the sample in the cavity. To enhance the signal-to-noise ratio, the angle of one of the quarter-wave plates in the cavity was modulated at a frequency of 10 Hz. The low optical activity as well as gas racemization (partial conversion of one pure enantiomer into a mixture) of optically active vapors could be detected.

More recently, a similar scheme for measuring optical rotation as well as circular dichroism (the differential absorption of left- and right-handed circularly polarized light) was developed, the difference being that multi-mode pulsed excitation is used so that mode-matching and a feedback system are not necessary [65, 66]. Furthermore, two detection channels (for the different polarizations of the transmitted light) are being utilized. The intra-cavity waveplates are aligned such that for an empty cavity, one channel (parallel to the input polarization) shows a decay trace whereas the perpendicular channel shows no response. Upon addition of an optically active gas to the cavity, the parallel channel decay trace will start to show oscillations and a signal will start to appear in the perpendicular channel. In practice this zero-background scheme is complicated and another detection scheme was used: the intra-cavity waveplate nearest to the output mirror was rotated by a few degrees so that both channels show a modulated ring-down trace (the modulation is due to the time-dependent rotation of the polarized light). The change in period between an empty and a filled cavity is a measure for gas-phase optical activity [65, 66].

## 1.3 Condensed media CRDS

Whereas CRDS was developed several decades ago and is now becoming a standard measurement technique in the gas phase, the extension towards condensed media remained limited until recently. The main challenge is the fact that for the high density of molecules inside the cavity, the Rayleigh scattering will no longer be negligible and the observed ring-down times will be very short. Also, available sample volumes tend to be much smaller than for gases. Furthermore, the introduction of a sample in the cavity is usually accompanied by the insertion of additional surfaces; the extra scattering and reflection losses at the intra-cavity surfaces will lead to even shorter ring-down times. For a reliable fit of the ring-down time, there should be sufficient data points on the ring-down transient. Therefore, both the excitation and detection instrumental response function (for example the pulse width and the rise time of the detector) should be negligible with respect to the measured ring-down times, and the data acquisition should be sufficiently fast.

With the speed of currently available digitizers, even for short decay transients enough data points are available for reliable fitting. For example, to fit a 70-ns decay curve up to 3 decay times (as is commonly done), 1050 data points are obtained using a 5-GS oscilloscope [27]. On-line fitting speeds in the kHz range can be obtained and the
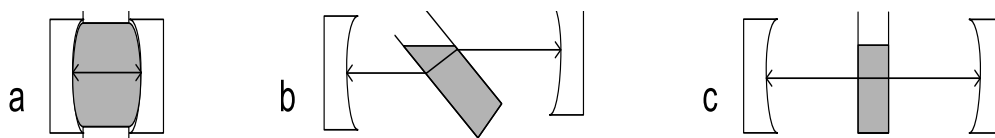
Figure 1.7: Three different geometries that can be used for introducing a liquid in a cavity: (a) filling the entire cavity with liquid, (b) inserting a cuvette at Brewster's angle and (c) inserting a cuvette at normal incidence.

unfavorable S/N ratios inherent to short ring-down times can be improved by averaging. It is good practice to average the fitted ring-down times rather than averaging the traces and subsequently fitting the resulting average trace. The fitting-before-averaging procedure is more time-consuming and requires fast software, therefore it is only possible at lower repetition rates. When using high repetition rates (in the kHz-range), the traces must first be averaged on the oscilloscope followed by fitting of the averaged curve.

Part 1 of this thesis is dedicated to the application of CRDS detection to LC analyses. For bringing a liquid in the cavity, three possibilities can be used (see also Fig. 1.7): to avoid the introduction of extra surfaces the entire cavity can be filled with the liquid [67]. When using a cuvette, it can be inserted at Brewster's angle (the angle at which the reflection for one polarization of the light impinging on a medium with a different refractive index will go to zero) to minimize the reflection losses [68]. Alternatively, a cuvette is used at zero degrees so that reflection losses are maintained in the cavity [59]. Two different approaches (Fig. 1.7a and c) will be explored and compared in chapters 2 – 5.

### 1.3.1 Studying solid-phase samples with CRDS

The first demonstration of CRDS using intra-cavity elements was published by Engeln *et al.* [63]; this paper was already mentioned in the section on polarization-dependent CRDS. The set-up consisted of a linear cavity in which an uncoated BK7 window was aligned at normal-incidence angle. Whereas the ring-down time of the empty 20-cm long linear cavity was on the order of several microseconds, insertion of the window decreased the ring-down time to 700 ns, but still long enough for reasonable measurements. The Verdet constant, which describes the Faraday effect or the strength of the optical activity induced by a magnetic field was measured for the BK7 window.

A further application is the measurement of one of the fundamental IR transitions of solid $C_{60}$ deposited on a ZnSe window [69]. Whereas the thickness of the solid sample was only 20 nm and the line width of 2 cm$^{-1}$ [70] was considerably smaller than the spectral bandwidth of the free-electron laser (8 cm$^{-1}$ between 8.1 and 8.7 $\mu$m), the measurement was sensitive enough to detect the absorbance feature of $C_{60}$. In a similar set-up, bulk and surface defects of thin a-Si:H films deposited on a glass substrate have been measured [71, 72].

Another possibility, rather than studying a thin film on a substrate placed inside the cavity, is using the mirrors of the cavity as a substrate [73]. This approach reduces the scatter losses 100-fold [69,71,72]. A molecularly thin film of iodine was applied by carefully dropping a slight excess iodine solution in acetone on each mirror followed by spin-drying. All iodine molecules that are not attracted to the surface will evaporate leaving a single monolayer of iodine molecules. The mirrors could be cleaned without any problem and no mirror degradation was observed after 50 deposition-cleaning cycles. A spectrum of solid-phase iodine was measured and the crystal structure of the molecular layer could

be deduced by comparison with bulk-iodine crystal absorption spectra. However, whereas this method is very powerful when molecules are deposited in a "soft" way (by evaporation of a solution), the mirrors will be irreversibly affected when the thin film is deposited using e.g. plasma deposition or ion beam sputtering, which limits its applicability.

### 1.3.2 Studying liquid-phase samples with CRDS

When filling a cavity completely with liquid (see Fig. 1.7a), direct contact between the mirrors and the liquid should not result in contamination and irreversible degradation. In our group we have good experiences with alcohols: if after use the mirrors are stored under dry methanol or isopropanol, their initial reflectivities are restored. In the case of direct contact with aqueous solutions for several hours, the mirror reflectivities degrade significantly (for example, [74]); but storage in a vacuum desiccator over $P_2O_5$ as a drying agent restores the mirror quality. A possible explanation could be that water causes swelling of the $\lambda/4$ dichroic layers thus affecting the mirror reflectivity. Nevertheless, no long-term effects are observed for repetitive exposure and cleaning [27,73,75,76]. In addition, since the mirrors are optimized for use in air or vacuum, a refractive index mismatch between the outer dielectric layer of the mirror and the liquid might in principle be disadvantageous. However, this effect appears to be insignificant, probably because the high reflectivity is due to many constructively interfering reflections from the stacked layers.

Alternatively, a cuvette can be placed inside a linear cavity but the intra-cavity surfaces will cause additional scattering and reflection losses (Fig. 1.7b). The reflection losses can be minimized by utilizing a Brewster's angle geometry. Ideally, the Brewster condition should be met for the four phase transitions (from air to quartz, from quartz to liquid and so on) (see Fig. 1.8). [77,78]. The disadvantage here is that the cell is only optimized for one set of refractive index differences i.e. for one particular solvent. Fortunately, this mismatch will be negligible for solvents that have similar refractive indices, such as water (n=1.333) and methanol (n=1.329). The development of cuvettes optimized for every phase transition is rather cumbersome, but a sufficient reduction in the reflection losses is already observed when the cuvette is close to the Brewster's angle for the air to quartz transition: the refractive index of common solvents are close to that of quartz and the liquid acts as an index-matching fluid [68].

A third option is to maintain the reflection losses inside the cavity by using a 0-degree geometry (Fig. 1.7c) [59]. In the set-up of Fiedler *et al.*, a broadband light source providing an output that is not as parallel as a laser source is used, so that the choice for the configuration in Fig 1.7c is obvious. Since the different rays have different angles, it is difficult to define one Brewster's angle and the 0-degree geometry yields lower optical losses.

In one of the first demonstrations of CRDS in the liquid-phase, one or two standard 1-cm cuvettes were placed under Brewster's angle in a linear cavity [68]. Xu *et al.* measured the fifth overtone spectrum of the C–H stretch of liquid benzene. A ring-down time of 0.8 $\mu$s was reported for a 48-cm cavity with a filled cuvette inside. The uncertainty of the ring-down times was quite large (0.01 $\mu$s), leading to a baseline noise of 0.1 to $1\cdot10^{-4}$ cm$^{-1}$ [68]. The authors noted that for the proper definition of the Brewster's angle of the cuvette, it is best to choose the solute/solvent mixture such that the refractive indices of the liquids are similar and preferably close to the refractive index of the quartz cuvette. The lowest baseline noise was obtained for pure benzene, whereas the baseline noise deteriorated for increasing concentrations of hexane.

A similar geometry was applied to the study of reaction kinetics of nitrate radicals with terpenes in solution [79]. In this study, nitrate radicals were produced by photolysis: part of the Nd:YAG beam pumping the dye laser was split off and directed at the cuvette perpendicular to the cavity axis. The absorbance of the terpene solution will decrease as terpene molecules react with the nitrate radicals. Since the reaction rate was on the order of one ring-down time, the rate constant of the nitrate radical reaction could be determined from one ring-down curve (after determination of the ring-down time in absence of the photolysis pulse). This approach of liquid-phase CRDS is especially useful for fast kinetic studies [79].

Excellent results can be obtained with liquid-filled cavities: a baseline noise of $10^{-6}$ cm$^{-1}$ was reported [67]; the standard deviation on the ring-down time of 358 ns was only 1.7 ns. Additional losses associated with intra-cavity elements are circumvented by filling the complete 21-cm cavity with liquid. The effective path length through the sample is equal to the cavity length, but the detection cell volume is as large as tens of ml. Hence the system is appropriate for measuring bulk properties of liquids rather than being a chemical analysis detection system. An important finding was that neither stirring nor a constant flow of liquid affected the measurement [67]. In a subsequent study, the kinetics of reduction of methylene blue was determined [80]. The concentration of analyte was very low: the reduction of 3 nM of methylene blue by an excess of ascorbic acid could be monitored. The fact that only low concentrations are needed can for example be useful when studying poorly soluble analytes [80]. CW-CRDS using the same set-up is also feasible: instead of the Nd:YAG-pumped dye laser, a broadband diode laser together with an AOM can be used [81]. The diode laser should be broad-banded in order to excite many transverse modes, thus avoiding the common problems with CW lasers (that are usually narrower than the FSR of the cavity). The switching rate of the AOM is determined by the build-up rate of light inside the cavity and could in principle be increased to 5 MHz. The actual repetition rate (10 kHz) was limited by the data transfer rate of the oscilloscope. Rather than the expected improvement in signal-to-noise ratio by a factor of a square-root of 1000 as compared to the 10-Hz system previously used, the sensitivity was only slightly improved [80, 81]. A higher repetition rate may also be advantageous in the kinetic study of fast reactions. As will be discussed below, in addition to the large-volume liquid-filled cavities the group of Zare also developed a microliter-sized Brewster's angle flow cell for use in analytical detection (see also Fig. 1.8).

Using a similar "wet mirror"set-up, single-mode CEAS of bacteriochlorophyll a in d$_6$-acetone was performed [82]. In this case a small-sized cavity was used. The 1.75-mm length cavity was locked to the narrow CW laser using a PZT mounted on the back mirror, measurements therefore had to be done in reflection rather than transmission mode. The limit of detection of this system was on the order of 1 nM [82]. Although little attention was paid to the detection cell volume, the probed volume was only several tens of $\mu$l, compatible with conventional-size FIA or LC.

Using a flowing liquid-sheet jet elegantly circumvents some of the disadvantages of the above-mentioned methods for introducing liquids [83]. A stable sheet jet is produced by firing a cylindrical jet at a flat surface. The stability and thickness of the jet depends on many parameters such as temperature, angle between the cylindrical jet and the flat surface, and the presence of air bubbles in the liquid. Despite the favorable ring-down time of 2.5 $\mu$s, the detection limit of a strong absorber was, relatively high, i.e. 71 nM due to the short path length through the jet. The technique might become useful for studying e.g. gas-liquid interfaces, but the high flow rate of 3.4 ml/s precludes use in analytical FIA or LC systems [83].

Instead of using a 0-degree cuvette in a linear cavity behind the laser, one can also insert the cuvette directly in the laser cavity containing the gain medium enabling intra-cavity laser absorption spectroscopy (ICLAS) measurements of liquids [84–86]. Using single-mode CEAS, limits of detection in the picomolar [84] to sub-nanomolar [86] range are feasible. A disadvantage of ICLAS is that the linear dynamic range is severely limited making this experimental scheme unsuitable for analytical purposes. In ICLAS, the sensitivity enhancement will become larger when approaching lasing treshold and experiments are usually performed close to the lasing treshold. When the absorption of the sample becomes a little higher, the light intensity in the laser cavity will fall below lasing treshold making measurements impossible.

### 1.3.3 Incoherent broad-band cavity-enhanced absorption spectroscopy: IBBCEAS

The principle of IBBCEAS was already explained in section 2.4.2, but considering the broad absorbance features in liquids, IBBCEAS is especially promising for liquid-phase studies. The relatively straightforward and economic IBBCEAS was implemented in a commercial bench-top double-beam absorption spectrometer utilizing a Xe arc lamp [50] or LEDs [87]. Both studies made use of a cuvette placed inside the cavity and integrated intensities were measured rather than ring-down times. A disadvantage of IBBCEAS, as with CEAS, is that the measurement depends on the stability of the light source.

In the first demonstration of liquid-phase IBBCEAS, Fiedler *et al.* carefully addressed the preferred geometry for the liquid-filled cuvette inside the cavity [50]. Since a collimated light beam rather than a more parallel laser beam is being used for the measurements (a projection of the light source is being made at the cuvette) it is difficult to define the appropriate Brewster's angle. Optical losses were minimal at a 0-degree geometry, provided that the back-reflection of the cuvette is being overlapped with the excitation beam, which is most conveniently done by mounting the sample cuvette on a mirror holder [50]. A double-beam setup is used with an additional mirror inside the reference beam to account for the specific spectrum of the mirrors. Comparison of single-pass and IBBCEAS measurements on the fifth overtone of the C–H stretch in benzene reveal that using mirrors with a reflectivity of 99% already enhances the signal by a factor of ten. The spectral range covered can be as broad as 200 nm [50]. Since the Xe arc lamp has an extremely high intensity, it is not a main problem to bring enough light in the cavity, so that the reflectivity of the mirrors could in principle be higher than 99%. An optimum should be sought between the enhancement factor, where higher reflectivities are advantageous, and the light intensity transmitted through the cavity. Since CEAS is based on the measurement of a small decrease in signal over a large background (as in conventional absorption spectroscopy), the intensity transmitted at the back mirror should be sufficient for detection with an insignificant shot noise level. Furthermore, the disadvantage of high-reflectivity mirrors is that they will be more narrow-banded, thus limiting the spectral range.

Whereas a high-quality Xe arc lamp is relatively expensive, liquid-phase IBBCEAS using affordable LEDs is more promising, especially since high-intensity and white LEDs are currently developing quite rapidly. Independently, Ball *et al.* [62] and Islam *et al.* [87] developed IBBCEAS using LED excitation for the gas phase and for the liquid phase, respectively. In the latter study different mirror sets (with a total reflectivity of 99, 99.9 and 99.45%) were used as well as narrow-band (20 to 35 nm) and white-light (from 450 to 700 nm) LEDs. Using a given narrow-band LED, limits of detection of various compounds
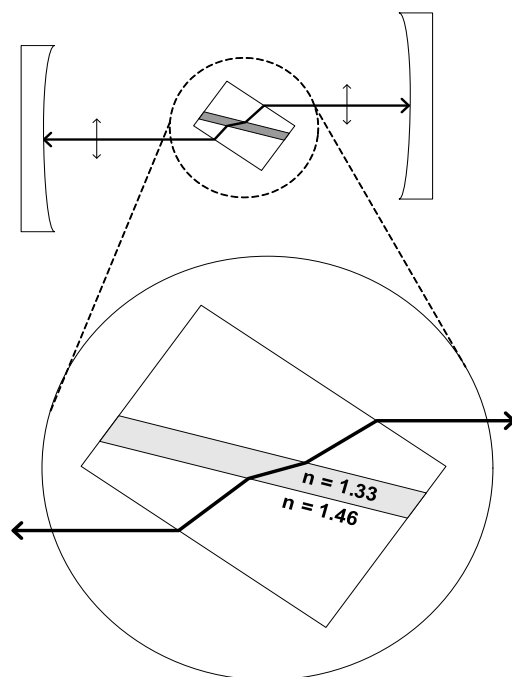
Figure 1.8: A Brewster's angle flow cell (inset) for use in cavity ring-down spectroscopy. All angles between air-quartz and quartz-liquid interfaces have been carefully optimized (adapted from [77]).

were lowest for the mirror set with a reflectivity of 99% and 2 or 3 times lower than with the white-light LED. The detector used in the study was a relatively cheap plug-in spectrometer with no possibilities for electrothermal cooling, which precluded the use of long integration times. The use of a more expensive cooled CCD camera will presumably allow for longer integration times thus enabling the use of mirror sets with a higher reflectivity yielding a larger enhancement factor [87].

Surprisingly, the lowest (steady-state) limit of detection obtained for the convenient and affordable liquid-phase IBBCEAS geometry (using the most favorable narrow-band LED and the 99% mirror set) is only five times higher than when using a more expensive and elaborate laser-based pulsed multi-mode CRDS as an LC detector at one wavelength [27,87]. IBBCEAS has not yet been applied in liquid-flow measurements, but this broad-band technique might become a promising detection technique in analytical chemistry.

### 1.3.4 CRDS absorption detection in liquid chromatography

LC separations with CRDS absorption detection have been demonstrated for each of the three geometries depicted in Fig. 1.7. Whichever geometry is chosen, a basic condition to make it compatible with LC without serious chromatographic bandbroadening is that the cell volume should be smaller than the injection volume. The baseline noise as obtained using the Brewster's angle flow cell (see Fig. 1.8) and a simple multi-mode pulsed CRDS set-up was on the order of $10^{-5}$ absorbance units. Due to the short path length through the flow cell (0.3 mm), the detection limit in LC separations was unfavorable: 0.5 to 5 $\mu$M for strong absorbers; comparable to conventional absorption detection [77]. In a subsequent study, single-mode CW-CRDS absorption detection was performed using the same Brewster's angle flow cell. The cavity was not locked to the laser; excitation was performed by switching on the laser, which frequency-shifted upon warming up. As soon

as the laser was in resonance with a cavity mode and the cavity transmitted laser light, the laser was switched off again and a ring-down curve was measured. After 100 $\mu$s the laser was switched on again and the measurement cycle started again. Whereas pulsed multi-mode CRDS shows a typical shot-to-shot variation of 1% of the ring-down time, in the single-mode set-up this was only 0.04% and an excellent baseline noise of $2 \cdot 10^{-7}$ was observed; limits of detection were on the order of several tens of nM [78].

In order to couple CRDS detection with LC, a liquid-only cavity flow cell with a volume of only 14 $\mu$l was constructed in our group by clamping the mirrors leak-tight around a 2-mm thick rubber spacer with an elliptical hole. The liquid flow could be introduced through capillaries inserted through the sides of the spacer (see Fig. 1.7c) [27, 75, 76]. A complete description of the experiments and the results obtained can be found in chapters 2, 3 and 4. Furthermore, an alternative approach, i.e. the normal incidence configuration using flow-through cuvettes, see Fig. 1.7b [88], was followed and compared to the performance of the liquid-only cavity. Details about the experiment and a comparison with the previously obtained results using the liquid-only cavity can be found in chapter 5.

CE (capillary electrophoresis) detector cell volumes are much smaller compared to conventional-size LC and too small for the CRDS cells described above. Nevertheless, CRDS absorption detection in CE studies has been demonstrated using fiber-loop CRDS [89]; this technique will be the subject of the next section.

### 1.3.5 Fibers for CRDS measurements

As repeatedly stressed above, the sensitivity of CRDS measurements depends on the reflectivity of the mirrors used and unfortunately highly-reflective mirrors are only applicable over a short wavelength range. Since this is one of the major disadvantages of CRDS, much attention has been paid to circumventing the need for mirrors. A few studies on fiber CRDS using retro-reflectors such as FBGs (fiber-Bragg gratings) [90] or highly-reflective coated fiber ends [91, 92] have been published. More interestingly, the use of fibers can in principle open an elegant way to circumvent the need for mirrors. An exponentially decaying ring-down transient can be obtained by looping an optical fiber upon itself.

The only limitation is the absorbance of the bulk material of which the core of the fiber is made. Fiber or fiber-loop CRDS is therefore most suited for studies at the telecom window wavelengths in the NIR, but it is of limited use at blue or UV wavelengths. Input and output coupling is possible by using commercially available couplers or by enabling light injection and detection by strongly bending the fiber at specific points. Many different modes of CRDS and EW-CRDS (discussed in more detail in the next section) have been explored.

Initially, since the introduction of a sample in a fiber or a fiber loop introduces significant scatter losses (analogous to intra-cavity elements in a linear cavity), only evanescent-wave applications of CRDS using fibers were envisioned. The light losses of a fiber depend on the difference between the index of refraction of the core and that of the cladding; induced changes of the refractive index can also be monitored. By removing the cladding, the fiber core will be exposed to the surrounding medium and additional losses of the light in the fiber can give information on the refractive index of the surrounding medium [90,91]. Hydrogen diffusion into and out of the cladding has been studied [92]. In addition to being sensitive to refractive index changes, light losses will also depend on the absorbance of the medium surrounding an exposed region of the core and this way a NIR spectrum of an overtone in 1-octyne was measured; the measurement principle is quite similar to ATR (attenuated total reflectance) spectroscopy in which only the evanescent wave associated

with a TIR event is penetrating into the sample [93].

Alternatively, a pressure sensor [94] and a strain gauge [95] were developed. In order to make a fiber ring-down set-up pressure-sensitive, only the fiber jacket has to be removed. Application of a certain pressure to the cladding changes its refractive index; the additional losses and therefore the ring-down time depend linearly on the applied pressures [94]. The idea behind the strain-sensing apparatus is that the transmitted intensity through a fiber decreases when pressure is applied to a section of a fiber. Using a fiber with a biconical taper (thinned stretch) a strain gauge sensor using the same principle has been developed as well [95]. The transmission of the biconical taper will also be affected by attachment of cells to the taper and single-cell detection using fiber-loop CRDS has been demonstrated [96]. Another possible application of fiber CRDS is the determination of additional losses in fibers due to, for example, bending [91, 97].

A first attempt to introduce a sample cell inside a fiber loop was performed using erbium-doped (i.e. active) fibers; these fibers were pumped just below lasing threshold and amplified the signal as it traveled around in the fiber loop [98]. The disadvantage of this set-up was that the accuracy and the repeatability of the measurement was determined by the repeatability of the amplification and is therefore rather limited; standard deviations on the obtained ring-down times were 20 %. Other methods for using active fibers in CRDS measurements were presented in a follow-up study [99]. Two fiber loops, one kept just above lasing treshold thus stabilizing the other (pumped just below lasing treshold) can be used. A more simple and straightforward method is directly firing a laser pulse in one fiber loop by briefly pumping it above lasing treshold. As far as we know, these systems have been characterized in detail with an empty sample cell, but gas-phase measurements were never published, possibly because the modified systems are still too unreliable and difficult to implement in gas-phase absorption spectroscopy [99].

Two fiber ends can be connected together using a commercially available splice connector. Such a connector is normally filled with an index-matching fluid in order to minimize losses, but can be replaced by a (flow of) liquid sample [100, 101]. The volume inside the splice connector is extremely small (about 10 pl) and it might therefore prove to be useful in absorption detection in analytical microdevices [102]. In a first demonstration of fiber-loop CRDS for transmission absorption measurements in the liquid phase, a 12-m fiber with splice connector was determined to have two ring-down times: one of 235 ns (corresponding to light coupled in the cladding) and one of 900 ns [100]. Due to the long round-trip times of the fiber loop, the individual pulses of light leaking out the fiber at a strong bend could be resolved. The limit of detection for a certain dye solution was 0.27 mM in a cell volume as low as 7 pl (the path length was only 4 $\mu$m). In another study, the phase-shift CW-CRDS method as developed by Engeln *et al.* [51] was applied to fiber-loop CRDS. Briefly, the sinusoidally modulated intensity as measured behind the fiber-loop cavity makes a certain phase difference with the sinusoidally modulated laser; this phase difference depends on the ring-down time of the cavity and therefore on the absorbance. Using phase-shift fiber-loop CRDS, the same dye and the same measurement wavelength as in [100], the limit of detection was improved 50-fold to $6\mu$M for a ten times longer path length (30 to 40 $\mu$m).

For the phase-shift absorption detection in CE separations, a home-built splice connector was created by encapsulating the capillary in a PMMA block and drilling a 150-$\mu$m diameter hole in the 360-$\mu$m outer diameter capillary so that the CE capillary and the fiber could be crossed (see Fig. 1.9) [89]. The used fiber ends were lensed by careful heating, thus minimizing losses in the splice connector. Different concentrations of a test mixture of non-covalently dye-labeled human serum albumin (HSA, one of the most abundant
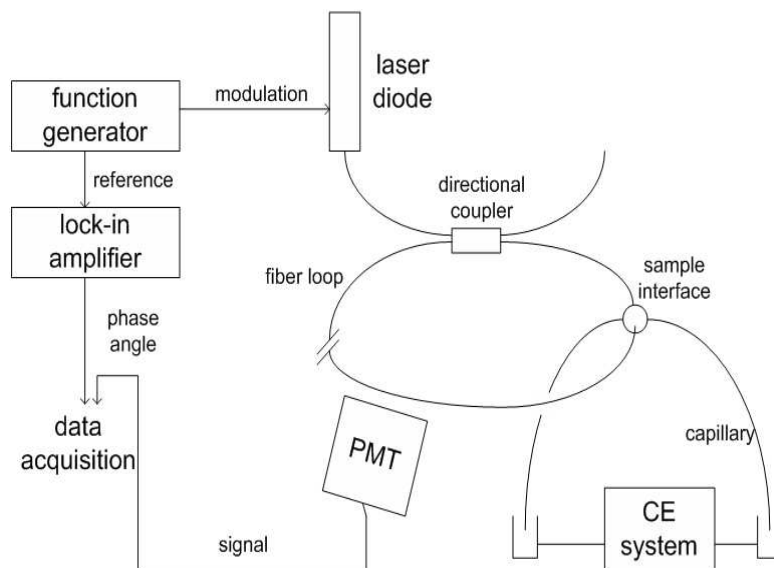
Figure 1.9: The set-up for phase-shift fiber-loop CRDS absorption detection in CE. PMT: photo-multiplier tube, directional coupler: needed for efficiently coupling light in fibers, lock-in amplifier: phase-sensitive detector (adapted from [89]).
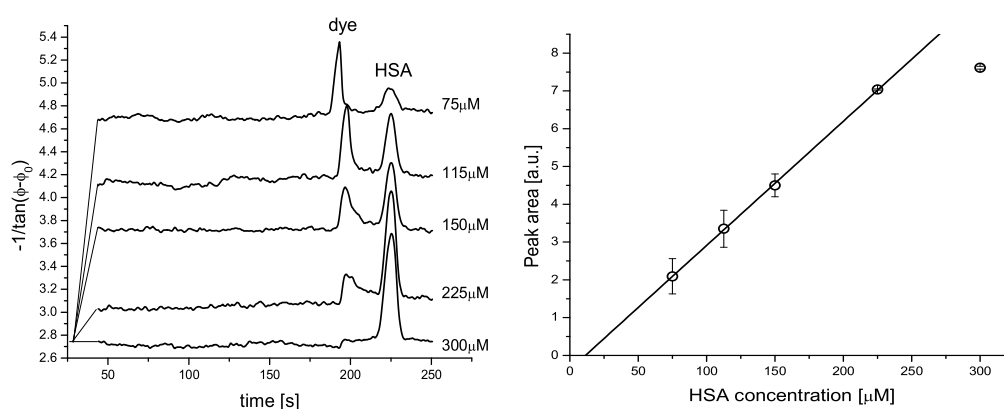


Figure 1.10: Electropherograms (CE flow profiles) of free dye and dye-stained HSA at different HSA concentrations, together with a calibration line showing the dye-HSA peak area as a function of the HSA concentration (Reproduced with permission from [89]. Copyright 2006 American Chemical Society.).

proteins in human blood) and the non-associated dye were separated (see Fig. 1.10). A concentration of 75 $\mu$M of labeled HSA could easily be detected.

## 1.4    Evanescent-wave CRDS

EW-CRDS is a new and rapidly evolving field: this technique combines the excellent sensitivity of CRDS absorption measurements with the surface specificity of EW spectroscopic techniques. In EW-CRDS, one or more of the reflections inside the cavity is a TIR event and only the evanescent wave (penetrating a few hundred nm in the sample) is being used for probing the sample. As a result, only molecules that are adsorbed at, or are near the surface are detected. In fact the set-up is quite similar to that of ATR spectroscopy, where a long, high-refractive index waveguide or prism is used in which the light undergoes several tens of TIR events before exiting the ATR crystal at the back side. However, this mode of EW absorption spectroscopy is usually not localized, the TIR reflections can be spaced millimeters apart and the ATR prisms are typically several centimeters long. Furthermore, the sensitivity of the ATR measurement is limited by the small number of TIR events.

In a proof-of-principle experiment, Pipino *et al.* demonstrated that CRDS is sensitive enough for detection of adsorption processes using the evanescent wave following a TIR reflection [103]. The set-up used a standard Pellin-Broca prism inside a cavity. The first demonstration of EW-CRDS using monolithic resonators employed a TIR ring cavity [103,104]. Similar to the above-mentioned fiber-loop EW-CRDS geometries [90–93], high-reflectivity mirrors are not needed and the TIR ring cavity can be applied to a broad wavelength range. In follow-up studies, monolithic (single-piece) or folded resonators with extremely low optical losses were used [105–107].

Unfortunately, these optical components need to be custom-made at high costs. Applying off-the-shelf or easy-to-produce custom-made optics is more straightforward and many different applications of TIR prisms placed inside CRDS cavities have been reported in the literature. Obviously, the additional intra-cavity surfaces cause reflection and refraction losses that affect the performance and achievable sensitivity levels. As has become clear in the previous section, upon insertion of intra-cavity elements the remaining ring-down times are often still sufficiently long for reasonable measurements. Losses can be minimized by utilizing a Brewster's angle at the entrance and exit faces of the prism [108,109], a high-quality anti-reflection coating [110–115] or a 0-degree geometry. An important advantage of the latter is that it permits polarization-dependent studies [116,117].

In part 2 of this thesis, several applications of EW-CRDS to the liquid phase will be described. In a first study, the feasibility of FIA on an intra-cavity prism surface (the set-up was comparable to the pulsed-laser set-up used in the group of Shaw [110]) without noticeable contamination or degradation of the prism surface was demonstrated. A follow-up study deals with the possibilities of surface-modified prisms: the TIR surfaces of the prisms are coated using organosilanes and the adsorption of the heme protein cytochrome C is studied.

### 1.4.1    Applications of EW-CRDS to the gas-phase

In an exploratory study, Pipino *et al.* inserted a Pellin-Broca prism in a cavity and one of its silica surfaces was exposed to iodine vapor. The advantage of using standard Pellin-Broca prisms is that they are designed to have entrance and exit faces at Brewster's angle, thus minimizing reflection losses. A Langmuir adsorption isotherm was measured, and
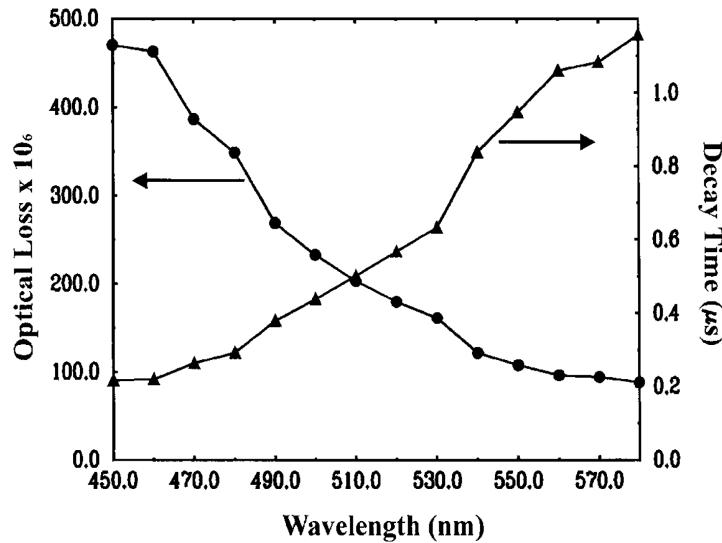
Figure 1.11: The ring-down times (triangles, right scale) as well as the optical losses (times $10^6$, circles, left scale), measured using the TIR ring cavity (Reproduced with permission from [105]. Copyright 1999 by the American Physical Society.).

repeated adsorption/desorption cycles showed the reversibility and repeatability of iodine vapor adsorption. The minimum detectable iodine coverage was determined to be 0.04 monolayer [104].

Following a previously published study about miniature fused-silica monolithic optical ring resonators [118], a TIR ring cavity was designed [103]. One of the sides was spherically polished, thus making the ring cavity into a stable optical resonator. The round-trip path length was 2.12 cm and the spherically polished side had an $R_c$ of 2.23 cm. In order to minimize scatter losses, the facets were polished to a surface roughness better than 0.05 nm r.m.s.. Light was coupled into and out of this cavity via frustrated TIR using two prisms equipped with PZTs in order to be brought in close contact with the ring resonator; in order to frustrate the TIR the prisms need to be brought within the evanescent wave associated with the TIR. The characteristics of this TIR ring (see Fig. 1.11) cavity can be used to determine the previously unknown optical purity of the used fused silica (Hereaus Suprasil 311) [105, 107, 116]. The ring-down times are between 200 and 1000 ns and considering the short round-trip time of 0.11 ns, the light can probe the four different surfaces 1800 to 9000 times in one ring-down event. In a subsequent study, the region between 1210 and 1650 nm was used for measuring the $3\nu$OH and $2\nu$OH stretch vibrations of $HNO_3$ adsorbed on silica [119].

Follow-up studies made use of an alternative design: a monolithic resonator (as schematically depicted in Fig. 1.12) was coated with high-reflectivity coatings at the edges. The first implementation using this design employed reflective coatings between 490 and 540 nm; ring-down times were between 1 and 1.2 $\mu$s, which is a factor of 2 improvement over the TIR ring cavity [105]. This geometry has been used to measure the molecular orientation of iodine at the silica interface; the minimum detectable coverage of iodine at the surface was calculated to be 0.004% of a monolayer, which is a factor of 1000 improvement over the intra-cavity Pellin-Broca [104, 105].

Utilizing high-reflectivity coatings with a center wavelength in the red region of the spectrum is expected to increase the performance of the folded resonators even more. A
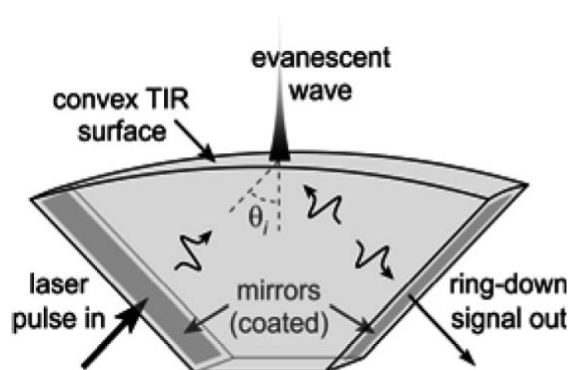
Figure 1.12: A monolithic folded resonator for EW-CRDS studies; the apex is atomically smooth with a convex curvature, entrance and exit faces are coated with a high-reflectivity coating (Reproduced with permission from [107]. Copyright 2005 by the American Physical Society.).

very interesting application showing the extreme sensitivity of this EW-CRDS mode is the measurement of a quasi-ice monolayer on the atomically smooth apex of the folded resonator. The coating of the folded resonator is centered at 1205 nm, where the frequency of the $2\nu OH + \delta OH$ mode of water should be. Ring-down times of the folded resonator are around 4.3 $\mu$s, and $s$ (perpendicular)- and $p$ (parallel)-polarized spectra are simultaneously recorded. Even though the absorption cross sections of vibrational overtones are much lower than the fundamental ones, a significant increase in peaks associated with surface-bound water is observed when going from a dry nitrogen environment to 10% relative humidity (see Fig. 1.13b). In addition, a doublet which does not respond upon dosing with water is observed (Fig 1.13a) and these peaks are therefore assigned to the $2\nu OH + \delta OH$ mode of surface silanol groups. The doublet is highly polarized indicating the presence of two distinct surface silanol groups, oriented perpendicular and parallel to the surface. Moreover, a decrease in linewidth of the water peaks indicates an increase of surface order as a full water monolayer is completed [107].

Using a folded resonator coated at 1650 nm, the absolute surface coverage as well as the molecular orientation of adsorbed trichloroethylene, cis- and trans-dichloroethylene were measured using a vibrational overtone [106]. In another application, using folded resonators with coatings centered at 1205 nm, in-situ measurements of surface dangling bonds during the growth of an a-Si:H layer on the silica resonator have been performed. For these measurements, the folded resonator had to be in an ultra-high vacuum set-up at 150 $^oC$, demonstrating that the design of the folded resonator is suitable for remote detection [120].

## 1.4.2 Applications of EW-CRDS to condensed media

Both the TIR ring resonator and the folded resonator used by Pipino and co-workers make use of an incident angle of 45 degrees; considering the refractive index difference between silica and aqueous solutions ($n_{water}$=1.33 and $n_{silica}$=1.46) such an angle of incidence will not provide TIR when extending these studies to the liquid phase. A minor change in the design of the resonators (i.e. using a 70 degrees angle) would permit the use of folded
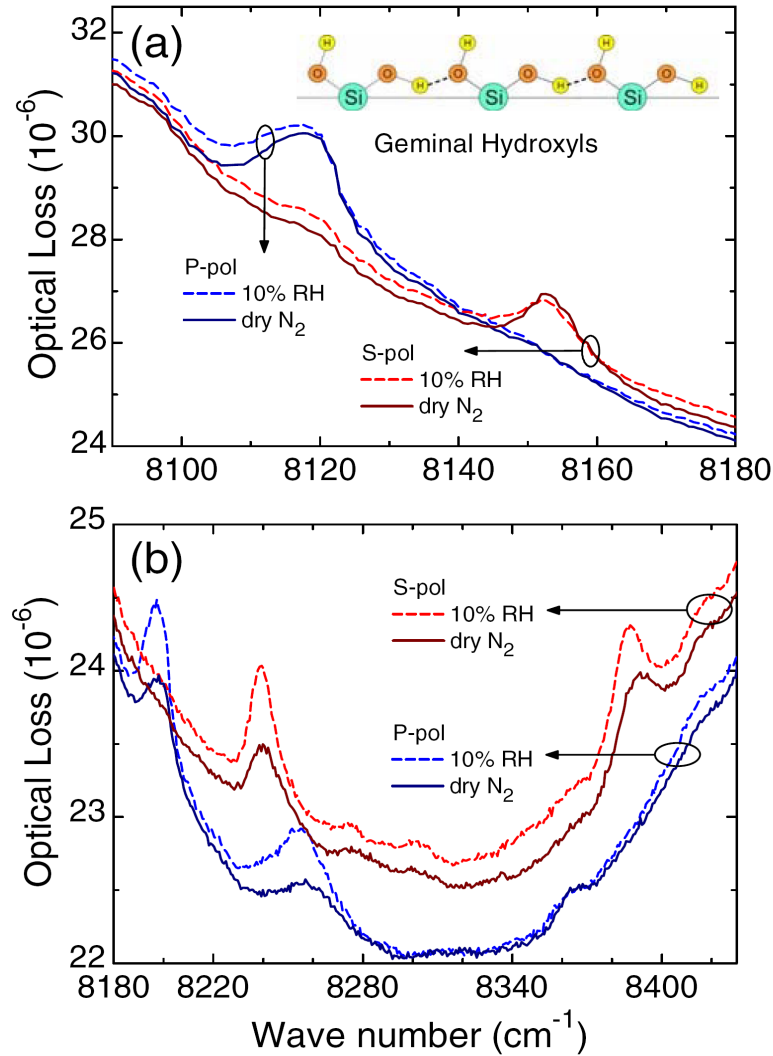
Figure 1.13: Vibration-combination bands of surface silanol groups (a) and adsorbed water molecules (b) as measured with the monolithic folded resonator coated at 1205 nm. The solid plots were measured under dry $N_2$ and the dashed plots are measured after equilibration at 10% relative humidity. The inset in panel a shows the H-bonded network of the surface hydroxyls. The background arises from the mirror reflectivity curve (Reproduced with permission from [107]. Copyright 2005 by the American Physical Society.).

resonators in liquid-phase studies but until now, as far as we know no efforts have been made in this direction.

As a first demonstration of the use of intra-cavity prisms, Shaw *et al.* inserted an anti-reflection coated conventional BK7 Dove prism in a linear cavity. Since the entrance and exit faces of commonly available Dove prisms are cut at 45 degrees, the reflection losses are considerable. However, the use of a high-quality anti-reflection coating (R≤0.025%) diminished the optical losses to a reasonable extent: while the empty cavity had a ring-down time of 15 $\mu$s, this value decreased to 150 to 200 ns upon insertion of the prism [110]. Considering the round-trip time of the cavity this corresponded to 70 passes over the sample surface within one ring-down time. A flow cell was constructed over the TIR surface by clamping an O-ring to the surface. This way the behavior of the different silanol groups at the surface could be studied. It is known that there are 0.8 to 8 OH groups per $nm^2$ at a silanol surface, divided in Q2 sites with two OH groups bound to a surface Si atom and Q3 sites with only one OH group bound to a surface Si; both sites have different pKa values. The electrophilic adsorbance of the positively charged dye Crystal Violet to the surface as a function of pH and competing metal cations gives insight in the mechanisms governing adsorbance [110].

In subsequent studies, Shaw and co-workers used a CW-CRDS approach in which a broadband diode laser was used in conjunction with an non-stabilized cavity [111–113]. The bandwidth of the laser is large enough to span many cavity modes; the laser power is shut off with a frequency of 6 kHz and after averaging of 256 traces on the digital oscilloscope, the data is transferred to the PC for further handling. Whereas the previous multi-mode pulsed approach yields a sensitivity on the order of $10^{-4}$ absorbance units, for this configuration it is below $10^{-5}$ [111]. This set-up has been used in the study of interfacial pH at the silica-water surface [112] by covalently attaching a derivative of a dye to the surface. The surface coverage of the dye was $5 \cdot 10^{-5}$ monolayer. Since the absorbance of the chosen dye is pH dependent, variation of the absorbance of the covalently bound species as a function of bulk pH can be compared to the absorbance variation of the dye in bulk solution, and is a measure of the interfacial pH [112]. Furthermore, gold nanoparticle adsorption and aggregation kinetics at the silica-water interface can be monitored (see Fig. 1.14) [113]. Upon addition of the citrate-stabilized gold colloid to the flow cell, the colloid will be destabilized at the silica-water surface and aggregation at the surface will take place. Absorbance of the colloid at 635 nm is due to surface plasmon excitation of the gold particles. After multilayer aggregation is complete, the gold-colloid/prism surface assembly can be used to detect refractive index changes smaller than $10^{-4}$ [113]. A medical application of the system, for example, is monitoring the hemoglobin adsorption from controlled urine samples for the diagnosis of hemoglobinurea [108].

The rate of solvent diffusion in a polymer film that is pressed to the TIR face of the prism has been studied. As solvents such as water or methanol penetrate into a poly(dimethylsulfoxane) film, the optical losses will increase. Insight in diffusion mechanisms in polymers may be useful in the development of chemical modifications that reduce permeation and degradation [114].

EW-CRDS was combined with electrochemistry by bringing an electrode close (25 to 250 $\mu$m) to the surface and electrogenerating the strongly absorbing $Fe(CN)_6^{3-}$ from weakly absorbing $Fe(CN)_6^{4-}$. The measurements were done employing a CW-CRDS set-up. Rather than using a broadband diode laser, the frequency of the laser was varied until excitation occurred, an AOM switched the laser off when the light intensity detected behind the cavity exceeded a certain value; measurements were performed at 100 Hz [115]. The authors realized that the reflection losses from the non-perpendicular surfaces of the
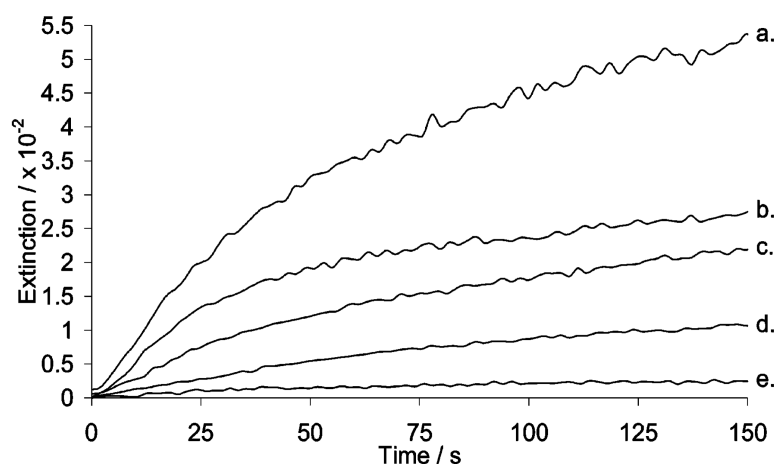
Figure 1.14: Increase in extinction upon adding citrate-reduced gold colloid to the flow cell on top of the Dove prism. Colloid concentrations are (a) 100%, (b) 80%, (c) 60%, (d) 40% and (e) 20% in water (Reproduced with permission from [113]. Copyright 2007 American Chemical Society.).

anti-reflection coated prism exit face might as well be used for detection of the ring-down transient: since the optical losses at the interfaces are much larger than at the high-reflectivity mirrors, more light intensity will reach the detector improving the signal-to-noise ratio of the decay transient [115].

Using a Brewster's angle for entrance and exit faces should decrease the optical losses considerably. In the set-up of Li *et al.* which utilizes a Brewster's angle Dove prism, the ring-down time is almost half that of the empty cavity (630 ns versus 1.5 $\mu$s) [89]. Nevertheless, the round-trip time of the cavity being 6.6 ns, the light will only make 95 passes in one ring-down time and the obtainable absorbance sensitivity is similar to that obtained when using a pulsed multi-mode CRDS set-up using the anti-reflection coated 45-degrees Dove prism [110]. The system was used for the determination of thermodynamic properties of a strongly adsorbing and a weakly adsorbing dye at the silica/acetonitrile interface [109].

The use of a normal-incidence geometry for the entrance and the exit faces of the prism permits for polarization-dependent studies, and measurement of the dichroic ratio can be used for determining the average molecular orientation of molecules in self-assembled thin films [116, 117]. An MB (Methylene Blue) film was produced by putting a 10-$\mu l$ drop of MB solution on the surface followed by evaporation of the methanol. The surface coverage is known from the concentration in the solution. At low concentrations (1/50 of a monolayer), the molecules lie almost flat on the surface whereas the molecules will be more vertically oriented at higher concentrations. In addition, since MB monomers and dimers have different extinction coefficients, the extent of dimer formation as a function of increasing MB coverage can be determined [116].

Using a similar right-angle geometry, the adsorption of hemoglobin from an aqueous solution were studied, as well as the average orientation of the hemoglobin molecules [117]. Adsorption studies were done using quiescent solutions of different hemoglobin concentrations in buffer; the authors assumed that photodegradation was negligible over

the 100-minute range of their measurement. The average orientation of hemoglobin on the silica surface was determined to be 54.8 degrees [117]. However, when the distribution of orientation angles is very large (the molecules are randomly oriented), the apparent average orientation angle as calculated from the dichroic ratio will be 54.7 degrees [116] and it is difficult to discern an average orientation around 54.7 degrees from a random orientation.

Despite the fact that the less sensitive pulsed multi-mode CRDS technique is used, the sensitivities obtained are similar to those obtained by Shaw *et al.* using CW-CRDS at high repetition rates [111–113] i.e. lower than $10^{-5}$ absorbance units. The anti-reflection coated and Brewster's angle configurations mentioned above all have sensitivities on the order of $10^{-4}$ absorbance units. The normal incidence approach seems to be most successful but the performance is still far removed from that of the TIR ring cavities and folded resonators of Pipino *et al.*, of which the sensitivity is estimated to be $10^{-7}$ absorbance units or better.

A main problem with the above-mentioned studies is that adsorption to the silica surface is irreversible and thorough cleaning using various acids and solvents is needed in between measurements. When developing a detection method in analytical chemistry, a set-up where repeated measurements can be performed without intermediate cleaning is needed. Chapter 6 of this thesis demonstrates that the amount (and irreversibility) of adsorption to the silica TIR surface can be set by variation of the eluent used as well as the flow rate. Furthermore, surface characteristics can be straightforwardly changed by covalently attaching a self-assembled monolayer on the TIR surface of the prism (see chapter 7). Surface modification can ultimately become a valuable tool in for example bio-sensing.

# Chapter 2

# Miniaturized Cavity Ring-Down Detection in a Liquid Flow Cell

[1]

## abstract

A novel method for applying cavity ring-down spectroscopy in the liquid phase, compatible with LC analyses, is presented. The core of the setup is a home-built cavity ring-down flow-cell (cell volume 12 $\mu$l), that is constructed using a silicon rubber spacer which is clamped leak-tight between two high-reflectivity mirrors. The mirrors are in direct contact with the liquid flow, which provides for a small path-length and short ring-down times. Inside the cavity there are no windows, reflection losses or Brewster angles to be considered. Due to the small size of the presented cavity geometry, the setup can be implemented in conventional-size LC apparatuses. With a flow injection setup a detection limit of 2.5 nM was obtained for Crystal Violet in ethanol, and the linear dynamic range of the system is at least two orders of magnitude. The method has the potential to become a powerful alternative for commercial LC UV/Vis absorbance detectors.

## 2.1 Introduction

In liquid chromatography (LC) direct optical absorption is the generic and commonly used method to detect absorbing analytes and their concentration in eluting compounds. Almost any analyte absorbs light in the visible or ultraviolet range, and standard absorption detection shares the advantages of simplicity and versatility. Since direct absorption techniques are based on monitoring attenuation of light intensity, they are fundamentally limited by the intensity fluctuations of the light sources employed, where currently $\Delta I/I$ values of $5 \times 10^{-5}$ are reached [77]. An option for improving the limit of detection (LOD) in LC lies in the increase of the optical path length without altering the detector cell volume, and therefore Z-shaped cells of typically 8 mm optical path length and 1 mm diameter are commonly used. With the use of Liquid Core Waveguide flow cells optical path lengths as long as 30 to 50 cm can be obtained [3, 4], but the number of applications is still limited. Considering the broad applicability of absorption detection in LC, it is highly relevant to improve sensitivity and detection limits, but at the same time the chromatographic restrictions of LC should be complied with. In view of chromatographic band-broadening effects, even in conventional-size LC the detector cell volume should be limited to typically 20 $\mu$L, while for micro- and especially nano-LC the constraints on detection volumes are obviously much more serious.

The invention of the cavity ring-down (CRD) detection technique [21] has introduced an elegant manner for improving sensitivity in direct absorption. CRD is based on the injection of a short laser pulse into an optical resonator with high-reflectivity mirrors, followed by the detection of the light leaking away through a mirror. Since its principle is based on measuring the rate of decay of an optical cavity, CRD in effect circumvents the common limitations of absorption measurements: the decay time is independent of the intensity of the light pulse exciting the optical resonator, and hence pulsed laser sources with pulse-to-pulse intensity fluctuations of $\Delta I/I$ in excess of $10^{-2}$ can be used without problem. Furthermore, the use of cavities in CRD inherently increases the interaction path length, since most of the light is detected after hundreds or thousands of round-trips. Numerous applications in gas-phase spectroscopy and dynamics, using the original pulsed variant of CRD, as well as cavity-enhanced and cavity phase-shift variants have been reported [15]. The extension to evanescent-wave absorption outside an optical resonator has shown promising applications for sensitively detecting films of solid [103, 105] or liquid material [110].

Application of CRD to detection in the liquid phase is still in its infancy, but at the same time the first reports bear great promise. Xu *et al.* demonstrated CRD detection for a study of weak overtone absorption in bulk benzene with an extended cell placed at Brewster angle inside a resonator to minimize Fresnel reflection losses [68]. A breakthrough, bringing CRD in the realm of LC, was established through the work of Snyder and Zare [77], who designed a cell aligned inside a CRD-resonator, having a double Brewster configuration to reduce reflection losses at both the air-glass and the glass-liquid interfaces. Their design involves an optical path length of 300 $\mu$m through the liquid flow within a resonator of 1 m, and ring-down transients of several $\mu$s are measured. Analysis of variations of the typical decay times yielded a LOD of 92 nM (at $\varepsilon = 9 \times 10^3$ M$^{-1}$cm$^{-1}$) for LC measurements in a cell volume of 10 $\mu$L (of which 0.5 $\mu$L illuminated). Hallock *et al.* demonstrated that the use of refractive index dependent Brewster-faced cells can be circumvented, since in some cases the liquid can be brought in contact with dielectrically-coated mirrors [67]. In their study on bulk liquids a single-pass path length of 20 cm was used and typical ring-down times of 200-400 ns were recorded.
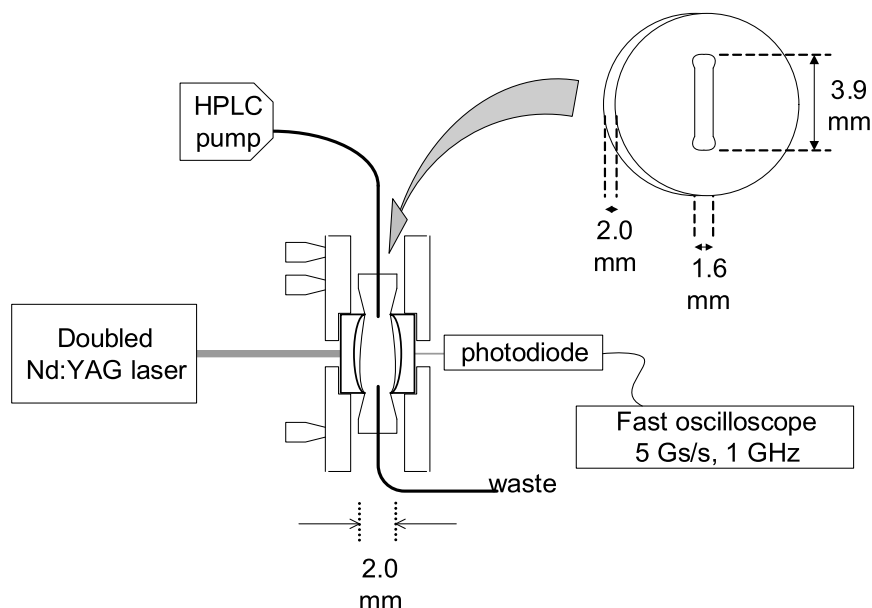
Figure 2.1: Schematic diagram of the flow cell (not to scale) and the set-up. The outer boundaries of the cavity ring-down flow cell are formed by the concave mirrors, pressed leak-tight to the sides of a silicon rubber spacer. Flow is introduced via capillary tubing (shown as thick black lines) inserted in the spacer, shown in detail at the upper right.

In the present study we report on a miniaturization of the thin flow-cell setup of Snyder and Zare [77] by forming a mini-resonator with two mirrors at a typical separation of 2 mm in contact with the fluid as in Ref. [67]. Whereas the flow-cell as suggested by Hallock et al. [67] is not suitable for HPLC detection purposes, the presented flow-cell with a volume of 12 $\mu$l meets the chromatographic demands on the detector cell volume. For the analysis of small variations in the resulting optical transients special care has to be taken to minimize the response time of the optical detection system. Our current limit of detection is estimated to be comparable to that of Ref. [77] in an experiment with flow injection, using Crystal Violet dissolved in ethanol. Several options to further increase the sensitivity of the miniature setup are envisioned and will be discussed.

## 2.2  Experimental section

The design of our miniature cavity ring-down flow cell, built from two highly reflective mirrors separated by 2 mm, is schematically depicted in Fig. 2.1. The mirrors, which are in direct contact with the liquid, are sealed in 10 cm diameter plate holders equipped with micrometer screws for cavity alignment. A 2 mm thick silicon rubber spacer determines the single-pass cavity length, while a hole in the spacer forms the flow cell (volume 12 $\mu$L). The shape of the hole is as elliptic as possible to sustain laminar flow inside the cell in order to minimize unwanted LC band broadening. The laser beam of maximum 1.6 mm diameter is directed through the flow cell and illuminates a volume of about 4 $\mu$L. Fused silica capillary tubing (external diameter 0.32 mm, internal 0.25 mm) is inserted in the spacer in order to introduce the liquid flow into the cell.
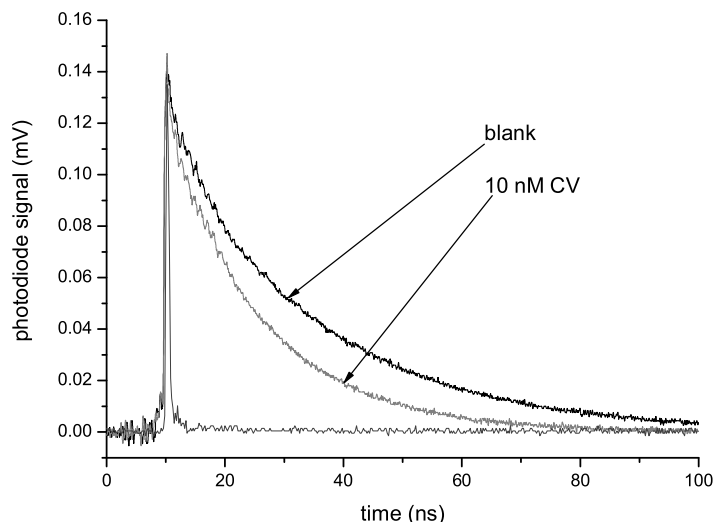
Figure 2.2: The cavity ring-down signal as measured on the oscilloscope for pure ethanol in flow (blank; upper curve) and after injection of 100 $\mu$L of a 10 nM CV-ethanol solution (lower curve). Also displayed is the temporal response curve of the detection system.

In view of the short single-pass optical path and the resulting short ring-down times, the instrument response function must be kept as short as possible. For this purpose we use laser pulses of 100 ps duration from a Q-switched, mode-locked and frequency-doubled (532 nm) Nd:YAG laser (Quantel, France), a fast sampling oscilloscope of 1 GHz analog bandwidth (Tektronix 5104 5 Gs/s) and a fast 4 GHz bandwidth photodiode (PHD400, Becker & Hickl, Germany). In combination they yield a response time of about 600 ps FWHM, negligible with respect to typical decay times observed of 20-30 ns. Laser pulses of 0.15 mJ incident pulse energy are coupled into the cavity at a repetition rate of 10 Hz, limited by the laser. With highly-reflective coated mirrors (REO Inc, Boulder, USA) having radius-of-curvatures (roc) of 50 mm the miniature cavity is easily aligned, in contrast to mirrors with roc = 20 or 50 cm.

All measurements are performed in flow on the test compound Crystal Violet (CV, color index 42555, 98% Aldrich Chem., Milwaukee, USA) dissolved in ethanol (Ethanol absolute $\geqslant$ 99.5%, Baker, Netherlands). The solvent is degassed by sonication prior to use; the extinction coefficient for CV in ethanol at 532 nm is determined at 54500 $M^{-1}cm^{-1}$. Flow (flow rate: 1 ml/min) is introduced with an LC-pump (Gynkotek Separations 300, Germany) combined with a six-port valve equipped with a 100 $\mu$L injection loop. Dilute solutions of CV in ethanol are injected in the continuous flow of pure ethanol for the CRD detection measurements.

## 2.3   Results and discussion

Fig. 2.2 displays some typical decay transients as recorded in pure ethanol and in a 10 nM CV-ethanol solution after injection of a 100 $\mu$L plug; the displayed transients are taken at the time window when the analyte plug has reached the flow cell. No signal averaging is applied. The fast transient corresponds to the photodiode signal of a laser pulse directly
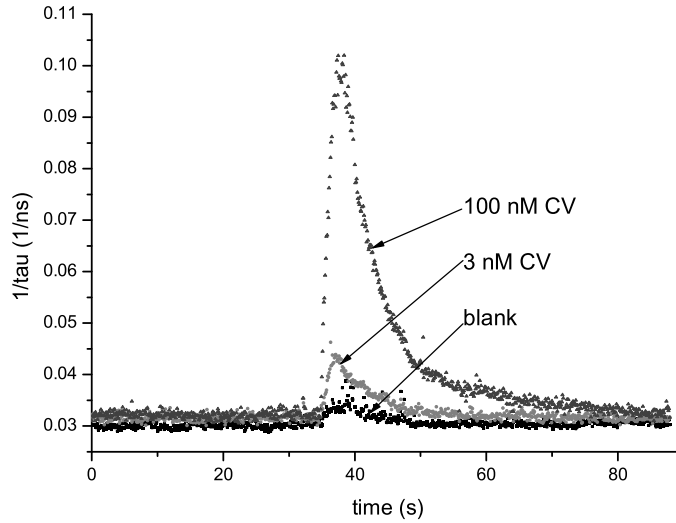
Figure 2.3: Recording of a time trace representing continuously monitored ring-down events after injection of an absorber in a flow of ethanol. From bottom up: blank; 3 nM crystal violet; 100 nM crystal violet.

measured and represents the instrument response function. All transients are registered by the oscilloscope at a maximum sampling rate of 5 Gs/s, so that 500 data points are available on a 100 ns decay transient (typically corresponding to $3\tau$). $1/e$ Decay times $\tau$ are extracted from the transients by fitting to a single-exponential decay. The ring-down signal is represented by the following function:

$$I(t) = I(0) \exp\left[-\left[(1 - R) + (\alpha_{\mathrm{anal}} + \alpha_{\mathrm{solv}})L\right]\frac{ct}{nL}\right] \tag{2.1}$$

where $\alpha_{\mathrm{anal}}$ denotes absorption by the analyte and $\alpha_{\mathrm{solv}}$ absorption and scattering by the solvent; both in $\mathrm{cm}^{-1}$. $R$ is the reflectivity, $c$ is the speed of light, $t$ is the time, $L$ is the path-length in the cavity and $n$ is the refractive index of the medium. Fitting yields values for $\tau$, the decay time with the analyte sample present, and for $\tau_0$, the decay time of the background, which includes effects of the limited mirror reflectivity and all absorption and scattering effects of the solvent. The absorbance due to the analyte then follows from:

$$\alpha_{\mathrm{anal}} = 2.303\,\varepsilon C = (n/c)\left[\frac{1}{\tau} - \frac{1}{\tau_0}\right] \tag{2.2}$$

where $\varepsilon$ is the molar extinction coefficient in $\mathrm{M}^{-1}\mathrm{cm}^{-1}$ and $C$ the concentration in M. We note that a $1/e$ decay time of 25 ns, as typically observed, corresponds to an effective absorption path length of 5.5 m. This explains the gain in sensitivity by the CRD-method; in a $1/e$ time interval the light pulses traverse the cavity 2750 times.

The fitting procedure is performed on-line (at 10 Hz) without loss of events, such that absorption in the flow cell can be monitored constantly. This allows for an on-line registration of time traces, during times when an injected plug is passing the CRD flow cell. Typical results of the absorption (proportional to $1/\tau$) in such time traces are presented in Fig. 2.3 comparing injected plugs of a blank, a 3 nM, and a 100 nM CV-ethanol sample.
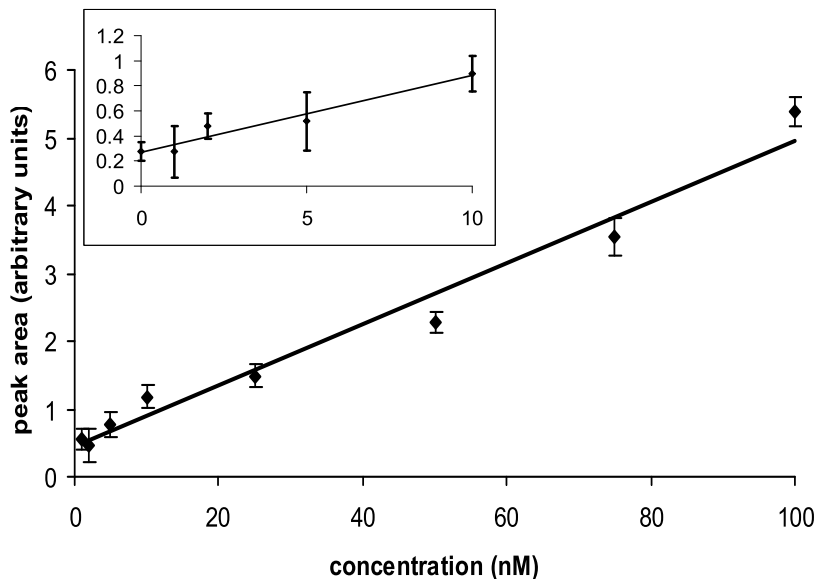
Figure 2.4: Calibration curve for CRD-detection of Crystal Violet in ethanol. In each case a 100 $\mu$L plug is injected at a flow rate of 1 mL/min, the area under the peaks in the $1/\tau$ traces is plotted versus concentration. Each data point represents an average over three measurements, with the error bar showing the standard deviation. The inset shows the measurements of the low CV concentrations in detail. For this measurement series, each data point is the average of at least six measurements, the error bar again shows the standard deviation.

The Figure shows that at higher concentrations only minor band broadening and limited tailing is observed, even less than usually dealt with in conventional-size LC.

A calibration curve was measured over a concentration range of 1 to 100 nM CV in ethanol. The integrated signal on the $1/\tau$ traces is plotted as a function of concentration in Fig. 2.4. The $R^2$ value for this calibration curve was 0.973 (for 8 points, each measured in three-fold), which indicates a satisfactory linear dynamic range over at least two orders of magnitude. For a 100 nM solution of CV, the absorbance over a distance of 5.5 m (corresponding to 1 $\tau$) is 0.3. Since deviations from the Lambert-Beer law are normally not seen for an absorbance lower than 1, no saturation effects are expected to take place.

The detection limit for a signal-to-noise ratio of 2 (2 times the standard deviation of the blank, $n = 5$) is determined at 2.5 nM for CV-ethanol solutions with $\varepsilon = 54500$ M$^{-1}$cm$^{-1}$ at 532 nm. It should be noted that this LOD is primarily a result of the rather large blank signals obtained; injection plugs of pure ethanol produce time traces deviating from background as shown in Fig. 2.3. This relatively high blank signal can not be attributed to carry-over of crystal violet remains, since the replacement of all possible contamination sources did not result in a lower blank. The LOD obtained with the set-up of Snyder and Zare [77] is comparable to ours; their LOD-value of 92 nM at $\varepsilon = 9000$ M$^{-1}$cm$^{-1}$ may be scaled to CV-ethanol solutions at 532 nm ($\varepsilon = 54500$) resulting in a LOD of 15 nM. The factor of 6 difference can be explained by their cell path length of 300 $\mu$m, which is a factor of seven shorter. The set-up of Ref. [77] (with a flow cell of 10 $\mu$L of which 0.5 $\mu$L illuminated) has proven to be suitable as an LC-detector. Similarly, the present

demonstration using injected plugs of dissolved analytes into a real flow cell closely mimics LC conditions.

In principle, there is no difference in terms of sensitivity between a CRD cavity of length $L = 1$ m (as in the case of Ref. [77]) with a short flow cell (of $d$ mm) inserted, or a geometry where $L = d$ (in the present case) as long as the absorption solely occurs in the analyte. Indeed similar sensitivities are found. A practical difference lies in the time of duration of the decay transients, which in the present case is as short as 100 ns for $3\tau$ analyzed transients, much shorter than in Ref. [77]. This has the advantage, not yet benefited from with the 10-Hz laser repetition rate, of scaling the experiment to a multiple MHz repetition rate, with the prospect of increasing the sensitivity via signal averaging.

The use of a miniature flow cell formed by mirror surfaces, bringing the eluent directly in contact with the di-electric coating, warrants some discussion on its behavior under operating conditions. Ring down times of 25-30 ns, obtained in air, represent mirror reflectivities of R $\approx$ 99.98%. The ring-down times are found to be slightly shorter (typically 20%) for the mirrors in contact with liquid ethanol for the same cavity geometry. Considering the refractive index ($n = 1.36$) for ethanol, however, a larger decay time is expected (see Eq. 2.1).

Such a decrease of the ring-down times could be explained by several effects. Higher overtones of the –OH vibrations in ethanol (fundamental around $\approx 3350$ cm$^{-1}$) are expected to cause absorption in the visible range. For example, the attenuation coefficient for water at 532 nm is $0.67 \times 10^{-3}$ cm$^{-1}$, including also Rayleigh scattering [121]. A possible additional effect is caused by lowering of the mirror reflectivity when liquid is brought into contact with the surface layer of the dielectric multi-layer coating. We note that the mirrors did not degrade significantly after extended use of the CRD-mirrors in contact with ethanol.

## 2.4 Conclusion

In this study, a new approach to implementing cavity ring-down absorption measurements in the liquid phase is presented. In this approach the liquid is in direct contact with the cavity mirrors, but in comparison with Ref. [67] the cell volume has been reduced by more than three orders of magnitude, making the setup fully compatible with LC. Despite the inherently short decays (ns instead of $\mu$s range), the sensitivity of the method is satisfactory, and our measurements in a liquid flow are as sensitive as previously reported measurements [77]. A considerable advantage of the system is that there are no surfaces in the cavity itself. Scattering losses are therefore minimal, and there are no Brewster's angles to be considered. Consequently, a large range of different eluents (with different refractive indices) can be successfully used. Furthermore, the short decay time ensures that the system can be improved, using higher repetition rate lasers (up to several MHz) and subsequent averaging.

A 3 nM injection plug of Crystal Violet in a continuous flow of ethanol could clearly be distinguished. When measuring the peak area under the $1/\tau$ traces as a function of concentration, a linear relationship is observed; the linear dynamic range is at least two orders of magnitude. Considering its linear response and small size, the presented cavity geometry can be implemented in conventional-size LC. The band-broadening that is observed when measuring in a flow is negligible.

A major challenge lies in the extension of sensitive CRD detection techniques to the ultraviolet range, where most analytes have strong(er) absorptions.

# Acknowledgment

# Chapter 3

# Improving the sensitivity of HPLC absorption detection by Cavity Ring Down Spectroscopy in a liquid-only cavity

1

## abstract

A previously described liquid-only cavity flow cell is used to assess the feasibility of improving absorbance detection limits in liquid chromatography (LC) using cavity ring-down spectroscopy (CRDS). In this miniaturized cavity there is an optical path length of only 2 mm between the mirrors, which at the same time form the walls of the flow cell. Typical ring-down times are 65 - 75 ns for the eluent blank. The performance of the presented flow cell compares favorably to conventional absorbance detection: the baseline noise is determined to be $2.7 \cdot 10^{-6}$ A.U. using averaging over 1 second. The concentration detection limits are between 15 and 20 nM (injected concentrations) for compounds with a molar extinction coefficient of 1.0 - $1.4 \cdot 10^{4}$ $M^{-1}cm^{-1}$ at the laser wavelength of 532 nm. The baseline noise as well as the absolute concentration detection limit is lowered by a factor of 30 as compared to measurements with a typical conventional absorbance detector. With an extra band broadening of only 15 %, the flow cell is suitable for LC analysis.

## 3.1 Introduction

Improving the limits of absorbance detection for non-fluorescent analytes by liquid chromatography (LC) is a main challenge in analytical chemistry method development. Several laser-based techniques have been or currently are explored for this purpose (for a review, see Ref. [5]). Such techniques are attractive especially if miniaturization is aimed at since, contrary to lamp emission, a laser beam can easily be focussed to a very small spot without significant loss of power. It should be noted, however, that conventional absorbance detection is based upon the measurement of a small intensity difference on a large background signal, so that the sensitivity is determined by the accuracy with which $\frac{\Delta I}{I}$ can be measured. Rather than a high-intensity light source, a stable source is required. Other absorbance detection schemes, in which a signal is measured against a zero-background are being explored.

For example, degenerate four-wave mixing is based upon the production of a thermal grating in an absorbing sample using two laser beams. A third laser beam is refracted off this thermal grating, generating a fourth laser beam with an intensity depending on the absorbance of the sample. When applied as a chromatography detector [122, 123], turbulence caused by the flow distorts the thermal grating, which puts limitations on this technique.

In thermo-optical absorbance measurements [124, 125], absorbance of the pump beam gives rise to a temperature increase in the sample that is proportional to both the absorbance and the pump laser intensity. A second beam, which is scattered off this so-called thermal lens, is utilized to evaluate the magnitude of the absorption. A disadvantage of this technique, which has successfully been applied as a chromatography detector [126, 127], is that all possible mechanical vibrations in the set-up should be eliminated.

Recently, a start was made with the implementation of cavity ring-down spectroscopy (CRDS) as an absorbance detector for LC [77, 78]. While CRDS is a well-established technique for gas-phase studies [17, 128], its application to the liquid phase has only recently gained interest [67, 68, 79–81, 101]. In principle, CRDS offers extremely high sensitivity due to its inherent multi-pass configuration. Furthermore, while the sensitivity of conventional or the aforementioned laser-based absorption techniques is ultimately determined by the stability of the light source, CRDS is based on measuring the decay rate of light that is stored within a stable high-finesse cavity after abruptly terminating the excitation beam, thus higher sensitivities can be obtained. After switching off the excitation beam, the light intensity as measured behind the cavity will decay over time $t$ according to:

$$I(t) = I(0) \exp\left[ -\left[(1-R) + (\alpha + S)L\right] \frac{ct}{nL} \right] \tag{3.1}$$

where $\alpha$ denotes the absorption by the analyte, $S$ is the absorption and scatter losses introduced by the solvent (both in cm$^{-1}$), $R$ is the reflectivity of the mirrors, $c$ is the speed of light, $L$ is the path length in the cavity and $n$ is the refractive index of the medium. Of course a more complex equation applies if the absorbing medium does not completely fill the cavity length, as in the design by Ref. [77, 78]. Fitting the resulting decay traces to the function $I(t) = I(0)e^{-t/\tau}$ yields values for the ring-down time $\tau$ when an absorber is present in the cavity, or $\tau_0$ for an empty cavity (i.e. blank solvent only). Losses due to the mirrors and absorption and scattering by the solvent are comprised in the latter value.

Exploratory studies indicate that CRDS is promising for detection in LC [77, 78]. In these studies a liquid flow cell that was carefully designed to approach the correct Brewster's angle at each of the four interfaces, was placed inside a cavity. Although the

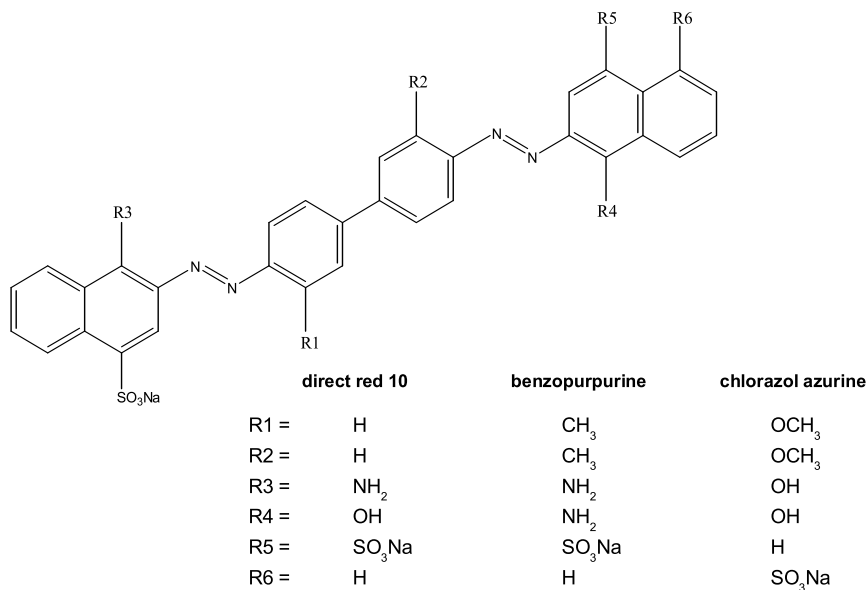| | direct red 10 | benzopurpurine | chlorazol azurine |
|---|---|---|---|
| R1 = | H | $CH_3$ | $OCH_3$ |
| R2 = | H | $CH_3$ | $OCH_3$ |
| R3 = | $NH_2$ | $NH_2$ | OH |
| R4 = | OH | $NH_2$ | OH |
| R5 = | $SO_3Na$ | $SO_3Na$ | H |
| R6 = | H | H | $SO_3Na$ |

Figure 3.1: Structures of the dyes in the test mixture: direct red 10 (FW = 697.66 g/mol), benzopurpurine (FW = 724.73 g/mol) and chlorazol azurine (FW = 758.70 g/mol).

effective path length of the cell was only 0.3 mm, the setup employed a 1-m cavity. This large mirror separation ensured that the decay transients were significantly longer than the laser pulses and the response time of the detection system.

As an alternative, one could develop a set-up in which there is only liquid between the mirrors. This has been explored by Hallock et al. for a cell of large dimensions [67]. In our previous study [75], the feasibility of applying this approach to a $\mu$l-sized flow cell was tested using flow injection measurements. This approach has some fundamental advantages: there are no losses due to scattering of additional surfaces in the cavity. Furthermore, since no Brewster's angles have to be considered, a large range of different eluents as well as gradient elution should be compatible with this configuration. Since $\tau$ is very short due to the small mirror separation, a repetition rate of several MHz followed by signal averaging could in principle be compatible with the proposed set-up. The disadvantage of the short decay time is that accurate determination of $\tau$ is more difficult. Short laser pulses and a fast read-out system are required, and the instrumental response time should be kept as short as possible in comparison to the decay.

This chapter shows that the second approach can also be successfully implemented as an LC detector. With our liquid-only cavity which has an optical path length of 2 mm and a volume of 12 $\mu$l, we report detection limits that are significantly lower than those achieved with a conventional absorbance detector provided with a U-shaped flow cell.

## 3.2 Experimental section

The performance of CRDS as a detector for LC separations was tested with a mixture of azo dyes (direct red 10, benzopurpurine, and chlorazol azurine, all obtained from Sigma-Aldrich) of which the structures are shown in Fig. 3.1 and the absorption spectra in
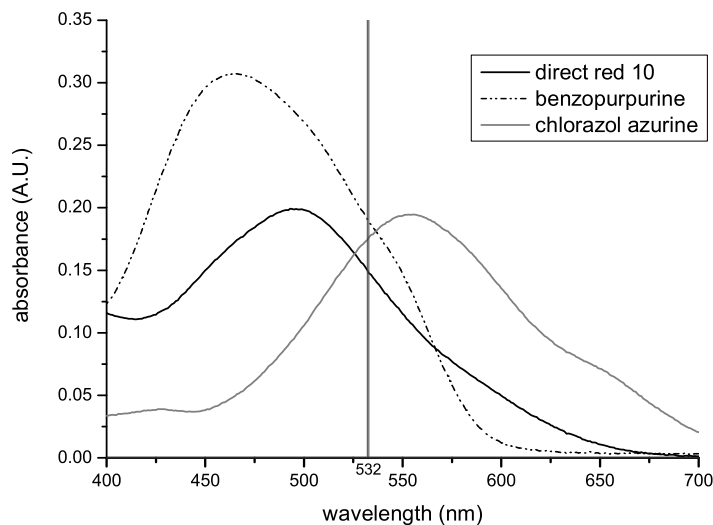
Figure 3.2: Absorption spectra of the separate dyes. The concentration of the dyes is 10 ppm in 100 mM aqueous potassium phosphate buffer, pH 7.4.

Fig. 3.2. All three have an extinction coefficient in the range of 1.0 - $1.4 \cdot 10^4$ $M^{-1} cm^{-1}$ at the laser wavelength of 532 nm, no fluorescence was observed for these compounds. The LC separation was carried out isocratically, the eluent was 50% (v/v) 10 mM potassium phosphate buffer (pH=7.4) in HPLC-grade methanol. The flow rate was set to 0.8 ml/min with an Applied Biosystems 400 solvent delivery system; 50 $\mu$l of sample was injected using a six-port injection valve. The column was a Chromsep Microspher (Varian) $C_{18}$ 100 x 4.6 mm (length x internal diameter) reversed phase column equipped with a guard column. For comparison, the same separation has been performed using a conventional UV-visible absorbance detector (Separations, Applied Biosystems 759a, 8 $\mu$l U-shaped flow cell with 8-mm optical path-length) that was set to 532 nm. This wavelength, quite appropriate for detection of the dyes concerned (see Fig. 3.2), was also used in the CRDS measurements.

The CRDS set-up was similar to the one described in our previous study focusing on flow-injection [75] and is schematically depicted in Fig. 3.3. Mirrors (R $\geq$ 99.996 % at 532 nm, 50 mm radius of curvature) were obtained from REO Inc. (Boulder, CO). In order to create the 12 $\mu$l flow cell, a 2 mm thick silicon rubber spacer with a near-elliptical hole was pressed leak-tight between the two mirrors. Flow was introduced via capillary tubing inserted in the spacer. The mirrors were in direct contact with the liquid flow. Although no noticeable degradation of the mirror quality during a day's work was observed, the mirrors needed cleaning with methanol at the end of each day and were stored in a desiccator overnight.

A Quanta-Ray Nd:YAG laser (Spectra-Physics) with the possibility of injection seeding, a repetition rate of 10 Hz and a pulse duration of 5 ns was operated at 532 nm. The transients were registered by a fast oscilloscope (Tektronix 5104 1-GHz) at a maximum sampling rate of 5 Gs/s, so that 2000 data points were available on a 400-ns time trace (typically corresponding to $5\tau$). Detection of the optical transient behind the cavity was done with a 4-GHz bandwidth photodiode (PHD400, Becker & Hickl) together with a 35-dB 1.8-GHz amplifier (Becker & Hickl). An auxiliary photodiode was employed to trigger
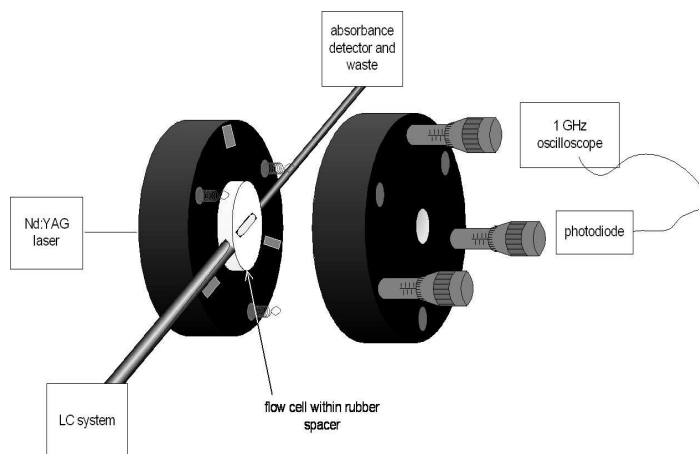
Figure 3.3: Schematic diagram of the flow cell (not to scale) and the set-up. The outer boundaries of the cavity ring-down flow cell are formed by the concave mirrors, pressed leak-tight to the sides of a silicon rubber spacer. Flow is introduced via capillary tubing inserted in the spacer. Note that the left and right part are mounted together during CRDS operation.

the detection system. Laser light of 1064 nm was rejected using a 532 nm band-pass filter.

The response function of the detection system was determined to be about 6 ns FWHM, therefore fitting of the decays was started 10 ns after triggering. Measurements were started 20 ns or 100 data points before triggering, and the offset was determined from the measured baseline. After subtracting the baseline, decay times (typically between 65 and 75 ns in eluent flow) were fitted on-line using a Levenberg-Marquardt non-linear least-squares fitting routine to yield a chromatogram expressed in $\tau$.

## 3.3 Results and discussion

### 3.3.1 Optimization of excitation source

The choice of a laser system differing from the one employed previously (a mode-locked and Q-switched Nd:YAG laser with pulses of 100 ps duration at 10 Hz [75]) warrants some further remarks. Since the presently used mirrors are of higher quality, the transients are longer and other, more convenient, laser sources with long pulse duration may also be utilized. Ring-down times in excess of 50 ns allow for response times of 5 ns without loss of sensitivity.

Firstly, a Coherent Infinity single-mode Nd:YAG laser, producing pulses of 2.4 ns duration and a variable repetition rate between 10 and 100 Hz, was implemented. This system delivered narrow-bandwidth laser pulses near the Fourier transform limit of 0.014 cm$^{-1}$. Secondly, a Spectra-Physics Quanta-Ray Nd:YAG laser was employed, equipped with an injection-seeder ensuring single-mode operation (generating a band-width of less than 0.01 cm$^{-1}$); in the non-seeding mode of operation a larger bandwidth of $\sim 1$ cm$^{-1}$ was obtained. In both cases the pulse duration was 5 ns.

The long coherence lengths, associated with the narrow bandwidths, caused strong interference effects in the high-finesse cavity, resulting in large pulse-to-pulse transmission variations (over orders of magnitude) combined with periodically changing ring-down times

(between 40 and 100 ns). These phenomena are related to coincidental matching of the laser mode to the cavity length $L$ at the instant of the laser pulse, where $L$ sensitively depends on vibrations and temperature drift of the setup. Under such conditions the common description of CRD, in terms of non-interfering multi-passing optical trajectories in a resonator exhibiting a "white", *i.e.* frequency-independent response [25], breaks down. The approach of a white cavity is applicable at short coherence lengths and under excitation of a non-confocal cavity, where many transversal modes tend to fill in the transmission spectrum, as was experimentally demonstrated by [24]. One of the features of non-interference white-cavity operation of a CRDS setup is that the transmission of the resonator equals $1 - R$, so that only a minute fraction of the incident light intensity reaches the detector.

The observed features can also be understood from a frequency-domain perspective. The free-spectral-range ($FSR = c/2L$) of our cavity of length $L = 2$ mm is 75 GHz, corresponding to 2.5 cm$^{-1}$. This mode-spacing is large with respect to the aforementioned laser bandwidths; hence, the single-mode laser frequency may or may not be in resonance with the cavity. However, when the injection-seeding in the latter Nd:YAG laser is blocked, the bandwidth is increased to $\sim 1$ cm$^{-1}$ and over a 1000 laser modes are supported.

At mirror reflectivities $R$ of 99.996 % the finesse $F$ of the cavity, equalling $F = \pi\sqrt{R}/(1 - R) = FSR/\delta\nu$ is very high ($F \approx 80000$) giving a modewidth of $\delta\nu = 3.2 \cdot 10^{-5}$ cm$^{-1}$. However, with a radius-of-curvature of 5 cm and $L = 2$ mm the cavity is sufficiently far from confocal, so that many transversal modes will be excited. Under conditions of the 1000 laser modes of the unseeded Nd:YAG laser exciting the high number of transversal modes of the miniature non-confocal resonator the condition of a white resonator, described by Naus *et al.* [25], was approached. Hence the unseeded Nd:YAG laser produced the stable CRDS detection conditions, that were employed in the present study. Miniature CRDS-setups, like the present one, are not easily operated with single-mode Nd:YAG lasers.

### 3.3.2 LC-CRDS

In order to establish the performance of CRDS as an absorbance detector, LC was performed of a test mixture containing the three dyes shown in Fig. 3.1. For further processing, the CRDS chromatograms expressed in $\tau$ were converted to $1/\tau$ and a 10 points moving average was applied. This averaging over 1 second corresponds to the time constant of an RC-circuit that is applied for electronic filtering in the conventional absorbance detector used in the comparison. A baseline ($1/\tau_0$) was fitted through the data and subtracted. The concentration of absorbing species in the cavity follows from:

$$\varepsilon C = \frac{n}{2.303c}\left[\frac{1}{\tau} - \frac{1}{\tau_0}\right] \tag{3.2}$$

wherein $\varepsilon$ is the molar extinction coefficient at 532 nm and $C$ the concentration of the absorbing species in the cavity. The resulting chromatograms could directly be converted to absorbance units (A.U.). To obtain the peak areas, Gaussian peaks were fitted through the peaks in the chromatograms.

A direct comparison between conventional absorbance detection and CRDS is shown in Fig. 3.4. A chromatogram was recorded using both detection systems in series. The eluent was first led into the CRDS flow cell and subsequently through the absorbance detector. Note the difference in peak heights between CRDS detection and our conventional absorbance detection in Fig. 3.4: since the path length is a factor of four lower for the CRDS flow cell, the peak height is also four times lower. The absence of photodecomposition
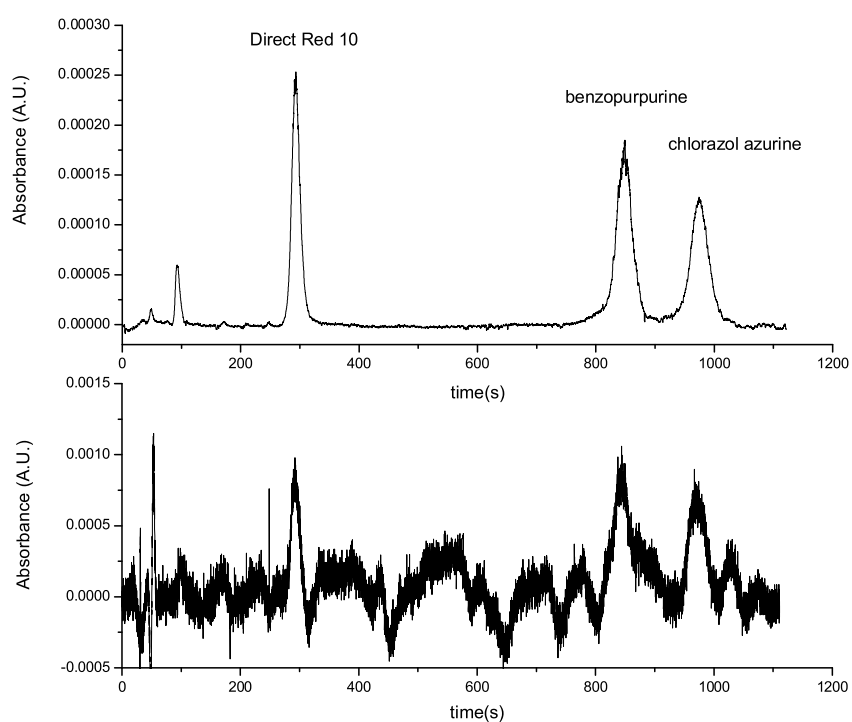
Figure 3.4: Chromatogram of a mixture containing direct red 10, benzopurpurine and chlorazol azurine as detected consecutively with CRDS (top) and a conventional absorbance detector (bottom), that were connected in series. The injected concentration of each of the dyes was 300 ppb.

of the dyes was demonstrated by reproducing the chromatographic separation with the laser turned off (not shown). Absorbance detection measurements with and without the CRDS flow cell in series using higher concentrations showed that the extra band broadening caused by the CRDS flow cell for the first eluting peak was less than 15 % so that the chromatographic resolution was almost fully conserved.

The detection limit of LC with CRDS detection was determined to be 15 - 20 nM (injected concentration) for the three azo dyes under study at 1 s averaging time. Since the absorbance detector showed a detection limit of at least 0.50 $\mu$M, the improvement of the detection limit was about a factor of 30. The peak-to-peak noise in the LC-CRDS chromatogram was only $2.7 \cdot 10^{-6}$ A.U. at 1 second averaging; much better than the conventional absorbance detector described in this study and comparable with the best instruments on the market [78, 129].

Previously, the feasibility of using the proposed liquid-only cavity as an absorbance detector was tested using flow-injection analysis [75]. With a compound having $\varepsilon = 5.45 \cdot 10^4$ M$^{-1}$cm$^{-1}$, detection limits of 2.5 nM were obtained. At low concentrations the measurements were hindered by a background signal: upon injection of a blank, a small but measurable peak was observed. Now, in on-line LC this blank peak appears at the chromatographic dead time, removed from the peaks of interest. However, this advantage is outweighed by the dilution inherent to LC separations.

Calibration curves of the dyes (see Fig. 3.5) show that LC-CRDS is linear over a concentration range of 12.5 to 300 ppb, the $R^2$ values being 0.9985 or better. The error bars also illustrate a satisfactory repeatability of the CRDS peak areas and the slopes of the calibration curves are directly proportional to molar extinctions of the analytes. As regards the upper limit, at 300 ppb the ring-down lifetime $\tau$ as measured at the maximum of a peak has decreased to 15 ns, and higher concentrations are likely to cause problems with the fitting of the transients due to the width of the instrumental response function. Since conventional absorbance detection is feasible at such concentrations, the limited dynamic range of the CRDS detection is not a serious drawback of the technique.

## 3.4  Conclusion

The liquid-only CRDS flow cell studied here has shown a good detection performance in conventional-size LC. While its contribution to the chromatographic band broadening is only minor, excellent concentration detection limits (15 - 20 nM injected) were obtained for the dyes concerned. The short ring-down times resulting from the 2-mm liquid-only cavity could still be quantified with sufficient precision for analyte concentrations up to the 300 ppb level; the peak-to-peak baseline noise corresponded to $2.7 \cdot 10^{-6}$ A.U.

These results are fully comparable with the alternative approach of references [77] and [78], in which a 0.3-mm path length flow cell inside a 1-m cavity was utilized. The main advantage of our liquid-only CRDS flow cell is that it is in principle applicable for all eluent compositions and also in gradient LC since no Brewster's angles need to be considered.

Further improvements of liquid-only CRDS will be achievable by utilizing a Z-shaped flow cell, which is currently under construction. Furthermore, the decay times dealt with in the present set-up are shorter than 100 ns. This will allow the use of MHz repetition rates, implying more efficient signal averaging. Future challenges will be to reduce the cell volume to make the system compatible with micro-LC and the use of shorter laser wavelengths to broaden the applicability range of LC-CRDS.
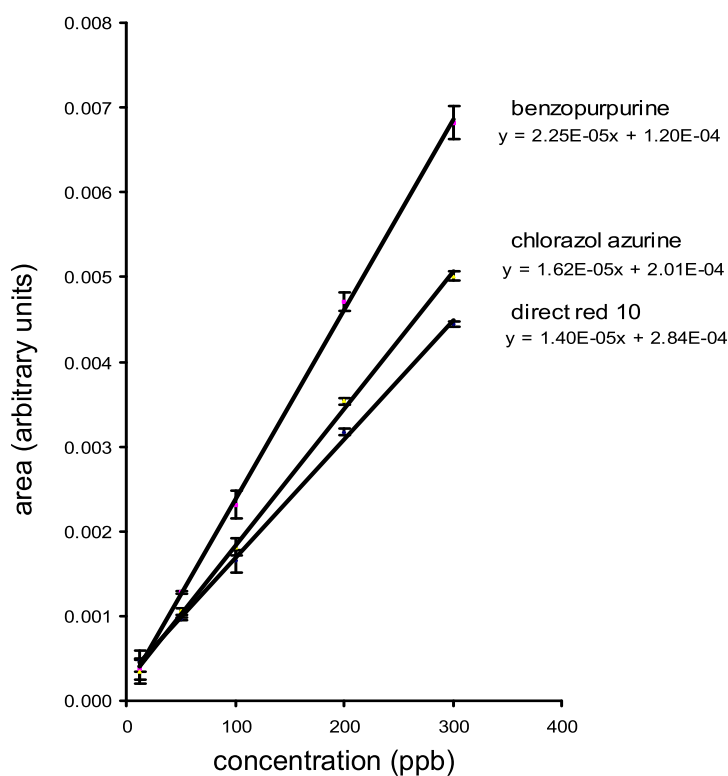
Figure 3.5: Calibration curves of Direct Red 10 ($\varepsilon_{532} = 1.0 \cdot 10^4$ M$^{-1}$cm$^{-1}$), benzopurpurine ($\varepsilon_{532}$ = 1.4$\cdot 10^4$ M$^{-1}$cm$^{-1}$) and chlorazol azurine ($\varepsilon_{532} = 1.3 \cdot 10^4$ M$^{-1}$cm$^{-1}$) as measured with CRDS detection shows a linear dynamic range up to at least 300 ppb. Each data point represents an average of three measurements, with the error bar showing the standard deviation.

# Acknowledgment

# Chapter 4

# Cavity ring-down spectroscopy for detection in liquid chromatography: extension to tunable sources and UV wavelengths

[1]

## abstract

In earlier studies, it was demonstrated that the sensitivity of absorbance detection in liquid chromatography (LC) can be improved significantly by using cavity ring-down spectroscopy (CRDS). Thus far the CRDS experiments were performed using visible laser light at fixed standard wavelengths, such as 532 nm. However, since by far most compounds of analytical interest absorb in the UV, it is of utmost importance to develop UV-CRDS. In this study, as a first step towards the deep-UV region, LC separations with CRDS detection (using a previously described liquid-only cavity flow cell) at 457 and 355 nm are reported for standard mixtures of dyes and nitro-polyaromatic hydrocarbons (nitro-PAHs), respectively. For the measurements in the blue range a home-built optical parametric oscillator (OPO) system, tunable between 425 and 478 nm was used, achieving a baseline noise is $2.7 \cdot 10^{-6}$ A.U. at 457 nm, improving upon the sensitivity of conventional absorbance detection (typically around $10^{-4}$ A.U.). An enhancement of the sensitivity can be seen at 355 nm as well, but the improvement of the baseline noise ($1.3 \cdot 10^{-5}$ A.U.) is much less pronounced. The sensitivity at 355 nm is limited by the quality of the UV-CRDS mirrors that are currently available: whereas the ring-down times as obtained at 457 nm are around $70 - 80$ ns for the eluent, they are only $20 - 25$ ns at 355 nm. Critical laser characteristics for LC-CRDS measurements, such as pulse length and mode structure, are given and prospects for going to shorter wavelengths are discussed.

---

## 4.1 Introduction

Liquid chromatography (LC) is used in many research areas including chemistry, biochemistry and environmental sciences. Quite often, the scope of these LC studies is to find traces of compounds or contaminants in complex mixtures. Hence, the development of sensitive detection methods is imperative.

Direct absorbance detection is often the detection method of choice due to its versatility and simplicity. Moreover, since absorbance detection is non-destructive, it can be used in tandem with other detection methods, e.g. mass spectrometry. However, the sensitivity of the method is ultimately determined by the precision at which the relative intensity change $\delta I/I$ can be measured. Since cavity ring-down spectroscopy (CRDS) is based on the measurement of the rate of decay of light exiting a high-finesse cavity rather than $\delta I/I$, it is no longer limited by fluctuations in $I$. Furthermore, since the light is detected after hundreds or thousands of round-trips through the cavity, the effective sample path length is dramatically increased.

In previous studies, the feasibility of using CRDS as a detector for LC separations was tested and different experimental schemes were explored [27, 75, 77, 78]. The set-up developed in our group uses the entire cavity for measurements: the optical path length of the absorbance cell was made to coincide with the length of the optical resonator [27, 75]. This design involves direct contact of the solvent fluids with the mirror coatings, but this was shown to cause no problems for typical LC separation eluents, such as 50% potassium phosphate buffers in HPLC-grade methanol. CRDS detection in pulsed CRDS schemes at 532 nm and averaging over 1 second led to an LC baseline noise level of $2.7 \times 10^{-6}$ A.U. [27].

A major drawback of the hitherto proven CRDS detection schemes is in the wavelength limitations. While the method has been demonstrated in the visible wavelength domain, most relevant molecules do not absorb in this range. Since absorbance detection in the UV is almost universal in LC, it is relevant to extend CRDS detection to shorter wavelengths. Both in case of a small liquid-only cavity and in the design with the Brewster cell inside a larger resonator, high-reflectance coatings are required to obtain detection sensitivities by CRDS that are competitive with conventional absorption detection. The present technology of manufacturing highly reflective coatings is a limiting factor at UV wavelengths, although significant progress is currently being made.

For the CRDS measurements at 457 nm, azo dyes were selected as model analytes. We then proceeded to CRDS detection at 355 nm, in order to develop a sensitive method for nitro-substituted PAHs (polycyclic aromatic hydrocarbons). Nitro-PAHs comprise a group of (non-fluorescing) environmental pollutants, that are highly carcinogenic compounds [130–132]. Whereas the mutagenic activity of their parent PAHs is indirect, nitro-substituted and oxygenated PAHs are direct acting mutagens. For example, the mutagenic activity of tobacco smoke can be correlated to the amount of subtituted PAHs. Nitro-PAHs originate from primary emission sources like exhaust gases (2-nitrofluorene or 1-nitropyrene) or unsubstituted polyaromatic hydrocarbons can be nitrated in the atmosphere (2-nitrofluoranthene or 2-nitropyrene) [133]. In the environment, these nitro-PAHs can be found in air particles and aerosols. Many studies concerning the amount of nitro-PAHs in air, particularly in urban air samples have been conducted, for example [133–135].

To determine nitro-PAHs in environmental samples, absorption detection generally is not sufficiently sensitive. Therefore a post-column derivatization to amino-PAHs is commonly used in order to use the more sensitive fluorescence detection technique [136–
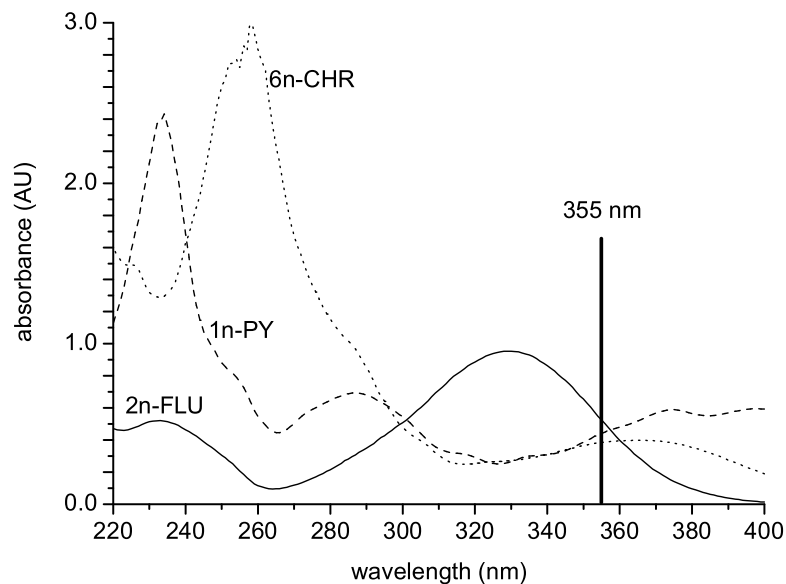
Figure 4.1: Absorbance spectra of the nitro-PAHs used in this study. Concentrations were 50 $\mu$M in eluent (80 % methanol, 20 % water).

138]. Of course, such an approach, although quite successful, complicates the detection system. That is why absorption detection modes such as CRDS might become of interest.

Here we report on extending CRDS methods for on-line LC detection progressively toward shorter wavelengths. Specifically for the blue region (420 - 480 nm) a tunable source of pulsed radiation, based on a compact optical parametric oscillator (OPO), was built and applied, demonstrating sensitive LC detection of azo dyes. In a second experiment it is demonstrated that UV-CRDS (at 355 nm) is feasible for sensitive detection of nitro-PAHs. The focus of the present work is on CRDS method development as such, where only isocratic separations are considered. Requirements as to the laser characteristics will be discussed.

## 4.2 Experimental section

### 4.2.1 Chemicals and LC separations

The LC separation of the azo dyes was carried out isocratically, the eluent was 50% (v/v) 10 mM potassium phosphate buffer (pH=7.4) in MilliQ water, 50% HPLC-grade methanol. For the separation of the nitro-PAHs, the eluent was 80% methanol, 20% MilliQ water. The azo dyes ($\varepsilon_{457} = 1.4 \cdot 10^4$ M$^{-1}$cm$^{-1}$ for Direct Violet 17 (891.8 g/mol), $\varepsilon_{457} = 1.5 \cdot 10^4$ M$^{-1}$cm$^{-1}$ for Direct Red 10 (697.7 g/mol) and $\varepsilon_{457} = 3.6 \cdot 10^4$ M$^{-1}$cm$^{-1}$ for benzopurpurine (724.7 g/mol)) and the nitro-PAHs ($\varepsilon_{355} = 10.2 \cdot 10^3$ M$^{-1}$cm$^{-1}$ for 2-nitrofluorene, (211.22 g/mol), $\varepsilon_{355} = 8.7 \cdot 10^3$ M$^{-1}$cm$^{-1}$ for 1-nitropyrene (247.26 g/mol) and $\varepsilon_{355} = 7.3 \cdot 10^3$ M$^{-1}$cm$^{-1}$ for 6-nitrochrysene (273.29 g/mol)) were all obtained from Sigma-Aldrich (Germany). Absorbance spectra of the nitro-PAHs are shown in Fig. 4.1.

For both experiments, the flow rate was set to 0.8 ml/min with an Applied Biosystems
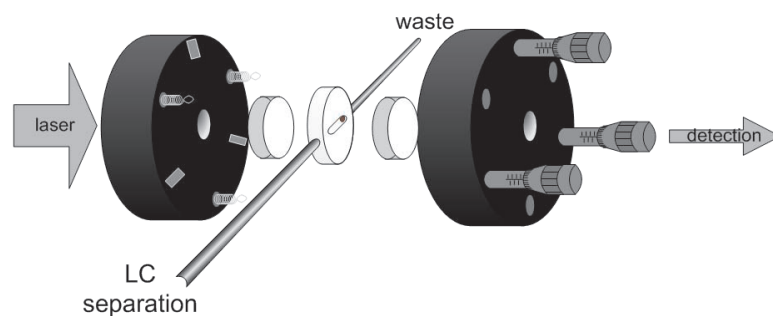
Figure 4.2: Schematic diagram of the liquid-only cavity flow cell (not to scale). The boundaries of the flow cell are formed by the high-reflectivity mirrors, clamped leak-tight to the sides of a silicon rubber spacer. Capillary tubing is inserted in the spacer for introducing the liquid flow. During operation the mirror separation is 2 mm, the detection volume is 12 $\mu$l.
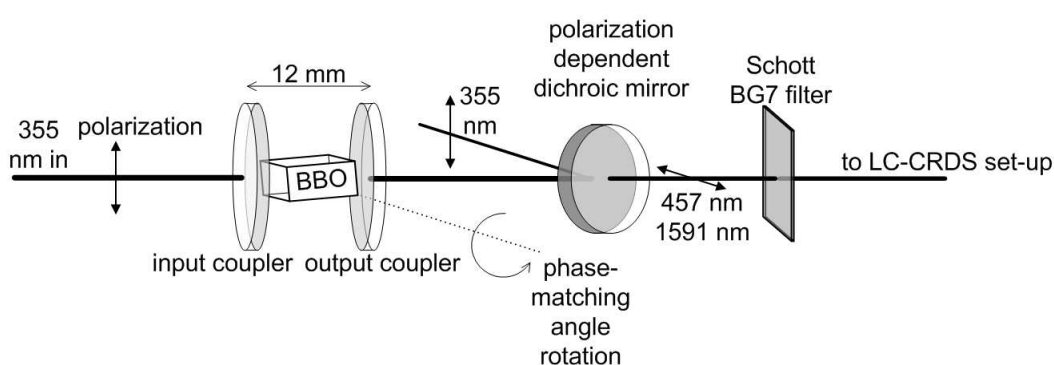


Figure 4.3: Schematic diagram of the wavelength-tunable OPO laser light source delivering laser pulses in the range 425 - 475 nm at a bandwidth of around 0.2 nm.

400 solvent delivery system; 50 $\mu$l of sample (dissolved in eluent) was injected using a six-port injection valve. The column was a Chromsep Microsphere (Varian) C$_{18}$ 100 x 4.6 mm (length x internal diameter) reversed phase column equipped with a guard column. For comparison, a similar separation was performed using a conventional UV-visible absorbance detector (Separations, Applied Biosystems 759a, 8 $\mu$l U-shaped flow cell with 8-mm optical path-length) that was set at the laser wavelength of the CRDS measurements.

### 4.2.2 Requirements for CRDS

As discussed previously [27], the bandwidth of the laser source is an important parameter for successful operation of CRDS in a miniature cavity of length $L = 2$ mm as in the present liquid-only cell design as depicted in Fig. 4.2. For such a cavity the longitudinal mode spacing is in the order of 2 cm$^{-1}$, while the mode width $\delta\nu$ is less than $10^{-4}$ cm$^{-1}$ for high-finesse resonators built from mirrors with reflectivities R $\geq$ 99.9 %. It is essential for a steady optical coupling of subsequent laser pulses into a passive resonator (that may be subject to temperature drift) that the bandwidth of the laser is sufficiently large: the choice of mirrors with radii-of-curvature (r.o.c.) strongly deviating from the chosen cavity length, such that the cavity is non-confocal and supports large numbers of transversal modes, improves the operation. Previously it was shown under conditions of $\lambda = 532$ nm and mirrors with r.o.c. $= 50$ mm that stable operation without mode-beating in the transmission of the miniature cavity could be established for laser bandwidths $\Delta\nu$ of 1 cm$^{-1}$, but for $\Delta\nu = 0.01$ cm$^{-1}$ severe mode beatings prevented stable operation. It should be noted that such a bandwidth does not put any restrictions to CRDS in the liquid phase where molecular absorption spectra show spectral bandwidths of more than 100 cm$^{-1}$. For this work, our choices for laser systems to be operated at the desired wavelengths of 355 nm and in the blue range were based on these considerations. In addition, the laser pulses should be of sufficiently short duration, i.e. much shorter than the obtainable ring-down transients, to not affect the detection sensitivity.

### 4.2.3 CRDS Measurements at 457 nm

For the measurements in the blue region a pulsed laser source was developed that matches the bandwidth and temporal characteristics required for CRDS measurements in the liquid-only cell design. A further practical requirement is to match the tunability of the source to the range of high reflectivity of the CRDS mirrors.

Such characteristics can be met by an optical parametric oscillator (OPO), based on a $\beta$-BaB$_2$O$_4$ (BBO) nonlinear crystal that is pumped at 355 nm. For most spectroscopic applications of OPOs complex pump-geometries, with injection-seeding [139] and oscillator-amplifier combinations [140], are developed to attain single-longitudinal mode operation. However, in a simplified scheme of an OPO, without any optical element besides the BBO-crystal and the two mirrors forming the resonator, pulses of typical bandwidths $\Delta\nu$ in the range of 0.25 nm (or 10 cm$^{-1}$), the desired characteristics for the liquid-only cell CRDS experiments, can be produced. The optical layout of such a home-built OPO system is shown in Fig. 4.3. In fact the system is identical to the power-amplifying OPO that was used in combination with a grazing-incidence optical parametric oscillator in Ref. [139]; here it is used as a stand-alone oscillator and, in the absence of injection-seeding, delivering optical bandwidth within the full phase-matching opening angle of the BBO-OPO. The cavity length only slightly exceeds the length of the crystal (10 mm) and is built from an incoupling plane mirror transmitting the UV of the pump source at 355 nm with a

reflectivity of 90% in the blue range, and a plane output coupler with $R = 70\%$. The BBO crystal is cut for type-I phasematching at an angle of $30^o$ and is manually rotated. The limited wavelength coverage of the OPO is due to the reflectivity properties of the mirrors spanning the cavity. The 355 nm pump light is dumped behind the OPO using a polarisation-dependent dichroic mirror, while the remaining light at 355 nm and at the OPO idler wavelength are filtered behind the OPO with a Schott BG7 filter.

This OPO is pumped by the third-harmonic output of a narrow-bandwidth Coherent Infinity 40-100 Nd:YAG laser with a pulse duration of 2.4 ns and a repetition rate that can be set between 10 and 100 Hz. The operation of the simple OPO-design, displayed in Fig. 4.3 was determined in a set of characterization measurements. With pump powers in the range 25 - 50 mJ/pulse a conversion efficiency of typically 20% is obtained across the range, where the finesse op the OPO is on the order of 20. The Coherent pump laser has the special property, due to a phase-conjugate mirror inside the amplifier system, that the beam profile is unaffected by thermal effects, when the repetition rate is varied in the range 10 - 100 Hz. The bandwidth of the OPO output steadily increases from 0.15 to 0.25 nm (or 8.5 to 11 cm$^{-1}$) over the interval 420–480 nm, while the pulse duration of the output pulses smoothly increased from 4.2 to 4.6 ns.

The CRDS set-up was similar to the one described in our previous studies [27,75]. Mirrors with R $\geq$ 99.993 % over a broad range from 450 to 480 nm, 200 mm (entrance mirror)/10 mm (exit mirror) radius of curvature were obtained from REO Inc. (Boulder, CO). In order to create the 12 $\mu l$ flow cell, a 2 mm thick silicon rubber spacer with a near-elliptical hole was pressed leak-tight between the two mirrors. Flow was introduced via capillary tubing inserted in the spacer. The mirrors were in direct contact with the liquid flow. Although no noticeable degradation of the mirror quality was observed during a day's work, the mirrors needed cleaning with methanol at the end of each day and were stored in a desiccator overnight.

Detection of the optical transient behind the cavity was done with a 4-GHz bandwidth photodiode (PHD400, Becker & Hickl) together with a 35-dB 1.8-GHz amplifier (Becker & Hickl). An auxiliary photodiode was employed to trigger the detection system. The transients were registered by a fast oscilloscope (Tektronix 5104 1-GHz) at a maximum sampling rate of 5 Gs/s, storing 2000 data points, covering a 400-ns time trace that typically corresponds to $5\tau$.

In measurements characterizing the mirrors, ring-down transients were probed to verify the mirror reflectivities in the empty-cell configuration. At wavelengths $\lambda < 450$ nm decay times of 25 ns were obtained, that gradually increased to 120 ns between 470 and 480 nm, at the optimum reflectivity of the mirror set. Despite the fact that 457 nm (chosen in order to obtain sufficient intensities on the photodiode) is somewhat displaced from the optimum, satisfactory results have been obtained at this wavelength. Typical decay transients during LC-CRDS operation at a preset wavelength of 457 nm were on the order of 75–80 ns; the pulse duration of the OPO pulses (4.5 ns) does not restrict the accurate determination of $\tau$ and therewith the sensitivity.

### 4.2.4   CRDS Measurements at 355 nm

The measurements at 355 nm were performed with the output of a Q-switched, mode-locked and frequency-tripled Nd:YAG laser (Quantel); the pulses have a duration of 100 ps, the wavelength of the system is fixed and the bandwidth at 355 nm is several cm$^{-1}$. Since relatively short ring-down times were expected, this laser was preferred over the above-mentioned pump laser because of its shorter pulse length. In combination with a
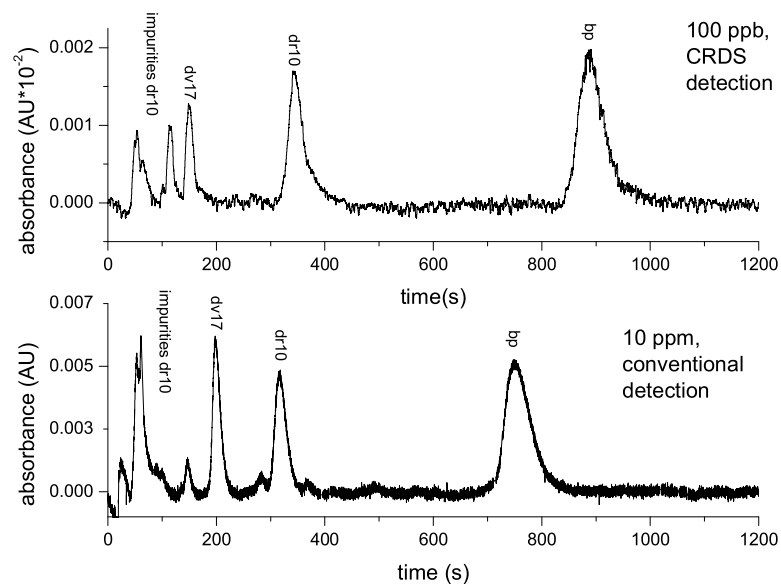
Figure 4.4: Chromatograms of a standard mixture of Direct Violet 17, Direct Red 10 and benzopurpurine as obtained for CRDS detection (upper panel) and conventional absorbance detection (lower panel) at 457 nm. Injected concentrations: 100 ppb (upper panel) and 10 ppm (lower panel). Retention time differences are due to differences between eluents used in the different runs.

sampling scope of 1 GHz analog bandwidth (Tektronix 5104; 5 GS/s) and a photomultiplier tube (Hamamatsu) a response time of 2 ns FWHM is achieved, sufficient for the analysis of typical decay transients in the 15 – 20 ns range. Again, the same liquid-only flow cell was used, now assembled from two highly reflective (at 355 nm) concave mirrors (Layertec, R $\geq$ 99.95 %, radius of curvature = 50 mm).

## 4.3   Results and discussion

Typical chromatograms for the dye mixture detected at 457 nm -where the dyes show extinction coefficients in the $10^4$ $M^{-1}cm^{-1}$ range- are shown in Fig. 4.4; the nitro-PAH mixture detected at 355 nm -a suitable wavelength, see Fig. 1- are shown in Fig. 4.5. In order to obtain these chromatograms in CRDS, the measured ring-down times are scaled to absorbance units as used in the Lambert-Beer law ($\varepsilon CL$) where $\varepsilon$ is the molar extinction coefficient in $M^{-1}cm^{-1}$, $C$ the concentration in M and $L$ the absorbance path length (2 mm in our case). The absorbance due to the analyte follows directly from the fitted $1/e$ decay times:

$$\alpha_{\mathrm{anal}} = 2.303\,\varepsilon C = (n/c)\left[\frac{1}{\tau} - \frac{1}{\tau_0}\right] \tag{4.1}$$

where $\tau_0$ is the fitted $1/e$ decay time, when only eluent is present in the cavity; this reduces to $\tau$ if an analyte passes the cavity, $n$ is the refractive index of the eluent and $c$ is the speed of light. Data were averaged over one second and a baseline ($1/\tau_0$) was subtracted.

   Chromatographic band-broadening due to imperfect flow profiles inside the liquid-only CRDS flow cell is estimated at 15%, which is generally acceptable from a practical point
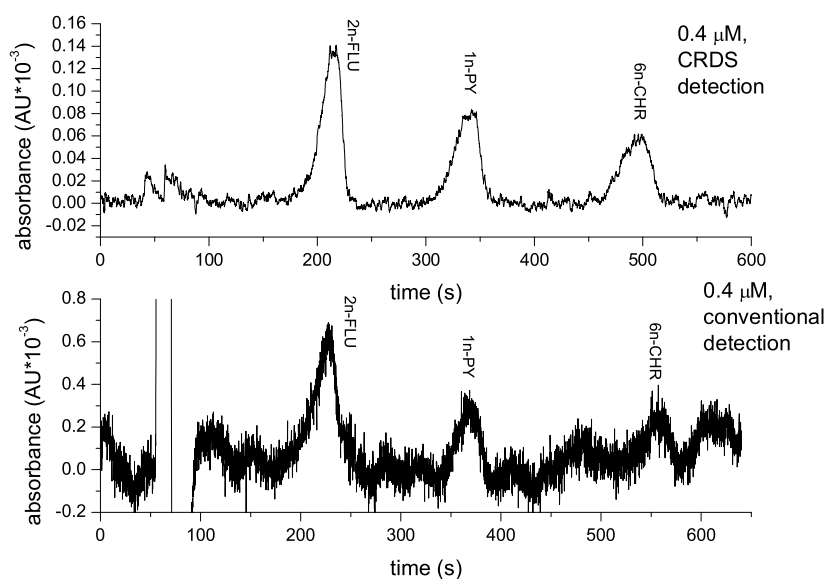
Figure 4.5: Chromatograms of a standard mixture of 2-nitrofluorene, 1-nitropyrene and 6-nitrochrysene as obtained for CRDS detection (upper panel) and conventional absorbance detection (lower panel) at 355 nm. Injected concentrations: 0.4 $\mu$M for both chromatograms.
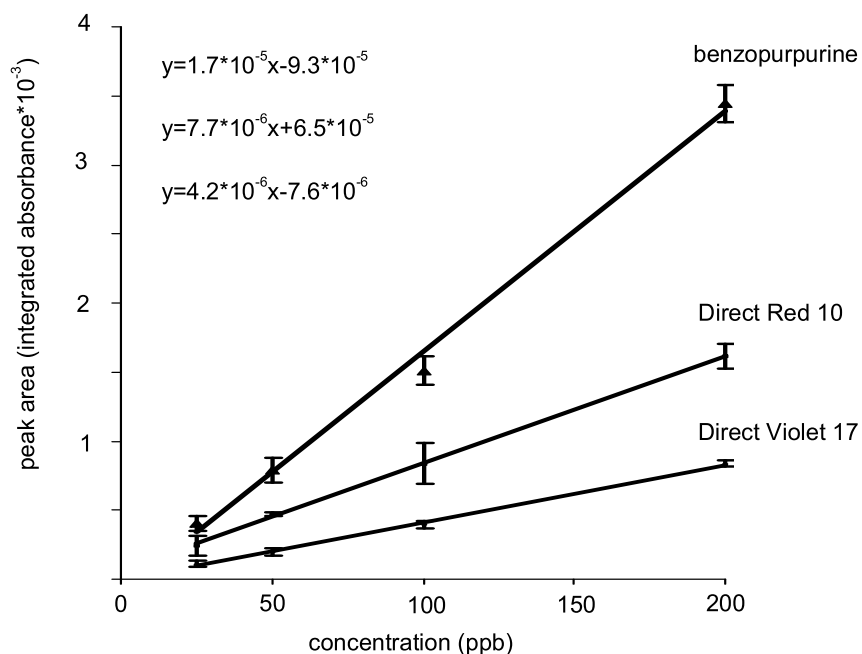


Figure 4.6: Calibration curves of Direct Violet 17, Direct Red 10, and benzopurpurine show that CRDS detection is linear up to at least 200 ppb. Each concentration was measured three times, the error bars show the standard deviation. $R^2$ values of the regression lines are 99.5% or better.
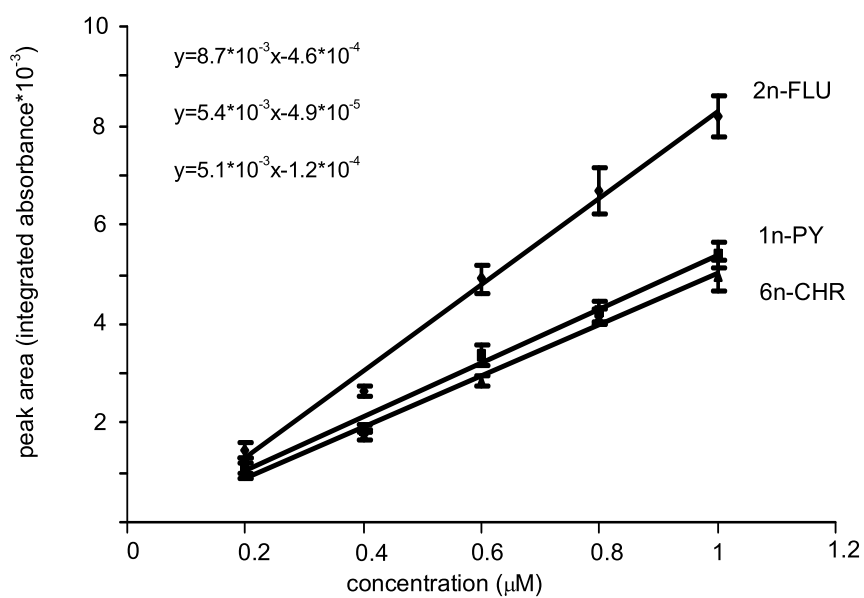
Figure 4.7: Calibration curves of 2-nitrofluorene, 1-nitropyrene and 6-nitrochrysene show that CRDS detection is linear up to at least 200 ppb. Each concentration was measured three times, the error bars show the standard deviation. $R^2$ values of the regression lines are 99.2%.

of view. Nonetheless, presumably the difference in chromatographic resolution explains why the impurities coming from Direct Red 10 are fully resolved in Fig. 4.4, lower panel, but not completely in Fig. 4.4, upper panel. Furthermore, note the different vertical scale in the two chromatograms: it accounts for the 100-fold concentration difference and the 4-fold difference in path lengths, i.e. 2 mm and 8 mm, respectively. The concentration detection limit of our LC-CRDS set-up at 457 nm ranges from 12 ppb (17 nM) for Direct Red 10 to 20 ppb (28 nM) for benzopurpurine.

Ring-down times for the baseline at 457 nm were typically between 70 and 80 ns (depending on the alignment and the cleanliness of the mirrors) which means that the light as detected after one ring-down time has traveled 15 – 18 meters (7500 – 9000 reflections) inside the cavity. The noise level of our CRDS detection at 457 nm was typically less than $2.7 \cdot 10^{-6}$ A.U., much lower than our conventional absorbance detector ($1 \cdot 10^{-4}$) and comparable to the best instruments available. The improvement in detectability is clear when one compares the S/N ratio in Fig. 4.4, upper panel, which is obtained for a hundred-fold lower concentration (100 ppb) with that in the lower panel with conventional detection (10 ppm). The used OPO-system has the advantage of increasing the repetition rate to 100 Hz, allowing for more data averaging, in comparison with the 10 Hz laser used at 355 nm.

The UV-CRDS system at 355 nm was tested using a mixture of three nitro-PAHs, the extinction coefficients are around $10^4$ M$^{-1}$cm$^{-1}$ (see Fig. 4.1). The resulting chromatograms are shown in Fig. 4.5 for CRDS detection (top) and conventional detection (bottom). With the available mirrors at 355 nm, the ring-down times for the baseline are 3- to 4-fold less favorable (i.e. 20 to 25 ns), so that only 100 to 125 data points can be sampled at 5 Gs/s to cover the relevant range of five decay transients. As a consequence the on-line fitting routine yields a less accurate value of $\tau$, and hence to a restricted detection limit compared to 457 nm CRDS.

The peaks in the chromatograms can be fitted by a Gaussian function, and as expected, the peak areas in the chromatograms show a linear dependence on the injected concentrations (see Fig. 4.6). The slopes of the regression lines are in accordance with the extinction coefficients of the azo dyes at 457 nm. The linear dynamic range of the LC-CRDS set-up extends from the detection limit (around 12 ppb) up to 200 ppb; at higher concentrations the ring-down transient becomes relatively short and the decay can no longer be fitted properly.

Similar plots were obtained for the nitro-PAHs, see Fig. 4.7. The different slopes are roughly in line with the extinction coefficients at 355 nm, although they do not exactly match, a feature that we did not investigate any further. The limits of detection are determined to be around 75 nM for 2-nitrofluorene, 100 nM for 1-nitropyrene and 150 nM for 6-nitrochrysene.

## 4.4   Conclusion

Sensitive liquid-phase CRDS detection using a liquid-only cavity flow cell is demonstrated at 457 nm and is competitive with the best instruments available. The baseline noise is only $2.7 \cdot 10^{-6}$ A.U., distinctly lower than obtained for conventional absorbance detectors where the baseline noise is typically of the order of $10^{-4}$ A.U..

The gain in sensitivity at 355 nm (baseline noise is $1.3 \cdot 10^{-5}$ A.U.) is less than in the blue range, although the difference in detection performance between CRDS and conventional UV absorbance detection as visualized in Fig. 4.5 is still quite appealing. As regards further extension of the CRDS detection techniques towards the UV region it should be

noted that the difference in sensitivity between 355 nm and 457 nm is mainly due to the limited reflectivity of the 355 nm mirrors at hand. There are no other main hindrances.

In gas-phase applications the CRDS technique was recently extended to deep-UV wavelengths. Sneep et. al. [22] performed measurements at wavelengths as short as 197 nm with mirrors of $R = 97\%$, Karaiskou et al. [74] covered the range of 200–205 nm with better quality mirrors of $R = 98.5\%$ and Wang et al. [141] used mirrors of $R = 99.85\%$ at 283.5 nm. For the application in LC-CRDS with the present liquid-only cell geometry a mirror quality of $R \geq 99.95\%$ is demonstrated to yield absorbance detection limits better than for conventional LC absorbance detectors. Suitable wavelengths would be 248 nm and 266 nm, covering the absorption maxima of many relevant molecules, and coincident with the fixed wavelengths of standard lasers (the KrF-excimer laser and the $4^{th}$ harmonic of the Nd:YAG laser), available in many laboratories.

Whereas UV CRDS measurements in the gas phase start to become successful [22,141], liquid-phase UV-CRDS is hampered by the rather stringent constraints on required mirror reflectivities, that can currently not yet be met at wavelengths in the deep UV.

## Acknowledgment

# Chapter 5

# Cavity ring-down spectroscopy for detection in liquid chromatography at UV wavelengths using standard cuvettes in a normal incidence geometry

1

## abstract

Liquid chromatography (LC) with cavity ring-down spectroscopy (CRDS) detection, using flow cuvettes (put under 0 degrees inside the ring-down cavity), is demonstrated. Fresnel reflections are maintained within the capture range of a stable cavity of 4 cm length. This method circumvents the need for specific Brewster's angles and possible mirror degradation is avoided. The flow cuvettes are commercially available at low cost. At 355 nm (the frequency-tripled output of a Nd:YAG laser), the system surpasses the performances of conventional absorbance detectors; the baseline noise was $1.3 \cdot 10^{-5}$ A.U. and detection limits (injected concentrations) were between 40 and 80 nM for nitro-PAHs with an $\varepsilon$ of 7.3 to $10.2 \cdot 10^3$ l·mol$^{-1}$cm$^{-1}$. The system was also tested at 273 nm, but in the deep UV the reflectivity (R $\geq$ 99.91 %) of the currently best available mirrors is still too low to show a significant improvement as compared to commercial absorbance detectors. **keywords:** cavity ring-down spectroscopy, liquid chromatography, detection method, flow cuvettes, nitro-polyaromatic hydrocarbons

---

## 5.1 Introduction

Liquid chromatography (LC) is used in many different research areas, often with UV absorbance detection. Especially for low concentrations or poorly absorbing analytes, the improvement of absorbance detection limits remains a relevant task.

Cavity ring-down spectroscopy (CRDS) is a laser-based absorption technique which owes its high sensitivity (i.e., low minimum detectable absorbance) to the multi-pass effect and the independence towards light source intensity fluctuations [15,25]. Since a considerable part of the light will only be detected after thousands of round-trips, the path length through the sample can be as large as meters or even kilometers. Furthermore, instead of light intensity differences, the rate of decay of the light is measured separately after each pulse. Thus, light source fluctuations play an insignificant role. In recent years, substantial progress has been made in applying CRDS to the liquid phase [67,68,79,80,100,101] and developing it as an LC absorption detector [27,75–78].

Previously, a liquid-only cavity flow cell in which the mirrors are clamped leak-tight around a 2-mm thick silicon rubber spacer has been tested extensively [27,75,76]. The spacer, with an elliptical hole of 3.9 mm long and 1.6 mm wide, acts as a 14-$\mu$l flow cell, and flow is introduced via capillary tubings inserted through the side of the spacer. Using a tunable pulsed laser source set at 457 nm and 100 Hz, a baseline peak-to-peak noise of $2.7 \cdot 10^{-6}$ A.U. was obtained. Since the path length in this system was larger than in refs [77,78] (2 mm, i.e. the full cavity length, compared to 300 $\mu$m) absolute concentration detection limits are better than reported by Bechtel *et al.* [78].

When solid surfaces (e.g. cuvettes or flow cuvettes) are placed inside a ring-down cavity, care is usually taken to minimize any possible reflection losses using the Brewster's configuration. However, when the cavity length is sufficiently short in order to preserve any reflections off intra-cavity surfaces, a zero-degree geometry can also be used [50,69,71,72]. As illustrated by Fiedler *et al.* [59], multi-mode excitation of a cavity gives rise to a certain angular distribution of the light beam, and a Brewster's angle can not accurately be defined. Actual losses can therefore be larger than the calculated Fresnel reflection losses (which should be negligible at Brewster's angle). Instead of minimizing reflection losses, it can be advantageous to capture the surface reflections on the normal of both sides of the cuvette inside a small, stable cavity. Reflection losses on the inside of the cuvette (where the liquid touches the cuvette surface) are much smaller due to the smaller difference in refractive indices.

In the present chapter it is explored whether - using an isocratic LC separation of a test mixture of nitro-polycyclic aromatic hydrocarbons (PAHs) as a model system - standard flow cuvettes can be used in LC-CRDS in a straight-forward normal incidence configuration, and whether they allow application in the ultraviolet region; for this purpose laser lines at 355 nm and 273 nm are involved. A major advantage of the normal incidence geometry is that there is no need for a carefully designed, custom-made flow cell. Since there are no Brewster's angles to be considered and the liquid is not in direct contact with the mirrors, a large range of eluents with different refractive indices, including more aggressive liquids such as acids, could be used.

## 5.2 Experimental section

The separation of the nitro-PAHs was carried out isocratically, the eluent was 80% methanol, 20% MilliQ water. Benzopurpurine and the nitro-PAHs (2-nitrofluorene, 1-nitropyrene and 6-nitrochrysene, see table 5.1) were obtained from Sigma-Aldrich (Germany). The flow

Table 5.1: Extinction coefficients at the applied laser wavelengths of the various compounds.

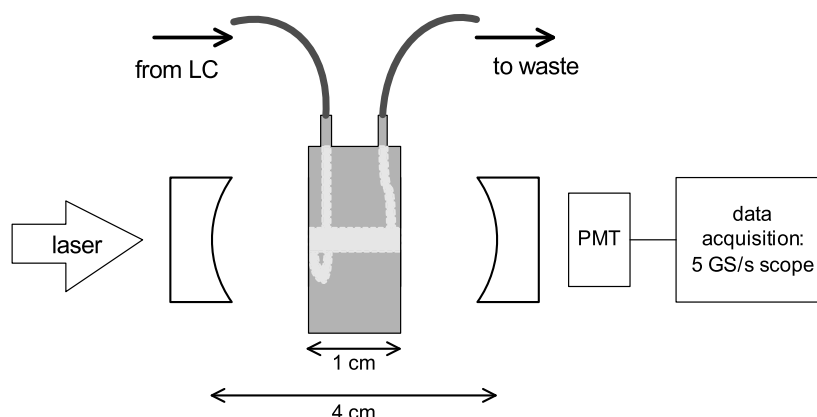| Compound | F.W. (g/mol) | $\varepsilon_{273}$(l·mol$^{-1}$cm$^{-1}$) | $\varepsilon_{355}$(l·mol$^{-1}$cm$^{-1}$) |
|---|---|---|---|
| benzopurpurine | 724.73 | $32 \cdot 10^3$ | $15 \cdot 10^3$ |
| 2-nitrofluorene | 211.22 | $2.7 \cdot 10^3$ | $10 \cdot 10^3$ |
| 1-nitropyrene | 247.26 | $11 \cdot 10^3$ | $8.7 \cdot 10^3$ |
| 6-nitrochrysene | 273.29 | $28 \cdot 10^3$ | $7.3 \cdot 10^3$ |



Figure 5.1: Schematic diagram of the set-up. CRDS measurements were performed using a cavity of 4 cm, in which the flow cuvette was placed under normal incidence. A laser beam of 1 mm diameter was coupled into the cavity without any mode-matching.

rate was set to 0.8 ml/min with an Applied Biosystems 400 solvent delivery system; 50 $\mu$l of sample (dissolved in methanol) was injected using a six-port injection valve. The column was a Chromsep Microsphere (Varian) C$_{18}$ 100 x 4.6 mm (length x internal diameter) reversed phase column equipped with a guard column. For comparison measurements, we used a Kratos spectroflow 757 UV-visible absorbance detector with an 8-mm path length and 12 $\mu$l volume (Applied Biosystems, CA), set at the laser wavelength of the CRDS measurements. Steady-state measurements were performed by adding 5-$\mu$l aliquots of 1 ppm or 5 ppm aqueous benzopurpurine solution to a standard quartz, 10 x 10 mm cuvette filled with 2 ml MilliQ water.

Quartz cuvettes and flow cuvettes, with a surface roughness of less than 0.2 $\mu$m and a parallelism of the windows better than 0.01 mm were obtained from Hellma, Germany. The cuvettes were mounted on a mirror mount permitting separate alignment in the previously aligned cavity. The flow cuvette used in the LC measurements had a volume of 80 $\mu$l, a path length of 10 mm and an aperture diameter of 3 mm. Using chromatograms measured with the UV-visible absorbance detector with and without the CRDS flow cuvette on-line, the extra band-broadening introduced by the CRDS flow cuvette was determined to be negligible (around 5 % for 1-nitropyrene).

For the CRDS measurements (see fig. 5.1), no mode-matching was performed, ensuring multi-mode excitation of our cavities (that are not temperature-controlled or locked to a specific laser mode). Transients were recorded using a photomultiplier tube (Hamamatsu) and a fast sampling oscilloscope of 1 GHz analog bandwidth (Tektronix 5104 5 GS/s).

Measurements at 355 nm were done using a Q-switched, mode-locked and frequency-tripled (355 nm) Nd:YAG laser (Quantel, France) delivering 100-ps, 1-mJ pulses at 10 Hz. A ring-down cavity of 4.0 cm length was made using two highly reflective (at 355 nm)

concave mirrors (Layertec, R specified as $\geq 99.95\%$, radius of curvature $= 500$ mm). Ring-down times for an empty cavity were 500 - 600 ns, from which it can be calculated that the actual reflectivity of these mirrors was 99.98%. The ring-down times would decrease to 60 - 70 ns when a cuvette filled with eluent blank was placed in the cavity. During elution of a 0.8 $\mu$M (injected concentration) 2-nitrofluorene plug, the ring-down time decreased down to 35 ns.

Mirrors with a radius of curvature of 500 mm, that were specified to have maximum reflectivity at 266 nm (the fourth harmonic of a Nd:YAG laser) were obtained from Research Electro-Optics Inc. (Boulder, USA). In order to determine the reflectivity and wavelength dependence of the mirror set, a reflection curve was taken using a frequency-doubled Quanta-Ray PDL-3 pulsed dye laser with coumarin 152, pumped by the 355-nm output (the third harmonic) of a Quanta-Ray Nd:YAG laser (Spectra-Physics) at a repetition rate of 10 Hz and a pulse duration of 5 ns. The energy of the pulses was 0.5 mJ. Despite the fact that the mirrors were designed for 266 nm, the optimum reflectivity (R $\geq 99.91\%$) was obtained at a longer wavelength, i.e. at 273 nm, presumably due to unexpected absorbance of the reflecting layers. Thus, all measurements were performed at 273 nm, using the Nd:YAG pumped, frequency-doubled PDL-3 laser system (instead of the quadrupled 266-nm output of the Nd:YAG laser). It should be noted that this reflectivity is far less favorable than the reflectivity at 355 nm.

The cavity at 273 nm was 3.8 cm long and typical ring-down times were 100 - 140 ns, decreasing to 12 - 18 ns when a flow cuvette with either eluent or MilliQ water was placed inside the cavity. For the standard 10 x 10 mm absorbance cuvette, the ring-down times were 20 - 25 ns. When 10 $\mu$M of 6-nitrochrysene was injected, the ring-down time decreased to 4 ns. Mainly due to the long pulses of the laser system giving an instrumental response time of 5.5 ns full width at half maximum, the precision at which the ring-down times can be measured determines the upper limit for higher absorbances.

## 5.3 Results and discussion

The intensity $I$ as measured behind the cavity decays according to:

$$I(t) = I(0) \exp\left[ -[(1-R) + (\alpha_{\text{anal}} + \alpha_{\text{solv}})l + \beta_{scatt}] \frac{ct}{n_{avg}L} \right] \tag{5.1}$$

where $\alpha_{\text{anal}}$ denotes absorption by the analyte and $\alpha_{\text{solv}}$ absorption and scattering by the solvents; both in cm$^{-1}$; $\beta_{scatt}$ is the loss due to scattering at the cuvette surfaces per pass; this does not include the reflections off the surfaces that remain in the resonator. $R$ is the reflectivity, $c$ the speed of light, $t$ the time, $L$ the length of the cavity, $l$ the path length through the sample, and $n_{avg}$ the weighted refractive index of the cavity. Fitting of the resulting curves to an exponential decay function yields ring-down times $\tau$, defined as the time over which the intensity has decreased to 1/e its original value. In order to obtain chromatograms in absorbance units ($\varepsilon \cdot C \cdot l$), we calculated:

$$\varepsilon Cl = \frac{\alpha_{\text{anal}}l}{2.303} = \frac{(L-l) + nl}{2.303c} \left[ \frac{1}{\tau} - \frac{1}{\tau_0} \right] \tag{5.2}$$

where $\varepsilon$ is the molar extinction coefficient in M$^{-1}$cm$^{-1}$ (as used in the Lambert-Beer law) and $C$ the concentration (in the flow cell) in M. $n$ is the refractive index of the liquid, $\tau$ the measured ring-down time when an analyte is passing, and $\tau_0$ is the ring-down time as measured when only eluent is present and includes background absorption and scatter losses. Data averaging over 1 second (also used in commercial absorbance detectors) is
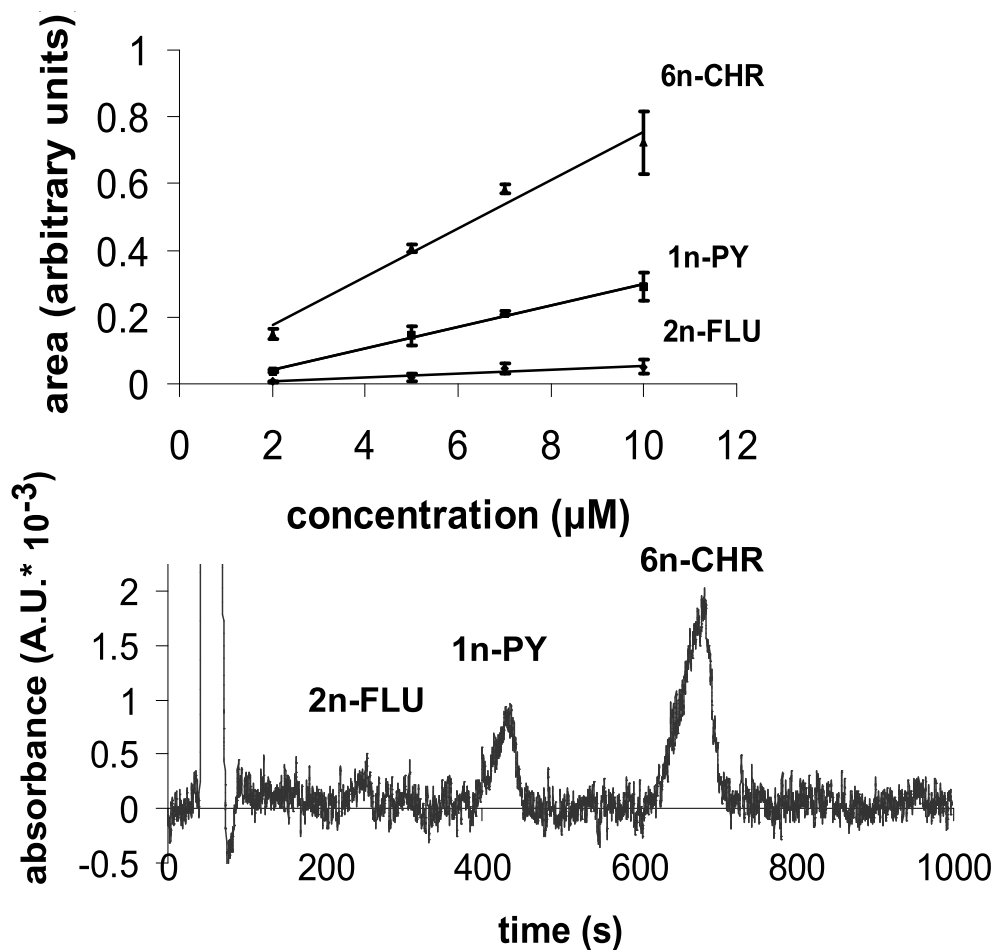
Figure 5.2: LC-CRDS chromatogram at 273 nm of a test mixture (injected concentration 1 $\mu$M of each compound) of the nitro-PAHs, together with calibration curves. Equations for the calibration curves: 2-nitrofluorene (2n-FLU) 0.0018x-0.0015, 1-nitropyrene (1n-PY) 0.0098x-0.0061, 6-nitrochrysene (6n-CHR) 0.0223x+0.0092. $R^2$ values were better than 0.98, except for 2-nitrofluorene which had an $R^2$ value of 0.91. Each concentration was measured three times, the error bars show the standard deviations.
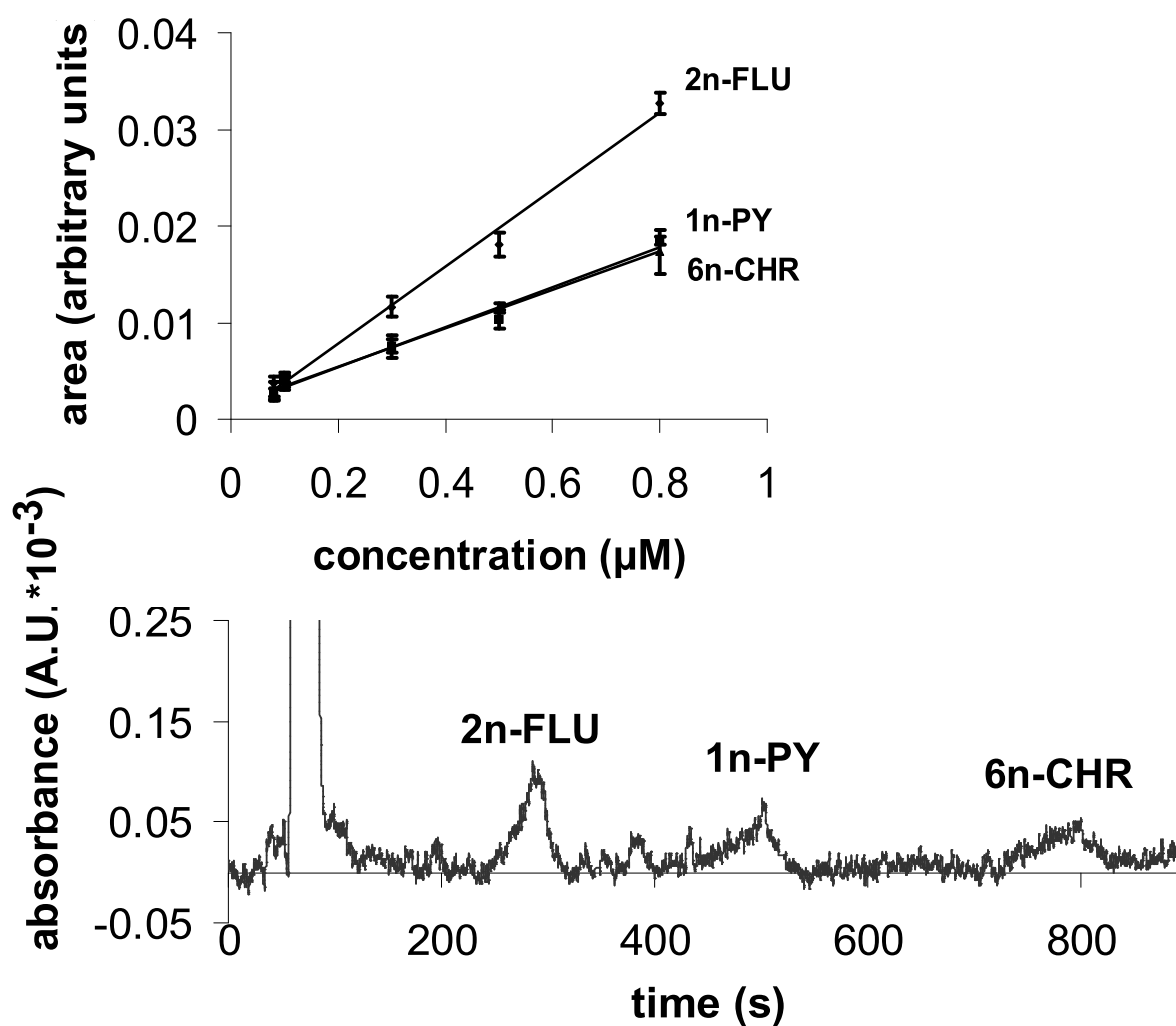
Figure 5.3: LC-CRDS chromatogram of a test mixture (injected concentration 80 nM of each compound) of the nitro-PAHs, together with the calibration curves as measured at 355 nm. Equations for the calibration curves: 2-nitrofluorene (2n-FLU) $0.0122x-5\cdot10^{-5}$, 1-nitropyrene (1n-PY) $0.0063x-0.0004$, 6-nitrochrysene (6n-CHR) $0.0061x+0.0004$. $R^2$ values were 0.98 or better. Each concentration was measured three times, the error bars show the standard deviation.

Table 5.2: Summary of the performance of the flow cuvette set-up at 273 and 355 nm in comparison with the previously used liquid-only cavity flow cell and a commercial absorbance detector, the detection limits are the injected concentrations of nitro-PAHs that result in a peak height three times the baseline peak-to-peak noise level.

| | 273 nm | 355 nm | liquid-only cavity, 355 nm [76] | UV-VIS detector |
|---|---|---|---|---|
| baseline noise (abs. units) | $4.2 \cdot 10^{-4}$ | $1.3 \cdot 10^{-5}$ | $1.3 \cdot 10^{-5}$ | $2 \cdot 10^{-4}$ |
| baseline ring-down times (ns) | 12 - 18 | 60 - 70 | 20 - 25 | N.A. |
| Conc. in flow cell (nM) | 50 - 470 | 4 - 6 | 20 - 27 | 75 - 100 |
| detection limits (nM) | 500 - 3000 | 40 - 80 | 80 - 150 | 500 - 1000 |

applied afterwards. Figs 5.2 and 5.3 show typical LC-CRDS chromatograms as obtained at 273 and 355 nm for concentrations near the detection limit of the systems.

In order to fully take chromatographic dilution effects into account, detection limits of the overall set-up were measured rather than calculated. A series of very low concentrations were injected and the corresponding peak heights were compared to the baseline noise close to that peak. A concentration which gives a peak that is three times higher than the baseline noise (r.m.s.) is considered as the concentration detection limit. One can also calculate the minimum detectable concentration (in the flow cell) directly from the standard deviation on $\tau_0$, but this will not take into account the chromatographic dilution and thus over-estimates the performance of the complete LC-CRDS system. Both types of detection limit are listed in Table 5.2.

Table 5.2 sums up some characteristics for the LC-CRDS detection of the separation of nitro-PAH test mixtures. Previously, LC-CRDS detection of the same nitro-PAH separation has been performed at 355 nm using the same laser and detection set-up and a liquid-only cavity flow cell [76]. For comparison, the results of that study are also included in the table. Note that three times the baseline noise (second row) corresponds to the concentration inside the flow cell at the detection limit (as listed in the third row). The bottom row lists the experimentally determined injected concentration detection limits. The latter are typically an order of magnitude larger because of the above-mentioned chromatographic dilution effect. At 273 nm, the sensitivity of CRDS detection in LC is very close to that of a commercial instrument (in both set-ups, detection limits were in the range of 0.5 - 3 $\mu$M for the different compounds). A significant improvement of the baseline noise and detection limits is seen at 355 nm, where the detection limits are in the range of 40 - 80 nM. In addition, at 355 nm, the present flow cuvette set-up has two-fold lower absolute detection limits compared to the liquid-only cavity geometry.

Calibration curves determined at 273 nm (between 2 and 10 $\mu$M) and at 355 nm (between 80 and 800 nM) show a good repeatability and linearity for the LC-CRDS measurements (see figs 5.2 and 5.3). Note that, at 273 nm, the calibration curve of 2-nitrofluorene is still acceptable, despite the fact that the extinction coefficients of 2-nitrofluorene and 6-nitrochrysene differ by an order of magnitude.

When considering the detection limits as obtained at 355 nm for the current flow cuvette system in comparison with those obtained for the liquid-only cavity flow cell, one would expect a factor of five improvement (since the path length through the sample is now 10 mm as compared to 2 mm). Due to the use of a different column, retention times were somewhat longer and peak widths were broader in comparison with [76], thus counteracting the advantage of the increased path-length. Overall, the gain in sensitivity with the current normal-incidence set-up is more than two-fold. Due to the low reflectivity

of the available mirrors at 273 nm, the performance of the system is severely limited by the accuracy with which the ring-down lifetime $\tau$ can be detected. Furthermore, the instrumental response function (about 5.5 ns full width at half maximum) is more than one quarter of the ring-down lifetime of 20 ns.

In order to further investigate the performance of liquid-phase CRDS at 273 nm, steady-state CRDS batch measurements (of 5-$\mu$l additions of 1 ppm or 1.38 $\mu$M benzopurpurine to 2 ml of MilliQ water) were carried out using a normal 1-cm square quartz cuvette. For 1 minute (600 shots) of averaging, the baseline peak-to-peak noise of the blank sample (pure MilliQ, giving a $\tau_0$ of 19.1 ns) was 1.1 ns; the detection limit was calculated to be at 15.8 ns (i.e. three times the noise level), this corresponded to the addition of 10 $\mu$l of benzopurpurine (making a total concentration of 7 nM benzopurpurine-solution in the cuvette). In a scanning absorbance spectrometer, of which the baseline peak-to-peak noise was about $3 \cdot 10^{-4}$ A.U., the detection limit at 273 nm was determined (in a similar way) to be about 20 nM, i.e. three times higher. We therefore concluded that CRDS in a normal incidence geometry can also be employed for batch absorbance measurements when very low concentrations need to be determined. The ring-down times and concentration detection limits were even better (due to longer averaging) than the results for LC separations taking into account the dilution effect in the column: the detection limit for 1-nitropyrene at 273 nm was 1 $\mu$M or $5 \cdot 10^{-11}$ mol injected. From the peak width, it can be calculated that this corresponds to a concentration of about 60 nM in the chromatographic peak. Corrected for the extinction coefficient differences, this would correspond to a concentration of 20 nM of benzopurpurine.

## 5.4 Conclusion

In this study, an LC-CRDS detection system employing a commercial flow cuvette in a normal incidence geometry is described for the first time. This geometry is simple to implement: instead of designing and producing a flow cuvette, the cuvettes used in this study are standard laboratory equipment. The absence of any Brewster's angle ensures that a wide variety of eluents with different refractive indices can be used. With this design, degradation of the mirrors is not an issue since they are not in contact with the solvents, thus permitting the use of more aggressive liquids such as acids and bases which would not be possible with a liquid-filled cavity.

The system was tested at 273 and at 355 nm. Whereas the reflectivity of the mirrors at 273 nm was inadequate and did not lead to an improvement of the sensitivity in absorbance detection, the sensitivity at 355 nm improved significantly (15-fold). The baseline peak-to-peak noise was only $1.3 \cdot 10^{-5}$ A.U., compared to $2 \cdot 10^{-4}$ A.U. of a commercial UV/Vis absorbance detector.

The normal incidence geometry systems has certain advantages over the liquid-only cavity flow cell as used in previous studies [27,75,76]. Despite the 80-$\mu$l detection volume, only a 5 % peak broadening was observed (for 1-nitropyrene), compared to about 15 % for the liquid-only cavity flow cell [76]. The absolute detection limits improved by a factor of 2 to 3. We are currently testing new options to improve the sensitivity of CRDS at 273 nm.

## Acknowledgment

kindly provided by Research Electro-Optics inc. (Boulder, Colorado) for test measurements.

# Chapter 6

# Evanescent-wave cavity ring-down spectroscopy for enhanced detection of surface binding under flow injection analysis conditions

1

## abstract

The feasibility of liquid-phase evanescent-wave cavity ring-down spectroscopy (EW-CRDS) for surface-binding studies under flow-injection analysis (FIA) conditions is demonstrated. The EW-CRDS set-up consists of an anti-reflection coated Dove prism inside a linear cavity (with standard or super-polishing of the total internal reflective (TIR) surface). A teflon spacer with an elliptical hole clamped on this surface acts as a 20-$\mu$l sized flow cell. The baseline noise of this system is of the order of $10^{-4}$ absorbance units; the baseline remains stable over a prolonged time and the prism surface does not become contaminated during repeated injections of the reversibly adsorbing test dyes Crystal Violet (CV) and Direct Red 10 (DR10). At typical FIA or liquid chromatography (LC) flow rates, the system has sufficient specificity to discriminate between species with different surface affinities. For CV a much stronger decrease in ring-down time is observed than calculated based on its bulk concentration and the effective depth probed by the evanescent wave, indicating binding of this positively charged dye to the negatively charged prism surface. The amount of adsorption can be influenced by adjusting the flow rate or the eluent composition. At a flow rate of 0.5 ml/min, an enrichment factor of 60 was calculated for CV; for the poorly adsorbing dye DR10 it is 5. Super-polishing of the already polished TIR surface works counter-productive. The adsorbing dye Crystal Violet has a detection limit of 3 $\mu$M for the standard polished surface; less binding occurs on the super-polished surface and the detection limit is 5 $\mu$M. Possible applications of EW-CRDS for studying surface binding or the development of bio-assays are discussed.

---

## 6.1 Introduction

Cavity ring-down spectroscopy (CRDS) is an absorbance spectroscopic technique that is based on the measurement of the decay rate of light after abrupt termination of the excitation of a high-finesse optical resonator. It has certain advantages over conventional absorbance spectroscopy: since it is a multi-pass technique, extremely low concentration detection limits are feasible. Alternatively, analytes with low extinction coefficients or in very thin layers can still be detected. Furthermore, since it is based on the measurement of the rate of decay of light rather than the measurement of $\Delta I/I_0$, sources with high intensity fluctuations such as pulsed lasers can be used. CRDS is well-established and wide-spread in the gas phase and applications of CRDS to liquid-phase studies are currently being developed [76, 78].

A special mode of CRDS that is gaining considerable interest is evanescent-wave cavity ring-down spectroscopy (EW-CRDS), a technique that combines the high sensitivity of the CRDS technique with surface-specificity. In EW-CRDS, one or more of the reflections inside the optical resonator are a total internal reflection (TIR) event. Only light of the evanescent wave associated with this TIR event is used for probing the sample. The evanescent wave decays exponentially with distance from the surface, and hence mostly species that are near, physisorbed or chemisorbed to the surface will interact with the radiation field. The penetration depth of the evanescent wave is typically on the order of one wavelength or less. This explains the current interest in evanescent-wave based techniques for detecting surface binding phenomena including bio-assays on surfaces [142–144].

Currently, three different implementations of EW-CRDS have been explored. The use of a monolithic ring cavity has already been suggested and demonstrated a decade ago [103, 104] by Pipino et al. In follow-up studies, monolithic or folded resonators were used [105–107]; this is an elegant solution to minimize intrinsic cavity losses, but the requirements on the surface quality, the morphology of the TIR surfaces and the purity of the resonator material are very stringent. The principle of fiber-loop CRDS has been explored by the group of O'Keefe, who constructed a high-finesse fiber cavity by utilizing fiber-Bragg gratings (FBGs) as reflectors [90]. Independently, this technique was developed in the groups of Loock and Lehmann by looping the fiber onto itself and using input and output couplers for the injection and detection of the pulse train [93, 100].

The use of intra-cavity elements is the most straight-forward method to create an EW-CRDS set-up [108–111, 114–117]: off-the-shelf or easy-to-produce custom-made optics can be used. Obviously, the surfaces placed inside the cavity cause reflection and refraction losses that affect the performance of EW-CRDS and the achievable detection limits. Possible intra-cavity elements include Dove prisms placed inside a linear cavity, standard right-angle prisms, and Pellin-Broca prisms. However, to ensure TIR at a silica-liquid interface, the angle of incidence on the TIR-surface should be larger than about $66^o$; hence, a linear cavity with a right-angle or Pellin-Broca prism is not appropriate for liquid-phase EW-CRDS studies on glass or quartz TIR surfaces. Usually, an anti-reflection coating is applied to minimize reflection losses at the entrance and exit surfaces.

Normal-incidence geometries have several advantages over non-normal incidence geometries. Firstly, when (relatively) small cavities are used, additional reflection losses of the surfaces can be maintained within the cavity [59]. In addition, both s- and p-polarized light can be used, permitting orientational studies using the dichroic ratio. The use of a triangular prism in a ring cavity was explored by the group of Zare, to determine the molecular orientation of a film of methylene blue at the air-silica interface [116].

The group of Shaw studied adsorption isotherms of Crystal Violet to silica as a function of pH and in the presence of other cations [110, 111] using an anti-reflection coated (R≤0.25%) Dove prism inside a cavity. Furthermore, the adsorption isotherm of hemoglobin from urine samples was determined in order to assess the feasibility of using EW-CRDS diagnosis in hemoglobinuria [108]. Adsorption of a charged and an uncharged dye at the silica/$CH_3CN$ surface has been measured by Fan et al. [109] using a similar set-up. Mazurenka et al. built an electrochemical cell on top of an anti-reflection coated, standard right-angle prism inside a ring cavity [115]. Simultaneous EW-CRDS and cyclovoltammetry measurements allowed the determination of concentration changes of chromophoric $[Fe(CN)_6]^{3-}$ upon oxidation of $[Fe(CN)_6]^{4-}$. Everest et al. used a custom-made Dove prism with entrance and exit faces at normal incidence [117]. The adsorption isotherm of hemoglobin to the silica interface as well as the average orientation of the hemoglobin transition dipole moment was measured.

Until now, liquid-phase EW-CRDS studies include steady-state measurements [108, 117] or measurements with an extremely low continuous flow (on the order of ml/hr) of sample in a 190-$\mu$l sized flow cell [110, 111]. The experimental conditions were such that adsorption equilibrium could be reached and thermodynamic properties could be measured; reversibility was not a critical factor. In contrast, our ultimate goal is the immobilization of biomolecules such as monoclonal antibodies and to detect compounds of interest showing interaction with these biomolecules using flow injection analysis (FIA) or liquid chromatography (LC). The use of biologically modified surfaces will be the subject of forthcoming studies. In this paper the test compounds Crystal Violet (CV) and Direct Red 10 (DR10) on unmodified surfaces are used to examine the performance of EW-CRDS detection under flow injection analysis (FIA) or liquid chromatography (LC) conditions. A generally encountered difficulty when using such test compounds is their irreversible adsorption to the TIR surface, necessitating rigorous cleaning (applying acids or alkaline solutions) or even etching of the surface after each measurement. An important next step in liquid-phase EW-CRDS is making such measurements compatible with FIA or LC by minimizing the flow cell dimensions, using flow rates on the order of ml/min, and having control over the adsorption process so that the TIR surface can be used over a prolonged time for repeated measurements.

In this study, flow injection measurements of the positively charged dye CV and the negatively charged dye DR10 are compared. The addition of an organic modifier to the eluent - as is quite common in reversed-phase LC - ensures a reversible chromatography-like adsorption process. The observed ring-down times are converted to absorbance units and compared with the predicted values in absence of adsorption based on the layer thickness probed by the evanescent wave; the difference indicates specific surface binding. The hydrophilic, negatively charged silica surface shows a strong preference for CV over DR10. The adsorption of CV could be dramatically increased by lowering the flow rate; for DR10 such effects are far less pronounced. It should be stressed that the scope of the present study is to explore conditions for the application of EW-CRDS in flow systems or LC, rather than the characterization of the test molecules used. Since the adsorption properties of CV had been investigated previously in several studies [110, 111], CV was chosen for testing the reversibility of adsorption to the surface.

## 6.2 Experimental section

Crystal Violet (CV, color index 42555, 98%, $\varepsilon_{532} = 5.3 \cdot 10^4$ $M^{-1}cm^{-1}$) was obtained from Aldrich Chem. (Milwaukee, USA) and Direct Red 10 (DR10, $\varepsilon_{532} = 1.0 \cdot 10^4$ $M^{-1}cm^{-1}$)
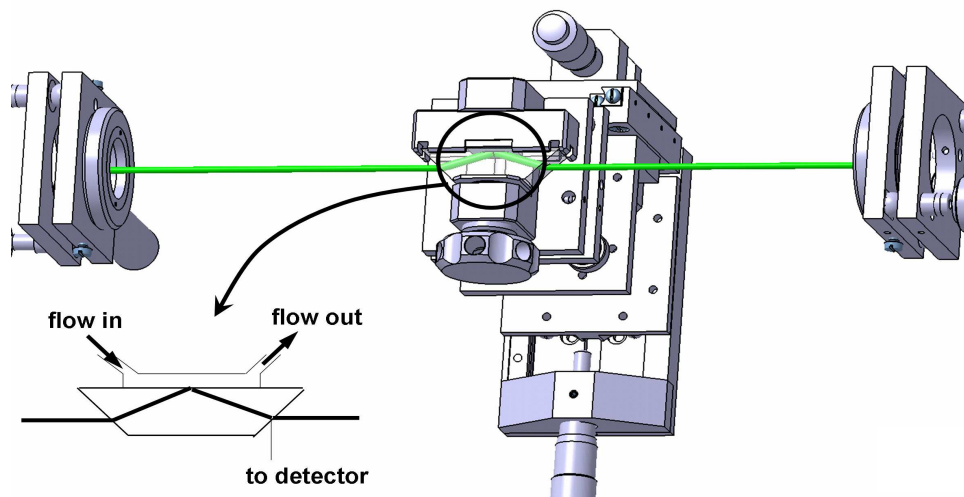
Figure 6.1: Schematic picture of the EW-CRDS set-up (not drawn to scale). An anti-reflection coated Dove prism is mounted on a mirror holder in a 70-mm long linear cavity. The effective pathlength with the prism in place, taking into account the refractive index, is 85 mm. Reflection loss at the $45^o$ exit surface is used for detection of the transient. A teflon spacer with an elliptical hole is clamped leak-tight on the TIR face of the prism, flow is delivered by PEEK tubing connected with finger-tights. The mirror holder, mounted on an x,z-stage permitting horizontal and vertical movement, enables two degrees of freedom for tilting and in-plane rotation.

was obtained from Sigma-Aldrich (Seelze, Germany). Solutions of CV, diluted from a 0.2 mM stock-solution in Milli-Q and DR10 were prepared in the eluent that was used. The eluent was 50% (v/v) 10 mM potassium phosphate buffer (pH = 4.3, 7.4 or 8.8) in HPLC-grade methanol, a flow of 0.5, 0.3 or 0.1 ml/min was delivered using an LC-pump, 100 $\mu$l of sample was injected using a six-way injection port. The eluents were degassed by sonication before use. In order to test the influence of the buffer and the ionic strength on adsorption of CV to the surface 10 mM HEPES (4-(2-Hydroxyethyl)piperazine-1-ethanesulfonic acid) buffer at pH 7.4, as well as 100 mM phosphate and HEPES buffers, were used in the eluent with 50% of methanol as well. A cell with a volume of 20 $\mu$l was constructed by clamping a 1-mm thick teflon spacer with an elliptical hole of 9.4 x 3.5 mm on top of a Dove prism (see Fig. 6.1). Two anti-reflection coated (R $\leq$ 0.25% at 532 nm, n = 1.52, $45^0$ facets) BK7 Dove prisms (Casix, Fuzhou, China) were used, one with a surface roughness rms $\leq$ 1.5 nm, $\lambda/2$ at 632.8 nm as received from the manufacturer("standard polish") and one with a custom polishing (Layertec, Germany, surface roughness rms $\leq$ 0.2 nm, $\lambda/10$ at 632.8 nm). Cleaning was performed by simply wiping the TIR surface of the prism with water or methanol.

A cavity was constructed using mirrors (R $\geq$ 99.996 % at 532 nm, 50 mm radius of curvature) from REO Inc. (Boulder, CO, USA). Alignment of the Dove prism inside the linear cavity was relatively easy: the laser was centered on the entrance and exit mirror holders, using two pinholes, and was then optimized with the mirrors in place. In absence of the Dove prism, this yielded a ring-down time of several microseconds. Next, the mirrors were replaced with the pinholes again, and the Dove prism (which was already in place on the prism mount) was inserted by vertical movement of the prism mount using

a micrometer screw. A combination of horizontal and angle movement of the prism was used to make sure that the beam path is not altered by the Dove prism. The prism mount was subsequently moved out of the beam path and the mirrors were inserted and aligned again by optimizing the ring-down transient behind the linear cavity. The Dove prism was inserted again, and the PMT was moved under an angle of 90 degrees of the cavity axis so that the scatter losses of the exit face of the Dove prism (R≤0.25% on each pass) are detected [115]. This ensures that more light (0.25% on each pass, rather than 0.004%) will reach the detector. Ring-down times for both the super-polished and standard polished TIR surfaces were between 20 and 25 ns, indicating that the surface roughness of the TIR-surface of the prisms does not contribute significantly to the total losses of the system. This short ring-down time is on the order of the maximum achievable ring-down time with the current cavity: with the anti-reflection coatings specified at R≤0.25% per surface and with two surfaces per pass, 200 passes are expected. Considering the relatively short cavity (85 mm) this corresponds to a ring-down time of 57 ns. Of course, additional reflection and scatter losses will take place resulting in a ring-down time on the order of 20 to 25 ns. The fact that about 10% of the original ring-down time of the empty cavity is maintained after insertion of an intra-cavity element is quite common (for example, [110]).

Laser pulses at a wavelength of 532 nm, 2.4 ns duration and a nominal bandwidth of $\approx 10$ cm$^{-1}$ were used to excite the cavity. As previously discussed, excitation with narrow-band radiation from injection-seeded Nd:YAG lasers would result in mode-beating on the transients [25] and therefore the 532 nm radiation at sufficiently large bandwidth was produced through the use of an optical parametric oscillator (OPO) pumped with the 3$^{rd}$ harmonic of a Coherent Infinity single-mode Nd:YAG laser (Santa Clara, CA, USA) at 355 nm [76]; this laser has the advantage that the repetition frequency can be varied between 10 and 100 Hz without modifications to the beam profile.

For the CRDS measurements no mode-matching was performed, ensuring multi-mode excitation of the cavity. The optical pathlength was $L = 85$ mm (including a correction for the Dove prism with $n = 1.52$). A scheme of the set-up is shown in Figure 6.1; the laser beam was p-polarized with respect to the 45$^o$ facets of the prism. Transients were recorded using a photomultiplier tube (Hamamatsu, Shimokanzo, Japan) and a fast sampling oscilloscope of 1 GHz analog bandwidth (Tektronix 5104 5 GS/s). An auxiliary photodiode was used to trigger the detection system. Typically, the first 15 ns of the detected trace, which contains the instrumental response function, was rejected; 65 ns (corresponding to about three ring-down times $\tau_0$) of the remaining trace was fitted. A moving average of 1 second or 100 data points was applied afterwards. Absorbance units ($\varepsilon Cl$) were derived from the ring-down times via:

$$\varepsilon Cl = \frac{\alpha_{anal}l}{2.303} = \frac{L}{2.303c}\left[\frac{1}{\tau} - \frac{1}{\tau_0}\right] \tag{6.1}$$

where $\varepsilon$ is the molar extinction coefficient in M$^{-1}$cm$^{-1}$ at 532 nm, $C$ the concentration in M and $l$ the effective path-length of the evanescent wave through the sample in cm. $L$ is the cavity length (85·10$^{-3}$ m), $c$ is the speed of light, $\alpha_{anal}$ is the absorption coefficient in cm$^{-1}$, $\tau$ and $\tau_0$ are the ring-down times in presence or absence of analyte. In the case of adsorption to the surface, the local concentration $C$ will increase, leading to a shorter ring-down time $\tau$.
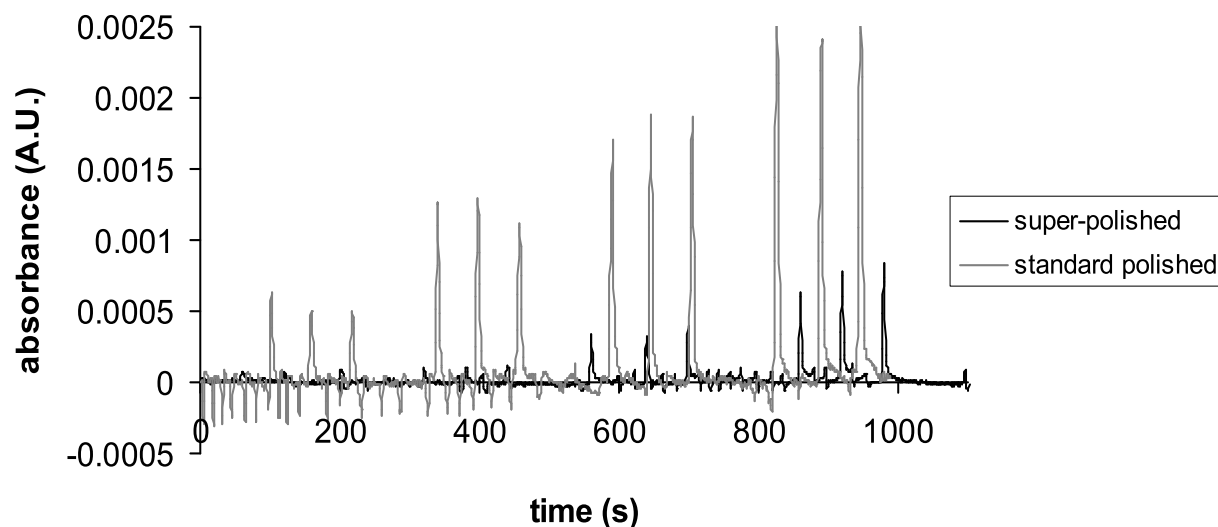
Figure 6.2: Influence of surface roughness. FIA profiles showing triplicate injections of respectively 5, 10, 15 and 20 $\mu$M of CV in 10 mM potassium phosphate buffer, pH = 7.4, on the super-polished and the standard polished TIR surface. The flow rate was 0.5 ml/min. The values on the y-axis are in absorbance units.

## 6.3    Results and discussion

In view of our future applications, the performance of EW-CRDS is examined at flow rates that are compatible with FIA and LC (0.1 - 0.5 ml/min). Under such flow rate conditions no real Langmuir adsorption isotherm was observed for CV, indicating that the adsorption equilibrium could not be reached. Nevertheless, even at pH 4.3, where by far the largest fraction of the silanol groups is not dissociated (a silica surface typically consists of 19% geminal or Q2 (pKa = 4.5) and 81% vicinal or Q3 (pKa= 8.5) silanol sites [111]), adsorption of CV can still be observed indicating that in addition to ionic interactions (induced) dipole interactions also play a role. For DR10, adsorption effects appear to be far less important. The baseline of the absorption curve remained stable over a prolonged time and after repetitive injections of adsorbing dye; the prism surface did not degrade and could be used for days without cleaning. The baseline drift is acceptable (stable baselines for 45-minute measurements have been observed) and the tailing of the CV and DR10 peaks is comparable with the tailing observed in LC studies at a flow rate of 0.5 ml/min. This demonstrates that the surface of the prisms does not become contaminated and irreversibility of adsorption does not play a major role; the surface can be used for measurements over a prolonged timescale.

Typical flow-injection profiles of low CV concentrations (5 - 20 $\mu$M) at 0.5 ml/min can be seen in Figure 6.2. Spikes on the baseline are sometimes observed due to the presence of air bubbles in the flow cell, despite the fact that all eluents were sonicated before use. At this flow rate the response of the system to CV does not change significantly with pH over the range of 4.3 to 8.8 (data not shown). The absolute absorbances observed in our flow system at 0.5 ml/min (linear flow 5.3 mm/s) are more than an order of magnitude lower than those observed by Fisk et al. [111] under semi-stationary conditions in a purely aqeous buffer. On the standard polished surface, the response of CV is much stronger than on the super-polished surface, which is also obvious from the detection limits being 3 $\mu$M for the standard polished TIR surface and 5 $\mu$M for the super-polished TIR surface. These
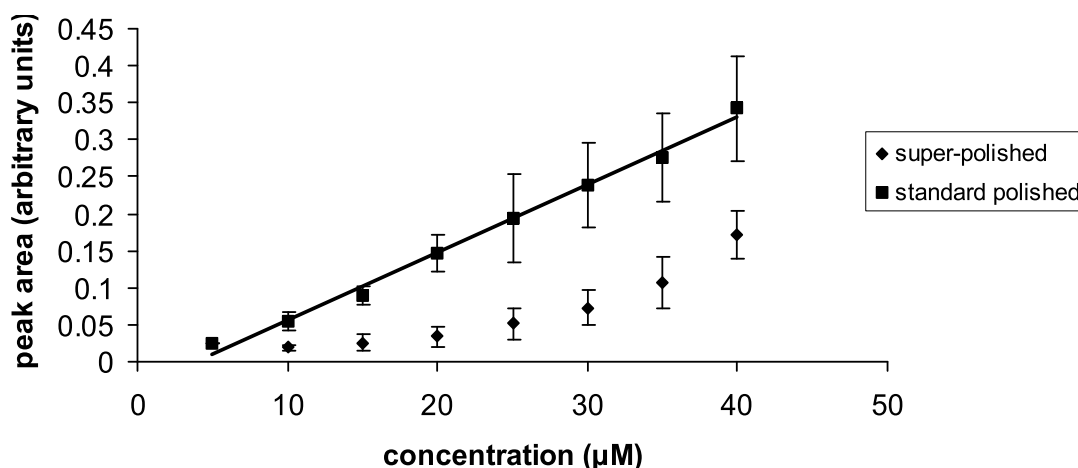
Figure 6.3: Response curves of CV at a flow rate of 0.5 ml/min and a pH of 7.4 as observed on the standard polished and the super-polished TIR surface. Each concentration was measured in three-fold; the error bars represent one standard deviation.

results indicate that for analytical purposes standard polished surfaces seem to be more appropriate. For the repeated injections the peak height variation is acceptable: typically 15 %. Memory effects are not observed.

In Figure 6.3, flow injection peak areas for CV are plotted as a function of concentration at 0.5 ml/min. Unexpectedly, the super-polished TIR surface gives a non-linear response to CV, whereas for the standard polished surface a linear regression line is obtained. Overall, at lower concentrations the performance of the standard polished TIR surface is better, while at higher concentrations the responses on the two different surfaces are more similar. Upon reducing the flow rates to 0.3 or 0.1 ml/min, a similar non-linear response to the CV concentration is observed for the standard polished surface (data not shown). We assume that the higher surface area of the standard polished surface is advantageous in the detection of low concentrations of CV. Additionally, the surface roughness of the standard polished prism might cause a turbulent flow at high flow rates, ensuring a more efficient exchange between the boundary layer and the bulk solution and thus stimulating further binding of CV. The flow regime inside the flow cell (laminar or turbulent) may be estimated from the Reynolds number [111]:

$$Re = \frac{\rho u d}{\mu} \tag{6.2}$$

where $\rho$ is the density of the fluid (the density of water, 998 kg m$^{-3}$ is assumed), $\mu$ is the dynamic fluid viscosity ($0.8909 \cdot 10^{-3}$ N s m$^{-2}$) and d is the thickness of the flow cell ($10^{-3}$m). u is the flow velocity; with the flow cell volume of 14 $\mu l$ and length of 9 mm, this is 5.3 , 3.2 , or 1.1 mm s$^{-1}$ for 0.5, 0.3 and 0.1 ml/min, respectively. Calculated Reynolds numbers are 5.9, 3.6 and 1.2 and the flow is likely to be turbulent (the critical Reynolds number is around 1, flows above this number are turbulent). Especially at low flows the flow regime will become more laminar, and as mentioned before, a nonlinear concentration dependence can be seen on the standard polished surface upon lowering the flow rate as well. It seems therefore possible that the flow is in a transition from turbulent to laminar at the utilized flow rates and is more turbulent on the standard polished surface.

Contrary to CV, the DR10 response is linear for both the super-polished and standard polished TIR surface, also at low flow rates (see further below).
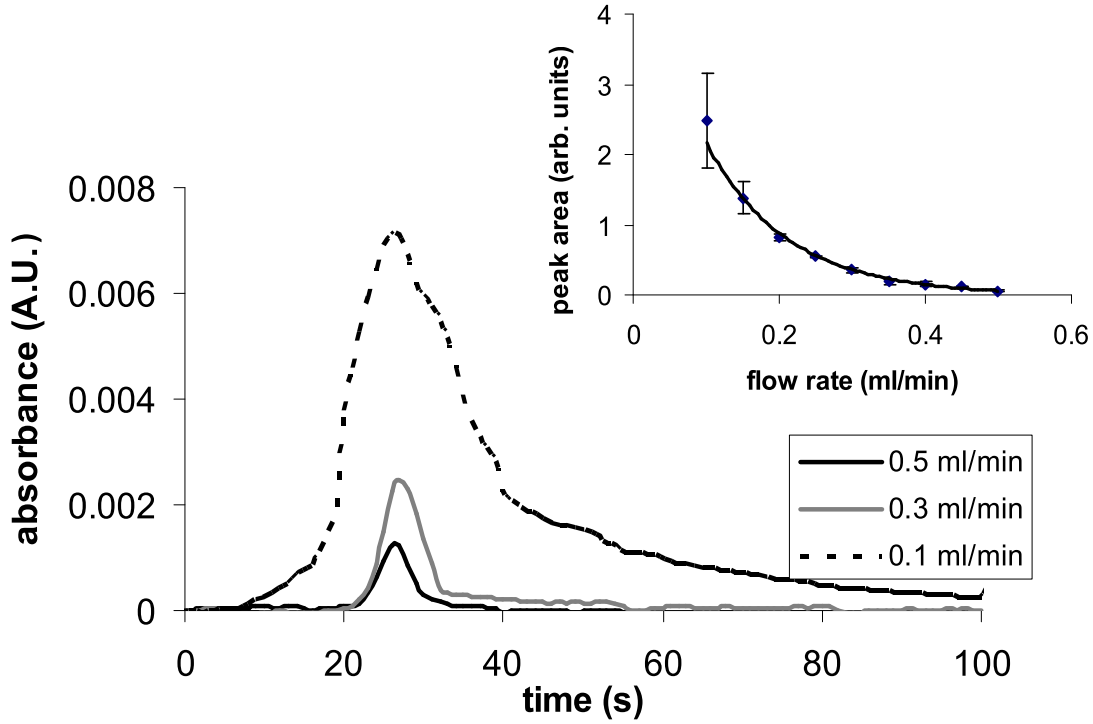
Figure 6.4: Influence of flow rate on CV adsorption. Flow profiles showing an injection of 20 $\mu$M of CV in 10 mM potassium phosphate buffer, pH = 7.4 on the super-polished TIR surface. Flow rates are 0.1, 0.3 and 0.5 ml/min, sample injection volume 100 $\mu$l. Profiles were horizontally shifted for ease of comparison. The values on the y-axis are in absorbance units. The inset shows the peak area as a function of flow rate as measured for 20 $\mu$M of CV on the standard polished TIR surface.

At low flow rates (0.1 ml/min) the tailing increased considerably (see Figure 6.4), but within a time-span of minutes the ring-down time eventually increased to the original value again. The width of the CV peak corresponds roughly to 1/flowrate, whereas the area of the peak corresponds to $(1/\text{flowrate})^2$. At a flow rate of 0.5 ml/min and a pH of 4.3 (where most silanol groups will be neutral) the tailing was far worse than at pH 7.4 and 8.8 (data not shown), indicating that the adsorption of CV to silica is of a more irreversible nature.

For bulk absorbance, one can calculate the optical path-length from the effective depth $d_e$ for p-polarized (in the plane of the beam and the surface normal) light [145]:

$$d_e = \frac{n_{21}\lambda(2sin^2\theta - n_{21}^2)cos\theta}{n_1\pi(1 - n_{21}^2)[(1 + n_{21}^2)sin^2\theta - n_{21}^2](sin^2\theta - n_{21}^2)^{1/2}} \tag{6.3}$$

where $\theta$ is the angle of incidence ($72.8^0$ in our case), $\lambda$ is the wavelength of the light (532 nm) and $n_1$ and $n_2$ are the refractive indices of BK7 (1.52) and the liquid medium (1.33), respectively, and $n_{21} = n_2/n_1$. In the literature on infrared spectroscopy this effective pathlength is commonly used to compare absorbances in transmission mode with those obtained with an attenuated total reflection (ATR) geometry. For our setup we calculated a $d_e$ of 403 $\pm$ 10 nm. The contribution of the bulk absorbance at a CV concentration of 20 $\mu$M using this $d_e$ value is calculated as $4.2 \cdot 10^{-5}$ A.U., assuming that the extinction coefficient of adsorbed CV equals that in bulk solution. This is much lower than the measured values: at a flow rate of 0.5 ml/min, the measured absorbance for the standard polished TIR surface is about $2.5 \cdot 10^{-3}$ A.U. while it is $8 \cdot 10^{-4}$ A.U. for the super-polished TIR surface (see

Fig. 6.2). In fact, the observed absorption in EW-CRDS on the standard polished surface is about 60 times larger than expected based on the CV bulk concentration, indicating a significant enrichment at the surface. For DR10 the bulk absorbance at the detection limit of 100 $\mu$M is calculated to be $4 \cdot 10^{-5}$ A.U. assuming that the extinction coefficients of adsorbed and bulk species are the same. The measured absorbance is on the order of $2 \cdot 10^{-4}$ A.U. (data not shown), indicating that the hydrophilic dye DR10 also exhibits adsorption, but to a far lesser extent than CV.

To estimate the surface coverage in the case of CV, the relatively large footprint of the laser at the TIR surface (about 7 mm$^2$) should be considered. Assuming a probed layer thickness of roughly 400 nm, the detected volume is about 3 nl and the absolute detection limit is 9 fmol at the concentration limit of detection of 3 $\mu$M. Taking into account the enrichment factor of 60, the probed layer actually contains about 0.5 pmol of CV on the probed surface area. Estimates for the number of available silanol sites range from 0.8 to 8 per square nm. [111], which would correspond to 10 to 100 pmol on the probed surface (for the super-polished TIR surface). At this CV concentration, the actual surface coverage will therefore be on the order of $10^{-2}$ relative to the number of silanol groups.

Both CV and DR10 are hydrophilic dyes; the former is positively charged above pH 3, whereas the latter is negatively charged above pH 4. At a flow rate of 0.5 ml/min, CV has a response that is about 10 to 15 times higher than that of DR10, indicating that the EW-CRDS detection system has sufficient specificity to discriminate between species with different surface affinities. Whereas the response of the system towards DR10 at a pH of 7.4 is only increased in width upon lowering the flow rate from 0.5 to 0.3 ml/min, the peak area of 20 $\mu$M of CV is 3 times higher at 0.3 ml/min. The CV response (peak area) increases roughly quadratically with decreasing flow rates (see Figure 6.4, inset). A higher surface specificity is obtained if CV is given enough time to become adsorbed to the surface (see Figure 6.5). Whereas for CV the performance of the standard polished TIR surface is better than that of the super-polished surface, the responses of both surfaces to DR10 are comparable.

Crystal Violet adsorption isotherms to silica with EW-CRDS have been measured in the group of Shaw [110, 111]; they used a syringe pump that delivered a very low flow of 4 ml/hour to a flow cell of 190 $\mu$l. Rather than using flow injection, they used a constant flow of CV solution at varying concentrations. They used purely aqueous buffer solutions without any modifier, causing the CV molecules to bind even more strongly to the surface, thus necessitating heavy cleaning after each measurement. Using a similar set-up, their concentration detection limit was about 0.3 $\mu$M of CV for a steady-state measurement, one order of magnitude lower than in our case. This difference should be attributed to a higher degree of surface binding achieved after complete equilibration which will additionally be higher in water than in 50/50 water/methanol.

In order to study the influence of buffer ions (type and concentration), additional experiments have been carried out using 50% of 10 mM HEPES buffer at pH 7.4 in methanol. As expected, the flow-injection profiles for 20 $\mu$M of CV were similar in shape, somewhat higher absorbances were obtained than in phosphate buffer. HEPES and phosphate buffers were also tested at a higher concentration: 100 mM in methanol (50%, v/v). The results are summarized in Table 6.1. The data were handled in the same way as for Figs. 6.3 and 6.5. It can be seen from the table that an increase in ionic strength leads to a decrease in CV adsorption. Furthermore, the signals as obtained for HEPES buffer are overall higher: this can be explained in a similar way. The ionic strength of a phosphate buffer containing a 10 mM mixture of $HPO_4^{2-}$ and $H_2PO_4^-$ will be higher than that of a 10 mM mixture of $C_8H_{17}N_2SO_4H$ and $C_8H_{17}N_2SO_4^-$.
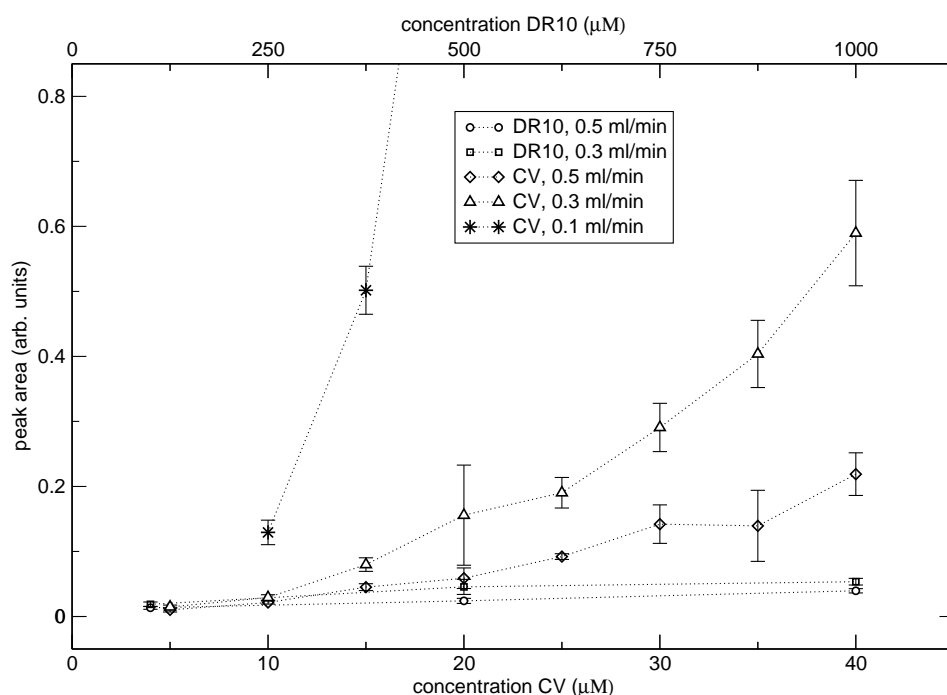
Figure 6.5: Response curves of CV and DR10 at different flow rates and pH = 7.4 as observed on the super-polished TIR surface. Each concentration was measured in triplicate; the error bars represent one standard deviation. Injected concentrations of CV were varied between 5 and 40 $\mu$M (lower scale); those of DR10 ranged from 100 – 1000 $\mu$M (upper scale), plotted in the same graph for ease of comparison. Lines between the points are guides for the eye. For a flow of 0.1 ml/min only 2 data-points are shown for CV since data points corresponding to higher concentrations are far off the shown vertical scale, for example, $40\mu$M of CV gave an area of 5.1.

## 6.4 Conclusion

In this study it has been demonstrated that EW-CRDS detection utilizing an anti-reflection coated Dove prism inside a linear cavity has distinct potential as a surface-selective detector in flow-injection and LC analysis. Only the analyte molecules present in a roughly 400-nm thick layer at the surface are detected, while the detection limits are, nevertheless, very low: 3 $\mu$M for Crystal Violet at a flow rate of 0.5 ml/min. Contamination or degradation of the surface is minimal, so that repeated measurements can be done over a prolonged time (days) without cleaning or re-aligning. At the applied flow rates the system is far from thermodynamic equilibrium. Nevertheless the discrimination between the strongly adsorbing CV and weakly adsorbing DR10 is quite efficient: already at 0.5 ml/min the response of the system towards CV is 10 times higher. This discriminating power between non-adsorbing and adsorbing molecules increases significantly upon lowering the flow rates. The EW-CRDS response for CV was 60 times higher than expected if only bulk solution absorbance would play a role in absence of any binding to the surface. For DR10 the enrichment factor as a result of binding was much smaller, i.e. 5 times.

It should be noted that the ring-down times in this study were of the order of 5 % of that of the empty cavity, mostly due to reflection losses. Therefore, substantial sensitivity improvement should be feasible. Using Brewster's angles for the entrance and exit faces of a Dove prism would lead to a decrease of only 40 % of the ring-down time [109]. However, such prisms are not easy to produce.

Table 6.1: Peak area of 20 $\mu$M of CV in eluents containing different buffers. Samples were dissolved in the same eluent as used.

| buffer | area (arb. units) | standard deviation (n=6) |
|---|---|---|
| 10 mM phosphate | 0.061 | 0.0035 |
| 100 mM phosphate | 0.025 | 0.0054 |
| 10 mM HEPES | 0.080 | 0.0071 |
| 100 mM HEPES | 0.037 | 0.0081 |

The current set-up is capable of reproducible surface-specific adsorption and desorption of the compound of interest at flow rates that are compatible with FIA and LC studies. Future applications of the EW-CRDS set-up include specific LC detection or biosensing. Since coating of silanol with for instance single stranded DNA or antibodies is well-studied and wide-spread in bioanalytical chemistry and biological techniques and coating runs are even commercially available, modification of the silica TIR face of the prism surface and surface-specific detection should be feasible.

## Acknowledgment

# Chapter 7

# Evanescent-wave cavity ring-down spectroscopy using surface-modified prisms

1

## abstract

Adsorption kinetics and molecular interactions on different surface interfaces are studied by means of evanescent-wave cavity ring-down spectroscopy, using total internal reflection surfaces onto which different self-assembled monolayers are covalently attached. The adsorption of cytochrome $c$ (a positively charged, spherical heme protein) to a negatively charged bare silica surface, to $C_{18}$-coated (hydrophobic) and to $C_3NH_2$-coated (positively charged) silica have been studied. The use of covalently attached monolayers to the silica total internal reflection surface is a first step towards the development of a biosensor that makes use of immobilized biomolecules for specific detection of analytes in solution.

---

[1] article under preparation

## 7.1 Introduction

Cavity ring-down spectroscopy is a sensitive mode of absorption spectroscopy that is based on the measurement of the rate of decay of light behind an optically stable cavity. This decay rate depends on reflection and scatter losses in the cavity; the additional presence of an absorber in the cavity will increase these losses and can thus be detected. In evanescent-wave cavity ring-down spectroscopy (EW-CRDS), one of the reflections in the cavity is a total internal reflection (TIR) event. Only the (exponentially decaying) evanescent wave associated with this TIR event is being used for absorbance measurements. Since the penetration depth of the evanescent wave is on the order of a wavelength, only molecules adsorbed at or near the surface are being probed. A strong feature of EW-CRDS, as with attenuated total reflectance (ATR) measurements, is the capability of measuring only molecules near the surface, and with a proper correction for bulk absorbance, also the molecules adsorbed in multiple layers on top of the first monolayer are detected. In contrast to other TIR techniques such as EW-fluoro-immunoassay or waveguide spectroscopy, EW-CRDS is spatially localized: a small sample volume is repeatedly probed. This permits miniaturization of the flow cell while maintaining an excellent sensitivity due to the multi-pass character of the measurement.

Techniques that are commonly used for studying adsorption kinetics of cytochrome $c$ (cyt $c$) to surfaces include electrochemistry and Raman spectroscopy. However, these techniques are not quantitative or are only capable of detecting the molecules in the first monolayer on the surface. Several studies have been described involving cyt $c$ adsorption to silica surfaces using ATR or waveguide absorption techniques [146–151]. Some of these studies involve the cyt $c$ adsorption to a surface-modified silica surface [147, 149, 150]. Unlike single-pass ATR absorbance spectroscopy, EW-CRDS is very sensitive due to its multi-pass character and therefore suitable for time-dependent studies (since the signal does not have to be integrated over a long time-span).

In a previous paper we have explored the possibility of using EW-CRDS as a detection technique in dynamic flow systems [152]. However, a crucial point as regards its potential as a detection system is the question whether modification of the TIR surface is possible without significantly affecting its total reflection qualities. This is the objective of the present study. We will show that self-assembled monolayers made in a one-step reaction from commercially available reagents provide a fast and user-friendly means of surface modification.

## 7.2 Experimental section

The set-up (see Fig. 7.1) is similar to the one used in a previous study [152]. Briefly, a cavity was constructed using mirrors (R $\geq$ 99.996 % at 532 nm, 50 mm radius of curvature) from REO Inc. (Boulder, CO, USA). Instead of the previously used 45-degrees anti-reflection coated prism, a 70-degrees Dove prism is used at normal incidence. The additional reflection losses at the intra-cavity surfaces are maintained in the cavity. The entrance and exit faces are polished to a flatness of $\lambda/10$ at 632.8 nm while the TIR face is polished to a flatness of $\lambda/2$. The rationale behind this modification is that the ring-down time of the cavity decreased from $1 - 1.5$ $\mu$s to $20 - 25$ ns upon inserting the 45-degrees prism suggesting that there is room for improvement: new designs with less reflection losses will provide increased sensitivity. Previously, we have found that superpolishing of the TIR face to a surface roughness of only 0.2 nm did not improve the ring-down time but worked counter-productive for the observed signal [152]. With the 70-degrees prism,
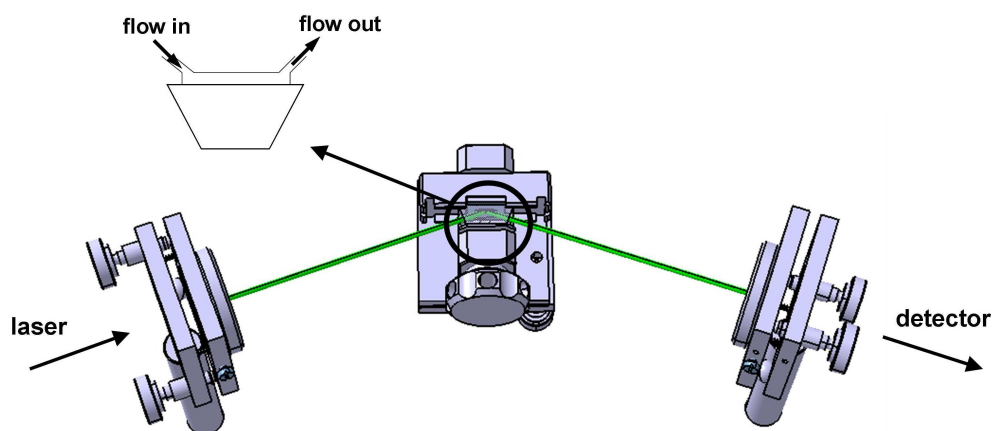
Figure 7.1: The cavity, as used for measurements, with the 70-degrees prism inserted. The prism is attached to a platform that permits tilting in two directions as well as rotation of the prism; the platform is mounted on an x,z table.
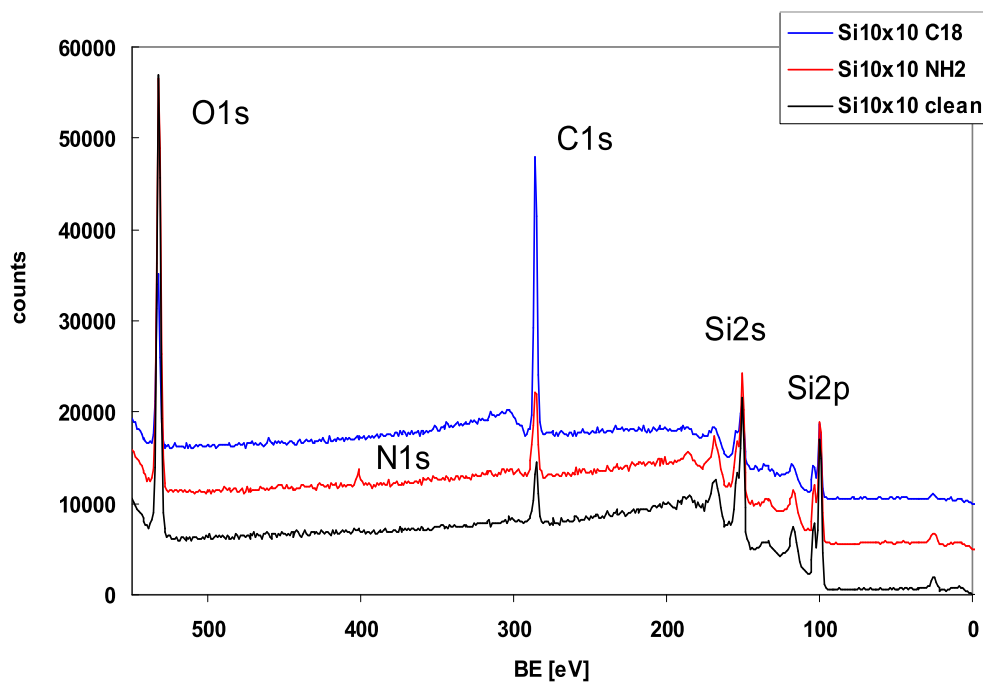


Figure 7.2: XPS survey of differently treated Si wafers. The elements oxygen (O1s), nitrogen (N1s), carbon (C1s) and silicon (Si2s, Si2p) are identified.

obtainable ring-down times were between 45 and 65 ns; they decreased to 30 – 45 ns for the highest concentrations of absorber used in this study. Laser pulses from an optical parametric oscillator (OPO), pumped with the 3$^{rd}$ harmonic of a Coherent Infinity single-mode Nd:YAG laser (Santa Clara, CA, USA), at a wavelength of 538 nm (the optimum of one of the two Q-transitions in the absorbance spectrum of cyt $c$) were used to excite the cavity at a repetition rate of 100 Hz. A moving average of 1 s or 100 data points was applied after fitting of the raw data. Transients were recorded using a photomultiplier tube (Hamamatsu, Shimokanzo, Japan) and a fast sampling oscilloscope of 1 GHz analog bandwidth (Tektronix 5104 5 GS/s).

Covalently bound monolayers were deposited on the TIR faces of the prisms by following a standard protocol for self-assembly from solution. Before the surface modifications, the prisms are thoroughly cleaned using chromic mixture ($K_2Cr_2O_7$ in $H_2SO_4$) followed by rinsing with abundant water. In order to obtain a uniform deposition of a silane monolayer, the surface was fully hydroxylated according to [153]: the prisms were immersed for 30 minutes in 1:1 (v/v) methanol:water followed by 30 minutes of immersion in 96% $H_2SO_4$. For the $C_{18}$-coating, trichloro-octadecylsilane ($\leq$90%, Sigma-Aldrich, Germany) was used as a reagent. This reagent is very reactive towards water and should be handled in an anhydrous environment (e.g. $N_2$-filled glove-box). The reaction is completed by immersion of the TIR-face of the prism for six hours in a solution of 20 $\mu$l of trichloro-octadecylsilane in 20 ml of toluene [154]. It should be emphasized that traces of water are appropriate since they accelerate the hydrolysis reaction. That is why the toluene (obtained from Riedel-de-Haen, Germany, containing 0.05% of water) was not dried prior to the reaction [155]. After the reaction, the prism was carefully cleaned and subsequently flushed with chloroform for 24 hours. For the $NH_2$-coating, after the cleaning and hydroxylation steps, the prism was immersed for 5 minutes in methanol. Subsequently, the TIR face of the prism was immersed for 15 minutes in an aqueous solution (1%, v/v) of triethoxy-aminopropylsilane ($\leq$90%, Sigma-Aldrich, Germany) in water followed by 5 minutes of ultrasonic cleaning in methanol and rinsing with abundant water [156]. Completion of the self-assembled layers was roughly estimated by monitoring the contact-angle between a drop of water and the surface. Whereas the contact-angle on a hydroxylated surface is 0 degrees, the hydrophobic surfaces will yield a contact-angle that is considerably larger. The coatings could be removed by leaving the prisms for several days in an abundance of chromic mixture.

The composition of the top surface after treatment was studied by XPS. Monochromatic Al-K$_\alpha$ X-ray radiation was used to investigate the top 10 nm. Compositional information can be obtained from the element specific binding energies. Furthermore, limited in-depth information can be extracted from the intensity ratios. For quantification XPS sensitivity factors from the Scofield library were used. In order to be able to accurately analyze composition, substrate charging was prevented by using silicon wafers instead of quartz prisms. Measurement of a treated prism and overlapping the oxygen signals to charge compensate, showed that a similarly treated Si wafer has the same top layer composition as the prism.

An XPS analysis of the clean and treated silicon wafer samples (see Fig. 7.2) shows that after treatment and transport through atmosphere, the elements oxygen (O1s), carbon (C1s) and silicon (Si2s, Si2p) are indentified on all samples. Only the $NH_2$-coated sample shows a trace of nitrogen (N1s) accounting for approximately 2% atomic concentration of the sample volume. The $C_{18}$-treated sample has the largest C1s peak, accounting for approximately 50% atomic concentration, whereas the amount of carbon present on the silica and somewhat higher for the $NH_2$-treated surface accounts for 10% atomic concentration. It can be estimated from the XPS analysis of the surfaces that a 100%-coverage
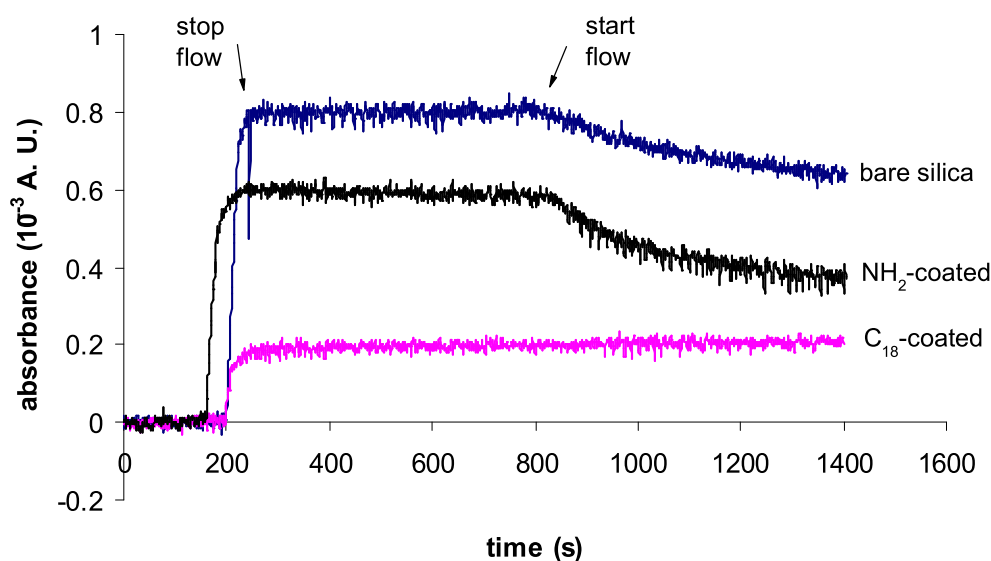
Figure 7.3: Flow profiles on the different surfaces; cyt $c$ concentration: 10 $\mu$M. From top to bottom: the bare silica surface, the NH$_2$-coated surface and the C$_{18}$-coated surface.

was obtained for the C$_{18}$-coated surface. The layer thickness on the C$_{18}$-modified wafer was measured to be on the order of 3 to 5 nm which corresponds to a monolayer with fully stretched C$_{18}$ chains [154]. Chlorine was not detected in the XPS surveys indicating that the reaction was complete. The NH$_2$-layer is immobilized using a different approach based on the less reactive triethoxysilane rather than trichlorosilane. The estimated monolayer coverage is only 50 to 75 %.

The extinction coefficient of our test molecule, the relatively small protein cytochrome $c$ (often used as a benchmark molecule), was determined to be $1.0 \cdot 10^4$ M$^{-1}$cm$^{-1}$ at 538 nm. Cyt $c$ has a net positive charge at a pH of 7.4 and is assumed to be spherical with a diameter of 3.0 to 3.5 nm [157]. Cytochrome $c$ adsorption experiments are performed using a stopped-flow approach: 100 $\mu$l of a cyt $c$ solution in 10 mM of potassium phosphate buffer at pH 7.4 is injected in a continuous flow (0.1 ml/min) of the same buffer. When the injection plug reaches the 14$\mu$l-sized teflon flow cell, that is clamped leak-tight on the TIR face of the prism, the flow is stopped. The evolution of the absorbance signal is monitored for a period of 10 to 15 minutes. No degradation of the absorbance signal is observed after prolonged time-spans, it is therefore assumed that photodegradation of cyt $c$ is negligible.

## 7.3 Results and discussion

### 7.3.1 Cytochrome $c$ adsorption to bare silica

First of all we explored the performance of the system before chemical modification of the TIR surface. A typical flow profile of a stopped-flow experiment is shown in Fig. 7.3: immediately after stopping the flow, the absorbance (measured by CRDS and eqn. 7.3.1) increases up to a constant level. Starting the flow again leads to a slowly decreasing absorbance. After performing the experiments, silica surfaces were cleaned by overnight reaction in chromic mixture. Later it was found that a 100-$\mu$l injection of 0.1 M H$_2$SO$_4$ in a flow of 0.05 ml/min also desorbs the cyt $c$ completely.

The absorbance in units $\varepsilon Cl$ can directly be related to the 1/e or ring-down time of
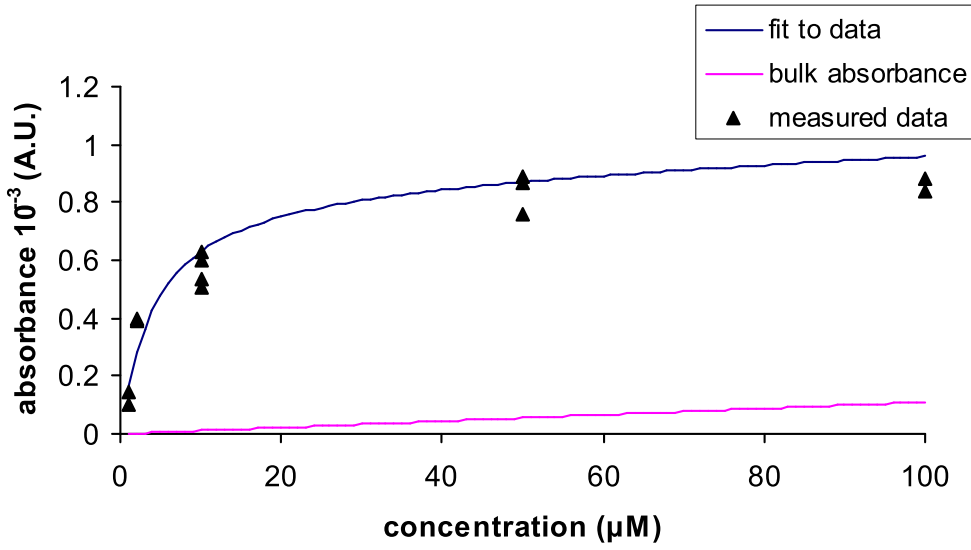
Figure 7.4: Average of three adsorption isotherms as measured on the bare SiOH surface, together with a fit to the data (regression coefficient 0.97). The straight line indicates the calculated bulk (background) absorbance using an effective penetration depth of 1100 nm. Data points were measured on different days using fresh solutions.

the measured decays via:

$$\varepsilon C_{eff} l = \frac{\alpha_{anal} l}{2.303} = \frac{n_{avg} L}{2.303 c}\left[\frac{1}{\tau} - \frac{1}{\tau_0}\right] \tag{7.1}$$

where $\varepsilon$ is the molar extinction coefficient in $M^{-1}cm^{-1}$ at 538 nm, $C_{eff}$ the effective concentration in the penetration layer in M and $l$ the effective path-length of the evanescent wave through the sample in cm, which is calculated as 1100 nm [145, 152]. $L$ is the cavity length (71 to 73 mm in this study), $n_{avg}$ the average refractive index, $c$ the speed of light, and $\alpha_{anal}$ is the absorption coefficient in $cm^{-1}$; $\tau$ and $\tau_0$ are the ring-down times in presence or absence of analyte. The baseline noise of the system is typically between 3 to $5 \cdot 10^{-5}$ A.U., a slight improvement over the set-up previously used (employing an anti-reflection coated 45-degrees Dove prism in a linear cavity) which showed a baseline noise on the order of $10^{-4}$ A.U. [152].

An isotherm (shown in Fig. 7.4) was measured in triplicate, the data were fitted to

$$A = \frac{A_{max} K C_{eq}}{1 + K C_{eq}} \tag{7.2}$$

where $A$ is the measured absorbance, $A_{max}$ is the absorbance as measured at maximum coverage (both in A.U. and corrected for the bulk absorbance using a penetration depth of 1100 nm), $K$ is the equilibrium constant for the adsorption (in $\mu M^{-1}$) and $C_{eq}$ is the equilibrium concentration in the bulk (in $\mu M$). Parameters obtained from the fits were: $A_{max}=(8.9\pm2)\cdot10^{-4}$A.U., $K=(23\pm14)\cdot10^4$ $M^{-1}$ and $\Delta G=(30\pm2)$ kJ/mol. The average fit is included in Fig. 7.4. An important - and most likely incorrect - assumption for the fits was that there is only one kind of adsorption site available for the cyt $c$ molecules. It is known that on a hydroxylated SiOH surface, two different silanol sites (the so-called Q2 and Q3 sites) exist and therefore two different adsorption sites should be taken into account [110, 158]. Furthermore, additional multi-layer adsorption is likely to take place

so that we are dealing with a multitude of adsorption sites: the surface and the different cyt $c$ layers.

It is illustrative to estimate the absorbance which would be measured for a complete cyt $c$ monolayer. From the cyt $c$ dimensions it is estimated that in a cyt $c$ monolayer with thickness of 3 to 3.5 nm, 0.6 - $0.7 \cdot 10^{12}$ molecules or 1 to 1.2 pmol are present in the laser spot (6 to 7 mm$^2$). Previously, monolayer coverage of 32 pmol/cm$^2$ amounting to 1.9 pmol in 6 to 7 mm$^2$ was measured with electrochemical techniques [159], quite close to this crude calculation. Using the extinction coefficient of $1.0 \cdot 10^4 \text{M}^{-1} \text{cm}^{-1}$ the absorbance of a monolayer should be 2 to $4 \cdot 10^{-4}$ A.U. Thus, the experimental results (maximum absorbance of $8.9 \pm 2 \cdot 10^{-4}$ A.U.) indicate that the maximum coverage on the three different surfaces is 2 to 3 monolayers. An assumption in this estimation is that the extinction coefficient of the adsorbed cyt $c$ is the same as for bulk (randomly oriented) molecules. This seems unlikely since, at least in the case of hydrophilic adsorption, cyt $c$ is known to be adsorbed with its heme group (and therefore with the transition dipole moment in the plane of the heme) almost perpendicular to the surface.

### 7.3.2 Cytochrome $c$ adsorption to modified surfaces

A future application of EW-CRDS is the development of a biosensor. Such a device requires the immobilization of a protein, an antibody or another biomolecule in order to monitor its interactions with analytes in the liquid mobile phase. Ideally, the biosensor will only exhibit specific interactions while non-specific binding of analytes is minimal. Of course, in EW-CRDS the crucial point is whether such an immobilization deteriorates the reflection quality of the TIR surface or not. To make EW-CRDS feasible the surface of the prism has to be modified in such a way that the measured ring-down signal is not strongly shortened with respect to the original signal measured on a bare prism. Various possibilities exist for the immobilization of proteins and antibodies on a silica surface. For example, one can add SH-groups to the "tail"of an IgG antibody in order to link the antibodies to a maleimide-activated NH$_2$-coated surface. Another possibility is using the non-specific binding on a hydrophobic surface (for example, C$_{18}$-coated surface); the disadvantage of this approach is that the active region of some of the immobilized antibodies may not be accessible for the antigen (analyte) anymore.

Previously, we determined that surface roughness (possibly induced by an imperfect layer on the surface) is not a serious problem: when using an EW-CRDS configuration with intra-cavity prisms, most optical losses will occur at the entrance and exit face of the prism rather than from scattering at the TIR surface. A higher surface roughness appeared to be advantageous for analytical purposes, presumably because imperfect (turbulent) flow results in more efficient contact between the analytes of interest and the surface [152].

In the present study we demonstrate that a user-friendly one-step protocol for attaching the C$_{18}$ or NH$_2$-layer is successful. Again, cyt $c$ was chosen as a test molecule. In Fig. 7.3, it is immediately seen that the adsorption on bare silica is about 2 to 4 times higher than on the coated surfaces. In view of the development of a biosensor this is a rather encouraging result, since a-specific binding is successfully being suppressed. On the C$_{18}$ surface, the flow profile shows no gradual decrease after re-starting the flow indicating that cyt $c$ is irreversibly attached to this layer. Such an irreversible binding is not unexpected since the aliphatic chains on the surface are known to denature the protein. The NH$_2$-surface should be positively charged at the used pH 7.4 and is therefore expected to repel cyt $c$. The fact that also for this layer some adsorption can still be seen suggests that the bare silica surface is not completely shielded or covered by the NH$_2$-layer.

## Cytochrome C adsorption to NH$_2$-coated surface



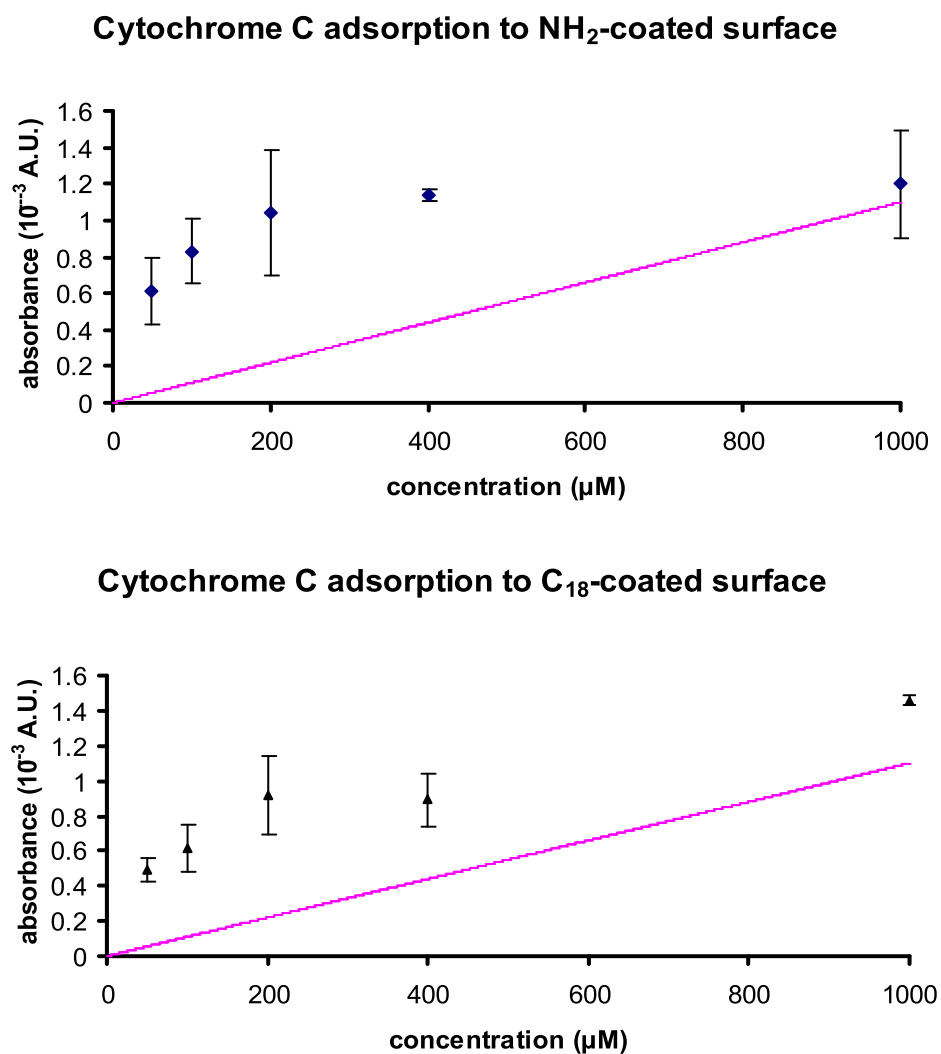## Cytochrome C adsorption to C$_{18}$-coated surface



Figure 7.5: Average of three adsorption isotherms as measured on the C$_{18}$ and NH$_2$ surfaces. Measurements have been performed in triplicate. The straight lines indicate the calculated bulk (background) absorbances using an effective penetration depth of 1100 nm. Data points were obtained on different days using fresh solutions.

For all three surfaces cyt $c$ adsorption is at least partly irreversible. Contrary to the bare silica surface, cleaning of the coated surfaces after performing an adsorption experiment is not trivial. The original ring-down time as measured on the clean $C_{18}$ and $NH_2$ surfaces is recovered after one night of flushing (at 2 ml/min) with pure methanol ($C_{18}$) or 1:1 methanol/water ($NH_2$). The nature of the interactions for the three surfaces will be different. In case of bare silica and $NH_2$-coated surface electrostatic interactions will be significant, whereas adsorption to the $C_{18}$ surface will be dominated by hydrophobic interactions while electrostatic contributions will be small. Especially for the $C_{18}$ surface, considerable irreversible binding should be expected, but flushing with abundant solvent is sufficient for completely removing irreversibly bound cyt $c$. A prism that was used for months yielded the same results as a newly coated prism.

Finally we tried to fit a Langmuir isotherm to the data points obtained for the $NH_2$- and $C_{18}$-coated surfaces, but this attempt was not successful. Presumably, the requirement of equilibrium conditions is not fullfilled. The measured adsorption isotherms for the two surfaces are shown in Fig. 7.5. One may argue that a fit of the data to a simple Langmuir isotherm is not adequate for the determination of thermodynamic parameters such as a maximum coverage. More appropriate would be a model which takes adsorption to three different adsorption sites (the surface, the first, oriented, cyt $c$ monolayer and the layers on top that are more randomly oriented). In the case of the $C_{18}$ surface where adsorption is due to hydrophobic rather than electrostatic interactions, only two sites should be taken into account since the first monolayer will probably not be oriented. However, it is clear that the affinity of the cyt $c$ towards the bare silanol surface is highest, followed by the $NH_2$-coated and the $C_{18}$-coated surfaces.

## 7.4   Conclusion

Surface modification of the TIR face of a prism used in EW-CRDS by self-assembly from solution has been demonstrated to be feasible. The use of surface modification could develop EW-CRDS into an interesting tool for sensitive absorbance spectroscopic studies of adsorption kinetics towards surfaces with different properties. Furthermore, in the present geometry reflection and scatter losses in the system are still very high and it is expected that an improved design of the prism used for EW-CRDS, for example the use of a folded resonator [105], can drastically increase the sensitivity of the system. Finally it is noted that the current design involving normal-incidence entrance and exit faces would allow for polarization-dependent studies: in that case the orientation of the adsorbed molecule could be calculated from the dichroic ratio.

## Acknowledgement

# Chapter 8

# Concluding remarks

Cavity ring-down spectroscopy (CRDS) is an extremely sensitive mode of absorption spectroscopy, suitable for application in trace detection. It is safe to state that cavity-enhanced techniques are to date the most sensitive modes of absorption spectroscopy, only rivaled by photo-acoustic absorbance spectroscopy (PAS). During the first years of its development, CRDS was exclusively applied to gas-phase studies. However, in the last decade various examples of different modes of CRDS applied to condensed media have also been reported, indicating its potential for these media as well.

Advantages of CRDS include the simplicity and robustness of the set-up as compared to for example the use of Herriot- or White-type absorbance cells, the absolute character of the measurements and the excellent sensitivity.

In chapters 2 – 5 of this thesis, the development of a CRDS-based absorbance detector suitable for conventional-size liquid chromatography (LC) detection and flow-injection analysis (FIA) is described. In the visible wavelength range (at 532 and 457 nm), the detection sensitivity of conventional absorbance detectors is surpassed by a factor of 100. This enhancement factor is even feasible using a tunable laser system that is tuned 13 nm off the design wavelength (470 nm) of the CRDS mirrors used. This shows that using one particular set of CRDS mirrors still provides some freedom in wavelength selection. To further improve user-friendliness, it might be advantageous to use a geometry which incorporates a flow cuvette at 0 degrees in a linear cavity although in such a set-up possible reflection losses play a significant role. This way, mirrors do not need cleaning on a daily basis and the set-up can be used for weeks without need for alignment.

A drawback of the CRDS technique is the limited linear dynamic range: a larger absorbance is associated with a shorter ring-down time and the upper limit of absorbance is determined by the number of data points that still result in a reasonable fit of the decay transient. The linear dynamic range of CRDS set-ups is typically limited to two orders of magnitude. Another disadvantage is the fact that high-reflectivity mirrors are currently not yet available in the UV wavelength range. This explains why, as demonstrated in chapter 5, the sensitivity enhancement for absorption detection in LC studies becomes less pronounced when moving to UV wavelengths. At 355 nm, the performance of the system was a factor of 10 lower than in the visible range. At 273 nm, the mirrors were of too low reflectivity for improving the sensitivity of LC absorption detection compared to conventional LC absorbance detectors.

In recent years several other groups have developed new CRDS methods. Especially promising is the development of cavity-enhanced absorption spectroscopy (CEAS), which can be used in conjunction with incoherent broad-band sources and mirrors with lower reflectivities but applicable over a larger wavelength range. This opens possibilities for

obtaining spectral information over a broader wavelength range, which is especially useful in condensed-media studies, where absorbance bands are usually much broader than in the gas-phase. Also useful in this respect is fiber-loop CRDS, although at present this technique is restricted to red or near-infrared (NIR) wavelengths due to substantial optical losses within the fiber material in the visible and UV wavelength region. Another promising mode is polarization-dependent CRDS: the off-resonance optical rotation of molecules of interest can be probed at any convenient wavelength.

A new and interesting development in CRDS is the rapidly evolving evanescent-wave (EW) approach, which combines surface specificity with extremely sensitive absorbance measurements. Many different implementations of this technique are currently being explored. However, also in this application there is a wavelength restriction. It is clear from Fig. 1.11 that upon shifting the wavelength to the UV range, the prism material becomes less transparent.

Chapter 6 of this study reports on the development and application to flow-injection analysis (FIA) of an EW-CRDS set-up based on an intra-cavity Dove prism. For analytical chemical purposes the reversibility of the surface binding processes is crucial: a method is needed where repetitive measurements can easily be performed without contamination or degradation of the total internal reflection (TIR) surface of the prism. We observed that when the flow rate as well as the amount of organic modifier used are carefully chosen, repeatable results can be obtained without the need for rigorous cleaning after each measurement. Furthermore, as described in chapter 7, organosilanes can be used to covalently attach a self-assembled monolayer to the TIR surface of the prism, thus influencing surface properties and interactions. Covalently attached self-assembled monolayers may ultimately provide a platform for developing bio-sensors.

# Bibliography

[1] D. Herriot, H. Kogelnik, R. Kompfner, Off-axis paths in spherical mirror interferometers, Appl. Opt. 3 (1964) 523–526.

[2] J. White, Long optical paths of large aperture, J. Opt. Soc. Am. 32 (1942) 285–288.

[3] C. Gooijer, G. P. Hoornweg, T. de Beer, A. Bader, D. J. van Iperen, U. A. T. Brinkman, Detector cell based on plastic liquid-core waveguides suitable for aqueous solutions: one-to-two decades improved detection limits in conventional-size column liquid chromatography with absorption detection, J. Chrom. A 824 (1998) 1–5.

[4] T. Dallas, P. K. Dasgupta, Light at the end of the tunnel: recent analytical applications of liquid-core waveguides, Trends. Anal. Chem. 23 (2004) 385–392.

[5] T. de Beer, N. H. Velthorst, U. A. T. Brinkman, C. Gooijer, Laser-based non-fluorescence detection techniques for liquid separation systems, J. Chrom. A 971 (2002) 1–35.

[6] M. J. Navas, A. M. Jimenez, Thermal lens spectrometry as analytical tool, Crit. Rev. Anal. Chem. 33 (2003) 77–88.

[7] F. Li, A. A. Kachanov, R. N. Zare, Detection of separated analytes in subnanoliter volumes using coaxial thermal lensing, Anal. Chem. 79 (2007) 5264–5271.

[8] J. Wu, T. Odake, T. Kitamori, T. Sawada, Ultrasensitive detection for capillary zone electrophoresis using laser-induced capillary vibration, Anal. Chem. 63 (1991) 2216–2218.

[9] J. M. Rey, M. W. Sigrist, Differential mode excitation photoacoustic spectroscopy: A new photoacoustic detection scheme, Rev. Sci. Instr. 78 (2007) 063104.

[10] R. L. Farrow, D. J. Rakestraw, Detection of trace-molecular species using degenerate 4-wave mixing, Science 257 (1992) 1894–1900.

[11] G. P. Hoornweg, T. de Beer, N. H. Velthorst, C. Gooijer, Forward degenerate four-wave mixing as a detection method in liquid separation systems: Improving detection limits by means of a Fabry-Perot interferometer, Appl. Spectr. 51 (1997) 1008–1011.

[12] B. Paldus, A. Kachanov, An historical overview of cavity-enhanced methods, Can. J. Phys. 83 (2005) 975–999.

[13] D. Atkinson, Solving chemical problems of environmental importance using cavity ring-down spectroscopy, Analyst 128 (2003) 117–125.

[14] S. Brown, Absorption spectroscopy in high-finesse cavities for atmospheric studies, Chem. Rev. 103 (2003) 5219–5238.

[15] G. Berden, R. Peeters, G. Meijer, Cavity ring-down spectroscopy: Experimental schemes and applications, Int. Rev. Phys. Chem. 19 (2000) 565–607.

[16] K. Busch, M. Busch, Cavity Ring-Down Spectroscopy : An Ultratrace Absorption Measurement Technique, Oxford University Press, Oxford, UK, 1999.

[17] M. D. Wheeler, S. M. Newman, A. J. Orr-Ewing, M. N. R. Ahsfold, Cavity ring-down spectroscopy, Faraday Trans. 94 (1998) 337–351.

[18] J. Scherer, J. Paul, A. O'Keefe, R. Saykally, Cavity ringdown laser absorption spectroscopy: history, development, and application to pulsed molecular beams, Chem. Rev. 97 (1997) 25–51.

[19] J. M. Herbelin, J. A. McKay, M. A. Kwok, R. H. Uenten, D. S. Urevig, D. Spencer, D. J. Benard, Appl. Opt. 19 (1980) 144–147.

[20] D. Z. Anderson, J. C. Frisch, C. S. Masser, Mirror reflectometer based on optical cavity decay time, Appl. Opt. 23 (1984) 1238–1245.

[21] A. O'Keefe, D. A. G. Deacon, Cavity ring-down optical spectrometer for absorption measurements using pulsed laser sources, Rev. Sci. Instr. 59 (1988) 2544–2551.

[22] M. Sneep, S. Hannemann, E.-J. van Duijn, W. Ubachs, Deep-ultraviolet cavity ring-down spectroscopy, Opt. Lett. 29 (2004) 1378–1380.

[23] H. Kogelnik, T. Li, Laser beams and resonators, Appl. Opt. 5 (1966) 1550–1567.

[24] G. Meijer, M. Boogaarts, R. Jongma, D. Parker, Coherent cavity ring down spectroscopy, Chem. Phys. Lett. 217 (1994) 112–116.

[25] H. Naus, I. H. M. van Stokkum, W. Hogervorst, W. Ubachs, Quantitative analysis of decay transients applied to a multimode pulsed cavity ringdown experiment, Appl. Opt. 40 (2001) 4416–4426.

[26] J. Martin, B. A. Paldus, P. Zalicki, E. H. Wahl, T. G. Owano, J. J. S. Harris, C. H. Kruger, R. N. Zare, Cavity ring-down spectroscopy with fourier-transform-limited light pulses, Chem. Phys. Lett. 258 (1996) 63–70.

[27] L. van der Sneppen, A. Wiskerke, F. Ariese, C. Gooijer, W. Ubachs, Improving the sensitivity of HPLC absorption detection by cavity ring down spectroscopy in a liquid-only cavity, Anal. Chim. Acta 558 (2006) 2–6.

[28] R. T. Jongma, M. G. H. Boogaarts, I. Holleman, G. Meijer, Trace gas-detection with cavity ring-down spectroscopy, Rev. Sci. Instr. 66 (1995) 2821–2828.

[29] J. T. Hodges, J. P. Looney, R. D. van Zee, Laser bandwidth effects in quantitative cavity ring-down spectroscopy, Appl. Opt. 35 (1996) 4112–4116.

[30] M. Sneep, D. Ityaksov, I. Aben, H. Linnartz, W. Ubachs, Temperature-dependent cross sections of $O_2$-$O_2$ collision-induced absorption resonances at 477 and 577 nm 98 (2006) 405–424.

[31] H. Naus, W. Ubachs, Experimental verification of Rayleigh scattering cross sections, Opt. Lett. 25 (2000) 347–349.

[32] R. D. van Zee, J. T. Hodges, J. P. Looney, Pulsed, single-mode cavity ringdown spectroscopy, Appl. Opt. 38 (1999) 3951–3960.

[33] D. Romanini, A. A. Kachanov, N. Sadeghi, F. Stoeckel, Cw-cavity ring down spectroscopy, Chem. Phys. Lett. 264 (1997) 316–322.

[34] D. Romanini, A. A. Kachanov, F. Stoeckel, Diode laser cavity ring down spectroscopy, Chem. Phys. Lett. 270 (1997) 538–545.

[35] D. Romanini, A. A. Kachanov, F. Stoeckel, Cavity ringdown spectroscopy: broad band absolute absorption measurements, Chem. Phys. Lett. 270 (1997) 546–550.

[36] X. Zhan, O. Viattinen, E. Kauppi, L. Halonen, High-resolution photoacoustic overtone spectrum of acetylene near 570 nm using a ring-dye-laser spectrometer, Chem. Phys. Lett. 180 (1991) 310.

[37] Y. He, M. Hippler, M. Quack, High-resolution cavity ring-down absorption spectroscopy of nitrous oxide and chloroform using a near-infrared CW diode laser, Chem. Phys. Lett. 289 (1998) 527–534.

[38] K. J. Schulz, W. R. Simpson, Frequency-matched cavity ring-down spectroscopy, Chem. Phys. Lett. 297 (1998) 523–529.

[39] G. von Basum, H. Dahnke, D. Halmer, P. Hering, M. Mürtz, Online recording of ethane traces in human breath via infrared laser spectroscopy, J. Appl. Phys. 95 (2003) 2583–2590.

[40] H. Dahnke, D. Kleine, P. Hering, M. Mürtz, Real-time monitoring of ethane in human breath using mid-infrared cavity leak-out spectroscopy, Appl. Phys. B 72 (2001) 971–975.

[41] E. R. Crosson, K. N. Ricci, B. A. Richman, F. C. Chilese, T. G. Owano, R. A. Provencal, M. W. Todd, J. Glasser, A. A. Kachanov, B. A. Paldus, T. G. Spence, R. N. Zare, Stable isotope ratios using cavity ring-down spectroscopy: determination of $^{13}C/^{12}C$ for carbon dioxide in human breath, Anal. Chem. 74 (2002) 2003–2007.

[42] H. W. A. Berkelmans, B. W. M. Moeskops, J. Bominaar, P. T. J. Scheppers, F. J. M. Harren, Pharmacokinetics of ethylene in man by on-line laser photoacoustic detection, Tox. and Appl. Phar. 190 (2003) 206–213.

[43] J. B. Paul, L. Lapson, J. G. Anderson, Ultrasensitive absorption spectroscopy with a high-finesse optical cavity off-axis alignment, Appl. Opt. 40 (2001) 4904–4910.

[44] V. L. Kasyutich, C. E. Canosa-Mas, C. Pfrang, S. Vaughan, R. P. Wayne, Off-axis continuous-wave cavity-enhanced absorption spectroscopy of narrow-band and broadband absorbers using red diode lasers, Appl. Phys. B 75 (2002) 755–761.

[45] M. Gupta, T. Owano, D. S. Baer, Quantitative determination of singlet oxygen density and temperature for oxygen-iodine laser applications, Chem. Phys. Lett. 400 (2004) 42–46.

[46] A. O'Keefe, Integrated cavity output analysis of ultra-weak absorption, Chem. Phys. Lett. 293 (1998) 331–336.

[47] A. O'Keefe, J. J. Scherer, J. B. Paul, CW integrated cavity output spectroscopy, Chem. Phys. Lett. 307 (1999) 343–349.

[48] T. Gherman, D. Romanini, Mode-locked cavity-enhanced absorption spectroscopy, Opt. Ex. 10 (2002) 1033–1042.

[49] T. Gherman, D. Romanini, I. Sagnes, A. Garnache, Z. Zhang, Cavity-enhanced absorption spectroscopy with a mode-locked diode-pumped vertical external-cavity surface-emitting laser, Chem. Phys. Lett. 390 (2004) 290–295.

[50] S. Fiedler, A. Hese, A. Ruth, Incoherent broad-band cavity-enhanced absorption spectroscopy of liquids, Rev. Sci. Instr. 76 (2005) 023107.

[51] R. Engeln, G. von Helden, G. Berden, G. Meijer, Phase shift cavity ring down absorption spectroscopy, Chem. Phys. Lett. 262 (1996) 105–109.

[52] S. DeMille, R. H. deLaat, R. M. Tanner, R. L. Brooks, N. P. C. Westwood, Comparison of CRDS to ICL-PAS and phase-shift CRDS spectroscopies for the absolute intensities of C–H ($\Delta\nu = 6$) overtone absorptions, Chem. Phys. Lett. 366 (2002) 383–389.

[53] E. K. Lewis, D. Reynolds, X. Li, G. de Villele, C. Leduc, D. L. Cedeno, C. M. I, Phase shift cavity ring down measurement of C–H ($\delta\nu = 6$) vibrational overtone absorptions, Chem. Phys. Lett. 334 (2001) 357–364.

[54] J. H. van Helden, D. C. Schram, R. Engeln, Phase-shift cavity ring-down spectroscopy to determine absolute line intensities, Chem. Phys. Lett. 400 (2004) 320–325.

[55] R. Engeln, G. Meijer, A Fourier transform cavity ring down spectrometer, Rev. Sci. Instr. 67 (1996) 2708–2713.

[56] E. Hamers, D. C. Schram, R. Engeln, Fourier transform phase shift cavity ring down spectroscopy, Chem. Phys. Lett. 365 (2002) 237–243.

[57] S. Fiedler, G. Hoheisel, A. Ruth, A. Hese, Incoherent broad-band cavity-enhanced absorption spectroscopy of azulene in a supersonic jet, Chem. Phys. Lett. 382 (2003) 447–453.

[58] A. A. Ruth, E.-K. Kim, A. Hese, The $S_0$ to $S_1$ cavity ring-down absorption spectrum of jet-cooled azulene: dependence of internal conversion on the excess energy, Phys. Chem. Chem. Phys. 1 (1999) 5121–5128.

[59] S. Fiedler, A. Hese, A. Ruth, Incoherent broad-band cavity-enhanced absorption spectroscopy, Chem. Phys. Lett. 371 (2003) 284–294.

[60] D. S. Venables, T. Gherman, J. Orphal, J. Wenger, A. Ruth, High-sensitivity in situ monitoring of $NO_3$ in an atmospheric simulation chamber using incoherent broadband cavity-enhanced absorption spectroscopy, Environ. Sci. Technol. 40 (2006) 6758–6763.

[61] A. A. Ruth, J. Orphal, S. E. Fiedler, Fourier-transform cavity-enhanced absorption spectroscopy using an incoherent broadband light source, Appl. Opt. 46 (2007) 3611–3616.

[62] S. M. Ball, J. M. Langridge, R. L. Jones, Broadband cavity enhanced absorption spectroscopy using light emitting diodes, Chem. Phys. Lett. 398 (2004) 68–74.

[63] R. Engeln, G. Berden, E. van den Berg, G. Meijer, Polarization dependent cavity ring down spectroscopy, J. Chem. Phys. 107 (1997) 4458–4467.

[64] J. Poirson, M. Vallet, F. Bretenaker, A. L. Floch, J.-Y. Thépot, Resonant cavity gas-phase polarimeter, Anal. Chem. 70 (1998) 4636–4639.

[65] T. Müller, K. B. Wiberg, P. H. Vaccaro, Cavity ring-down polarimetry (CRDP): a new scheme for probing circular birefringence and circular dichroism in the gas phase, J. Phys. Chem. A 104 (2000) 5959–5968.

[66] T. Müller, K. B. Wiberg, P. H. Vaccaro, An optical mounting system for cavity ring-down polarimetry, Rev. Sci. Instr. 73,3 (2002) 1340–1342.

[67] A. J. Hallock, E. S. F. Berman, R. N. Zare, Direct monitoring of absorption in solution by cavity ring-down spectroscopy, Anal. Chem. 74 (2002) 1741–1743.

[68] S. Xu, G. Sha, J. Xie, Cavity ring-down spectroscopy in the liquid phase, Rev. Sci. Instr. 73 (2002) 255–258.

[69] R. Engeln, G. von Helden, A. van Roij, G. Meijer, Cavity ring down spectroscopy on solid $C_{60}$, J. Chem. Phys. 110 (1999) 2732–2733.

[70] D. S. Bethune, G. Meijer, W. C. Tang, H. J. Rosen, W. G. Golden, H. Seki, C. A. Brown, M. S. de Vries, Vibrational Raman and infrared-spectra of chromatographically separated C60 and C70 fullerene clusters, Chem. Phys. Lett. 179 (1991) 181–186.

[71] A. H. M. Smets, J. H. van Helden, M. C. M. van de Sanden, Bulk and surface defects in a-Si:H films studied by means of the cavity ring down absorption technique, J. Non-Cryst. Solids 229-302 (2002) 610–614.

[72] I. M. P. Aarts, P. Hoex, A. H. M. Smets, R. Engeln, W. M. M. Kessels, M. C. M. van de Sanden, Direct and highly sensititve measurement of defect-related absorption in amorphous silicon thin films by cavity ring-down spectroscopy, Appl. Phys. Lett. 84 (2004) 3079–3081.

[73] D. Kleine, J. Lauterbach, K. Kleinermanns, P. Hering, Cavity ring-down spectroscopy of molecularly thin iodine layers, Appl. Phys. B 72 (2001) 249–252.

[74] A. Karaiskou, C. Vallance, V. Papadakis, I. Vardavas, T. Rakitzis, Absolute absorption cross-section measurements of $CO_2$ in the ultraviolet from 200 to 206 nm at 295 and 373 K, Chem. Phys. Lett. 400 (2004) 30–34.

[75] B. Bahnev, L. van der Sneppen, A. E. Wiskerke, F. Ariese, C. Gooijer, W. Ubachs, Miniaturized cavity ring-down detection in a liquid flow-cell, Anal. Chem. 77 (2005) 1188–1191.

[76] L. van der Sneppen, A. Wiskerke, F. Ariese, C. Gooijer, W. Ubachs, Cavity ring-down spectroscopy for detection in liquid chromatography: extension to tunable sources and UV wavelengths, Appl. Spectr. 60 (2006) 935–938.

[77] K. L. Snyder, R. N. Zare, Cavity ring-down spectroscopy as a detector for liquid chromatography, Anal. Chem. 75 (2003) 3086–3091.

[78] K. L. Bechtel, R. N. Zare, A. A. Kachanov, S. S. Sanders, B. A. Paldus, Moving beyond traditional UV-Visible absorption detection: Cavity ring-down spectroscopy for HPLC, Anal. Chem. 77 (2005) 1177–1182.

[79] A. J. Alexander, Reaction kinetics of nitrate radicals with terpenes in solution studied by cavity ring-down spectroscopy, Chem. Phys. Lett. 393 (2004) 138–142.

[80] A. J. Hallock, E. S. F. Berman, R. N. Zare, Ultratrace kinetic measurements of the reduction of methylene blue, J. Am. Chem. Soc. 125 (2003) 1158–1159.

[81] A. J. Hallock, E. S. F. Berman, R. N. Zare, Use of broadband, continuous-wave diode lasers in cavity ring-down spectroscopy for liquid samples, Spec. Techniques 57 (2003) 571–573.

[82] T. McGarvey, A. Conjusteau, H. Mabuchi, Finesse and sensitivity gain in cavity-enhanced absorption spectroscopy of biomolecules in solution, Opt. Ex. 14 (2006) 10441–10451.

[83] A. Alexander, Flowing liquid-sheet jet for cavity ring-down absorption measurements, Anal. Chem. 78 (2006) 5597–5600.

[84] E. Kleist, H. Betterman, Intracavity absorption measurements from liquid samples in an $Ar^+$-ion laser, Opt. Lett. 13 (1988) 449–451.

[85] J. Hicks, G. Patonay, Linearity consideration for near-infrared laser diode intracavity absorption spectrometer, Anal. Chem. 62 (1990) 1543–1545.

[86] U. Elejalde, J. M. Girkin, Real-time, ultralow concentration detection of analytes in solution by infrared intracavity laser absorption, Appl. Opt. 46 (2007) 3995–3999.

[87] M. Islam, L. Seetohul, Z. Ali, Liquid-phase broadband cavity enhanced absorption spectroscopy measurements in a 2 mm cuvette, Appl. Spectr. 61 (2007) 649–658.

[88] L. van der Sneppen, F. Ariese, C. Gooijer, W. Ubachs, Cavity ring-down spectroscopy for detection in liquid chromatography at UV wavelengths using standard cuvettes in a normal incidence geometry, J. Chrom. A 1148 (2007) 184–188.

[89] R. Li, H.-P. Loock, R. D. Oleschuk, Capillary electrophoresis absorption detection using fiber-loop ring-down spectroscopy, Anal. Chem. 78 (2006) 5685–5692.

[90] M. Gupta, H. Jiao, A. O'Keefe, Cavity-enhanced spectroscopy in optical fibers, Opt. Lett. 27 (2002) 1878–1880.

[91] T. von Lerber, M. W. Sigrist, Cavity ring-down principle for fiber-optic resonators: experimental realization of bending loss and evanescent-field sensing, Appl. Opt. 41 (2002) 3567–3575.

[92] D. E. Vogler, M. G. Müller, M. W. Sigrist, Fiber-optic cavity sensing of hydrogen diffusion, Appl. Opt. 42 (2003) 5413–5417.

[93] P. B. Tarsa, P. Rabinowitz, K. K. Lehmann, Evanescent field absorption in a passive optical fiber resonator using continuous-wave cavity ring-down spectroscopy, Chem. Phys. Lett. 383 (2004) 297–303.

[94] C. Wang, S. T. Scherrer, Fiber ringdown pressure sensors, Opt. Lett. 29 (2004) 352–354.

[95] P. B. Tarsa, D. M. Brzozowski, P. Rabinowitz, K. K. Lehmann, Cavity ringdown strain gauge, Opt. Lett. 29 (2004) 1339–1341.

[96] P. B. Tarsa, A. D. Wist, P. Rabinowitz, K. K. Lehmann, Single-cell detection by cavity ring-down spectroscopy, Appl. Phys. Lett. 85 (2004) 4523–4525.

[97] D. E. Vogler, A. Lorencak, J. M. Rey, M. W. Sigrist, Bending loss measurement using a fiber cavity ringdown scheme, Optics Lasers Engin. 43 (2005) 527–535.

[98] G. Stewart, K. Atherton, H.Yu, B. Culshaw, An investigation of an optical fibre amplifier loop for intra-cavity and ring-down cavity loss measurements, Meas. Sci. Technol. 12 (2001) 843–849.

[99] G. Stewart, K. Atherton, B. Culshaw, Cavity-enhanced spectroscopy in fiber cavities, Opt. Lett. 29 (2004) 442–444.

[100] R. Brown, I. Kozin, Z. Tong, R. Oleschuk, H.-P. Loock, Fiber-loop ring-down spectroscopy, J. Chem. Phys. 117 (2002) 10444–10447.

[101] Z. Tong, A. Wright, T. McCormick, R. Li, R. Oleschuk, H.-P. Loock, Phase-shift fiber-loop ring-down spectroscopy, Anal. Chem. 76 (2004) 6594–6599.

[102] H.-P. Loock, Ring-down absorption spectroscopy for analytical microdevices, Trends. Anal. Chem. 25 (2006) 655–664.

[103] A. C. R. Pipino, J. W. Hudgens, R. E. Huie, Evanescent wave cavity ring-down spectroscopy with a total-internal-reflection minicavity, Rev. Sci. Instr. 68 (1997) 2978–2989.

[104] A. C. R. Pipino, J. W. Hudgens, R. E. Huie, Evanescent wave cavity ring-down spectroscopy for probing surface processes, Chem. Phys. Lett. 280 (1997) 104–112.

[105] A. C. R. Pipino, Ultrasensitive surface spectroscopy with a miniature optical resonator, Phys. Rev. Lett. 83 (1999) 3093–3096.

[106] A. C. R. Pipino, J. P. M. Hoefnagels, N. Watanabe, Absolute surface coverage measurement using a vibrational overtone, J. Chem. Phys. 120 (2004) 2879–2888.

[107] I. M. P. Aarts, A. C. R. Pipino, J. P. M. Hoefnagels, W. M. M. Kessels, M. C. M. van de Sanden, Quasi-ice monolayer on atomically smooth amorphous $SiO_2$ at room temperature observed with a high-finesse optical resonator, Phys. Rev. Lett. 95 (2005) 166104.

[108] W. B. Martin, S. Mirov, D. Martyshkin, R. Venugopalan, Hemoglobin adsorption isotherm at the silica-water interface with evanescent wave cavity ring-down spectroscopy, J. Biomed. Opt. 10 (2005) 024025.

[109] H.-F. Fan, C.-Y. Hung, K.-C. Lin, Molecular adsorption at silica/$CH_3CN$ interface probed by using evanescent wave cavity ring-down absorption spectroscopy: determination of thermodynamic properties, Anal. Chem. 78 (2006) 3583–3590.

[110] A. M. Shaw, T. E. Hannon, F. Li, R. N. Zare, Adsorption of crystal violet to the silica-water interface monitored by evanescent wave cavity ring-down spectroscopy, J. Phys. Chem. B 107 (2003) 7070–7075.

[111] J. D. Fisk, R. Batten, G. Jones, J. P. O'Reilly, A. M. Shaw, pH dependence of the crystal violet adsorption isotherm at the silica-water interface, J. Phys. Chem. B 109 (2005) 14475–14480.

[112] J. P. O'Reilly, C. P. Butts, I. A. l'Anson, A. M. Shaw, Interfacial ph at an isolated silica-water surface, JACS communications 127 (2005) 1632–1633.

[113] J. D. Fisk, M. Rooth, A. M. Shaw, Gold nanoparticle adsorption and aggregation kinetics at the silica-water interface, J. Phys. Chem. C 111 (2007) 2588–2594.

[114] T. E. Hannon, S. Chah, R. N. Zare, Evanescent-wave cavity ring-down investigation of polymer/solvent interactions, J. Phys. Chem. B 109 (2005) 7435–7442.

[115] M. Mazurenka, L. Wilkins, J. V. Macpherson, P. R. Unwin, S. R. Mackenzie, Evanescent wave cavity ring-down spectroscopy in a thin-layer electrochemical cell, Anal. Chem. 78 (2006) 6833–6839.

[116] F. Li, R. N. Zare, Molecular orientation study of methylene blue at an air/fused-silica interface using evanescent-wave cavity ring-down spectroscopy, J. Phys. Chem. B 109 (2005) 3330–3333.

[117] M. A. Everest, V. M. Black, A. S. Haehlen, G. A. Haveman, C. J. Kliewer, H. A. Neill, Hemoglobin adsorption to silica monitored with polarization-dependent evanescent-wave cavity ring-down spectroscopy, J. Phys. Chem. B 110 (2006) 19461–19468.

[118] S. Schiller, I. I. Yu, M. M. Fejer, R. L. Byer, Fused-silica monolithic total-internal-reflection resonator, Opt. Lett. 17 (1992) 378–380.

[119] A. Pipino, M. Michalski, Climbing the vibrational ladder to probe the OH stretch of $HNO_3$ on silica, J. Phys. Chem. C 111 (2007) 9442–9447.

[120] I. Aarts, A. Pipino, M. van de Sanden, W. Kessels, Absolute in-situ measurements of surface dangling bonds during a-Si:H growth, Appl. Phys. Lett. 90 (2007) 161918.

[121] M. R. Querry, P. G. Cary, R. C. Waring, Appl. Opt. 17 (1978) 3587–3592.

[122] K. Fujiwara, K. Kurokawa, H. Uchiki, T. Kobayashi, Detection of trace iodine in solution by phase conjugate reflection, Spec. Letters 20 (1987) 633–643.

[123] T. de Beer, G. P. Hoornweg, G. J. Grootendorst, N. H. Velthorst, C. Gooijer, Forward-scattering degenerate four-wave mixing as a potential laser-based absorption detection method in liquid separation systems: Coupling to conventional-size liquid chromatography, Anal. Chim. Acta 330 (1996) 189–197.

[124] T. G. Nolan, W. A. Weimer, N. J. Dovichi, Laser-induced photothermal refraction for small volume absorbance determination, Anal. Chem. 56 (1984) 1704–1707.

[125] D. J. Bornhop, N. J. Dovichi, Simultaneous laser-based refractive index and absorption determinations within micrometer diameter capillary tubes, Anal. Chem. 59 (1987) 1632–1636.

[126] J. M. Saz, B. Krattinger, A. E. Bruno, J. C. Diez-Masa, H. M. Widmer, Thermo–optical absorbance detection of native proteins separated by capillary electrophoresis in 10 micrometer I. D. tubes, J. Chrom. A 699 (1995) 315–322.

[127] M. Qi, X.-F. Li, C. Stathakis, N. J. Dovichi, Capillary electrochromatography with thermo-optical absorbance detection for the analysis of phenylthiohydantoin-amino acids, J. Chrom. A 853 (1999) 131–140.

[128] G. Berden, R. Peeters, G. Meijer, Cavity ring-down spectroscopy: Experimental schemes and applications, Int. Rev. Phys. Chem. 19 (2000) 565–607.

[129] JMSTsystems, http://www.jmstsystems.com/docs/vuv–30rev4_2.pdf.

[130] J. Durant, W. Busby, A. Lafleur, B. Penman, C. Crespi, Human cell mutagenicity of oxygenated, nitrated and unsubstituted polycyclic aromatic hydrocarbons associated with urban aerosols, Mutation Research-Genetic Toxicology 371 (1996) 123–157.

[131] H. Tokiwa, Y. Nakanishi, N. Sera, N. Hara, S. Inuzuka, Analysis of environmental carcinogens associated with the incidence of lung cancer, Toxicol. Lett. 99 (1998) 33–41.

[132] J. Lewtas, M. Nishioka, B. Peterson, Bioassay directed fractionation of the organic extract of SRM 1649 urban air particulate and ambient matter, Int. J. Environ. Anal. Chem. 39 (1990) 61245–61256.

[133] H. Bamford, J. Baker, Nitro-polycyclic aromatic hydrocarbon concentrations and sources in urban and suburban atmospheres of the Mid-Atlantic region, Atm. Environ. 37 (2003) 2077–2091.

[134] P. Castells, F. Santos, M. Galceran, Development of a sequential supercritical fluid extraction method for the analysis of nitrated and oxygenated derivatives of polycyclic aromatic hydrocarbons in urban aerosols, J. Chrom. A 1010 (2003) 141–151.

[135] H. Söderström, J. Hajšlová, V. Kocourek, B. Siegmund, A. Kocan, M. Obiedzinski, M. Tysklind, P.-A. Bergqvist, PAHs and nitrated PAHs in air of five European countries determined using SPMDs as passive samplers, Atm. Environ. 39 (2005) 1627–1640.

[136] M. Murayama, P. Dasgupta, Liquid chromatographic determination of nitro-substituted polynuclear aromatic hydrocarbons by sequential electrochemical and fluorescence detection, Anal. Chem. 68 (1996) 1226–1232.

[137] M. Cerná, D. Pochmanová, A. Pastorková, I. Benes, J. Lenícek, J. Topinka, B. Binková, Genotoxicity of urban air pollutants in the Czech Republic: Part i. bacterial mutagenic potencies of organic compounds adsorbed on PM10 particulates, Mutation Res./Genetic Toxicology and Environmental Mutagenesis 469 (2000) 71–82.

[138] K. Hayakawa, N. Tang, K. Akutsu, T. Murahashi, H. Kakimoto, R. Kizu, A. Toriba, Comparison of polycyclic aromatic hydrocarbons and nitropolycyclic aromatic hydrocarbons in airborne particulates collected in downtown and suburban Kanazawa, Japan, Atm. Environ. 36 (2002) 5535–5541.

[139] J. M. Boon, W. E. van der Veer, J. W. Gerritsen, W. Hogervorst, Opt. Lett. 20 (1995) 380–382.

[140] J. Mes, M. Leblans, W. Hogervorst, Single-longitudinal-mode optical parametric oscillator for spectroscopic applications, Opt. Lett. 27 (2002) 1442–1444.

[141] C. Wang, F. Mazzotti, G. Miller, C. Winstead, Cavity ringdown spectroscopy for diagnostic and analytical measurements in an inductively coupled plasma, Appl. Spectr. 56 (2002) 386–397.

[142] P. Claudon, M. Donner, J. F. Stoltz, Potential interest of optical fibers as immunosensors - study of different antigen coupling methods, J. Mat. Sci Materials in Medicine 2 (1991) 197–201.

[143] T. Vo-Dinh, M. J. Sepaniak, G. D. Griffin, J. P. Alarie, Immunosensors: Principles and applications, ImmunoMethods 3 (1993) 85–92.

[144] J. L. Rodrigues, C. S. de Magalães, P. O. Luccas, Flow injection spectrophotometric determination of Al in hemodialysis solutions, J. Pharm. Biomed. An.

[145] N. J. Harrick, Infrared reflection spectroscopy, Harrick scientific corporation, New York, USA, 1987.

[146] D. S. Walker, H. W. Hellinga, S. S. Saavedra, W. M. Reichert, Integrated optical waveguide attenuated total reflection spectrometry and resonance raman spectroscopy of adsorbed cytochrome c, J. Phys. Chem. 97 (1993) 10217–10222.

[147] P. L. Edminston, J. E. Lee, S.-S. Cheng, S. S. Saavedra, Molecular orientation distributions in protein films. 1. Cytochrome c adsorbed to substrates of variable surface chemistry 119 (1997) 560–570.

[148] Z.-M. Qi, N. Matsuda, A. Takatsu, K. Kato, A kinetic study of cytochrome c adsorption to hydrophilic glass by broad-band, time-resolved optical waveguide spectroscopy, J. Phys. Chem. B 107 (2003) 6873–6875.

[149] W. Xu, H. Zhou, F. E. Regnier, Regio-specific adsorption of cytochrome c on negatively charged surfaces, Anal. Chem. 75 (2003) 1931–1940.

[150] Y.-Y. Cheng, S. H. Lin, H.-C. Chang, Probing adsorption, orientation and conformational changes of cytochrome c on fused silica surfaces with the Soret band, J. Phys. Chem. A 107 (2003) 10687–10694.

[151] C. M. Kraning, T. L. Benz, K. S. Bloome, G. C. Campanello, V. S. Fahrenbach, S. A. Mistry, C. A. Hedge, K. D. Clevenger, K. M. Gligorich, T. A. Hopkins, G. C. Hoops, S. B. Mendes, H.-C. Chang, M.-C. Su, Determination of surface coverage and orientation of reduced cytochrome c on a silica surface with polarized atr spectroscopy, J. Phys. Chem. C 111 (2007) 13062–13067.

[152] L. van der Sneppen, J. Buijs, C. Gooijer, W. Ubachs, F. Ariese, Evanescent-wave cavity ring-down spectroscopy for enhanced detection of surface binding under flow injection analysis conditions, Appl. Spectr. 62 (2008) 649–654.

[153] J. J. Cras, C. A. Rowe-Taitt, D. A. Nivens, F. S. Ligler, Comparison of chemical cleaning methods of glass in preparation for silanization, Biosensors and Bioelectronics 14 (1999) 683–688.

[154] P. Silberzan, L. Leger, D. Ausseree, J. J. Benattar, Silanation of silica surfaces. a new method of constructing pure or mixed monolayers, Langmuir 7 (1991) 1647–1651.

[155] M. E. McGovern, K. M. R. Kallury, M. Thompson, Role of solvent on the silanization of glass with octadecyltrichlorosilane, Langmuir 10 (1994) 3607–3614.

[156] J. R. Shallenberger, E. Metwalli, C. G. Pantano, F. N. Tuller, D. F. Fry, Adsorption of polyamides ond polyamide-silane mixtures at glass surfaces, Surface and interface analysis 35 (2003) 667–672.

[157] S. K. Chan, I. Tulloss, E. Margoliash, Primary structure of the cytochrome c from the snapping turtle, chelydra serpentina, Biochemistry 5 (1966) 2586–2597.

[158] H.-F. Fan, F. Li, R. N. Zare, K.-C. Lin, Characterization of two types of silanol groups on fused-silica surfaces using evanescent-wave cavity ring-down spectroscopy, Anal. Chem. 79 (2007) 3654–3661.

[159] R. A. Clark, E. F. Bowden, Voltammetric peak broadening for cytochrome c/alkanethiolate monolayer structures: dispersion of formal potentials, Langmuir 13 (1997) 559–565.

# List of publications

**Included in this thesis:**

B. Bahnev, L. van der Sneppen, A. E. Wiskerke, F. Ariese, C. Gooijer and W. Ubachs, *Miniaturized cavity ring-down detection in a liquid flow cell* , Analytical Chemistry 77 (2005) 1188 (chapter 2).

L. van der Sneppen, A. E. Wiskerke, F. Ariese, C. Gooijer and W. Ubachs, *Improving the sensitivity of HPLC absorption detection by cavity ring-down spectroscopy in a liquid-only cavity*, Analytica Chimica Acta 558 (2006) 2 (chapter 3).

L. van der Sneppen, A. E. Wiskerke, F. Ariese, C. Gooijer and W. Ubachs, *Cavity ring-down spectroscopy for detection in liquid chromatography: Extension to tunable sources and ultraviolet wavelengths*, Applied Spectroscopy 60 (2006) 931 (chapter 4).

L. van der Sneppen, F. Ariese, C. Gooijer and W. Ubachs, *Cavity ring-down spectroscopy for detection in liquid chromatography at UV wavelengths using standard cuvettes in a normal incidence geometry*, Journal of Chromatography A 1148 (2007) 184 (chapter 5).

L. van der Sneppen, J. B. Buijs, C. Gooijer, W. Ubachs and F. Ariese, *Evanescent-wave cavity ring-down spectroscopy for enhanced detection of surface binding under flow injection analysis conditions*, Applied Spectroscopy, 62 (2008) (chapter 6) 649.

**Additional publications:**

A. Bonifacio, L. van der Sneppen, C. Gooijer, and G. van der Zwan, *Citrate-Reduced Silver Hydrosol Modified with $\gamma$-Mercaptoalkanoic Acids. Self-Assembled Monolayers as a Substrate for Surface-Enhanced Resonance Raman Scattering. A Study with Cytochrome c*, Langmuir 20 (2004) 5858.

L. van der Sneppen, C. Gooijer, W. Ubachs and F. Ariese, *Cavity ring-down spectroscopy in chemistry* in 'Lasers in Chemistry' edited by M. Lackner, Wiley-VCH, in press.

L. van der Sneppen, C. Gooijer, W. Ubachs and F. Ariese, *Cavity ring-down spectroscopy in analytical chemistry* in 'Cavity ring-down spectroscopy: Techniques and applications' edited by R. Engeln and G. Berden, Blackwell publishing Ltd., in press.

L. van der Sneppen, C. Gooijer, W. Ubachs and F. Ariese, *Liquid-phase and evanescent-wave cavity ring-down spectroscopy as a tool in analytical chemistry* in 'Annual review of Analytical Chemistry' edited by J. Tang, E. S. Yeung and R. N. Zare, Annual Reviews, in preparation.

# Samenvatting

De analytische chemie houdt zich onder andere bezig met het scheiden van mengsels van stoffen waarna in het ideale geval de afzonderlijke componenten kunnen worden geïdentificeerd of gebruikt voor andere doeleinden, zoals de synthese van nieuwe verbindingen. Het scheiden van mengsels wordt zelfs wel voor forensisch onderzoek gebruikt; ik verwijs daarvoor graag naar de tv-serie CSI: New York. Soms zijn scheikundigen geïnteresseerd in stoffen, die slechts in een heel kleine hoeveelheid aanwezig zijn. Denk bijvoorbeeld aan een grondwatermonster dat getest moet worden op de aanwezigheid van schadelijke verontreinigingen. In zo'n geval moeten zo laag mogelijke concentraties van deze verontreinigingen teruggevonden worden.

Het scheiden van mengsels gebeurt vaak met chromatografie. Een vloeistofchromatografieopstelling bestaat uit een kolom gevuld met kleine vaste deeltjes (die de stationaire fase vormen) waar een constante stroom van vloeistof doorheen loopt. Een mengsel wordt op een bepaald moment op de kolom gebracht en door de vloeistofstroom langs de deeltjes in de kolom geleid. Stoffen die zich graag hechten aan de stationaire fase zullen er langer over doen om uiteindelijk het einde van de kolom te bereiken met de vloeistofstroom.

Het is belangrijk om te meten na hoeveel tijd de betreffende molekulen aan het einde van de kolom zijn beland, zodat ze eventueel opgevangen kunnen worden voor verdere analyses of verwerking. Om dat te kunnen bepalen, moet er een detector aan het eind van de chromatografiekolom worden geplaatst. Molekulen, die opgelost zijn in de constante vloeistofstroom, kunnen op verschillende manieren gedetecteerd worden. Een eenvoudige en breed toepasbare manier is het meten van kleurveranderingen van de vloeistofstroom op het moment dat "gekleurde"molekulen in het mengsel langs de detector komen. Detectie op deze manier wordt absorptiedetectie genoemd, omdat licht van een bepaalde kleur wordt geabsorbeerd, hetgeen resulteert in een kleurverandering.

Tijdens het eerste gedeelte van mijn promotie-onderzoek heb ik me bezig gehouden met het ontwikkelen van een nieuw soort absorptiedetector. Deze absorptiedetector maakt gebruik van twee spiegels die recht tegenover elkaar staan en zo een optische trilholte of cavity vormen. Als een lichtpuls op zo'n trilholte valt, zal slechts een heel klein deel in de trilholte komen, het grootste deel wordt gereflecteerd. Vervolgens zal de lichtpuls weerkaatsen tussen de spiegels, terwijl bij iedere spiegel er een klein beetje licht naar buiten lekt. Gedurende de tijd dat de hoeveelheid opgeslagen licht heen en weer gaat in de trilholte, wordt het licht dat aan de achterkant naar buiten lekt met een lichtgevoelige detector gemeten. Aangezien er licht verloren gaat bij iedere reflectie in de trilholte, zal deze hoeveelheid licht telkens afnemen totdat uiteindelijk de lichtintensiteit in de trilholte is uitgedoofd. Dit lichtverval wordt een ring-down genoemd. De snelheid waarmee deze afname plaatsvindt is afhankelijk van de kwaliteit van de spiegels: als de reflectiviteit hoog is en er dus weinig naar buiten lekt per reflectie, zal dit verval langzaam gaan.

Als er in de trilholte echter molekulen aanwezig zijn die licht absorberen, zal het verval worden versneld. Tijdens een meting, waarbij bijvoorbeeld tien keer per seconde een

lichtpuls op de trilholte valt en het lichtverval na iedere puls gemeten wordt, zal de snelheid waarmee het licht vervalt toenemen zodra er zich absorberende molekulen in de trilholte bevinden. Deze meettechniek, die cavity ring-down spectroscopie wordt genoemd, is erg gevoelig: de lichtpuls kan in een fractie van een seconde vele duizenden keren weerkaatsen tussen de spiegels voordat hij helemaal is uitgedoofd. De afstand, waarover absorptie gemeten wordt, is daarmee duizenden malen groter geworden. Zelfs hele lage concentraties van molekulen zijn daarom nog te meten met deze techniek.

Tijdens mijn promotie-onderzoek heb ik een gevoelige absorptiedetectie-methode, gebaseerd op cavity ring-down spectroscopie, ontwikkeld. Zo'n twintig jaar geleden, toen cavity ring-down spectroscopie nog maar net ontwikkeld was, werd deze vooral toegepast voor absorptiemetingen aan gassen. In dat geval wordt de ruimte tussen de spiegels wordt gevuld met een gas en er kan direct gemeten worden. Enkele jaren geleden is men begonnen met het meten aan vloeistoffen, maar dit is technisch moeilijker te realiseren. Hoe kan een trilholte het beste met een vloeistof gevuld worden? Is het beter om een cuvet (een klein, rechthoekig buisje dat gevuld kan worden met vloeistof) tussen de spiegels te zetten, zodat de spiegels niet te vervuild raken door het directe contact met vloeistof? In dit proefschrift zijn mijn bevindingen met beide oplossingen beschreven, en het is gebleken dat de cuvet de meest gebruiksvriendelijke oplossing is. Het is dan niet nodig na elke dag meten de spiegels te reinigen en de trilholte opnieuw uit te lijnen. De beste CRDS metingen bleken ongeveer 100 keer gevoeliger dan met absorptiedetectoren die op dit moment gebruikt worden.

Het tweede deel van mijn promotie-onderzoek ging nog een stap verder. Er is gebruik gemaakt van een opstelling, met in de trilholte nog een derde reflectie: een totale interne reflectie. Totale interne reflectie is een verschijnsel dat kan optreden als licht op een grensvlak tussen glas en lucht valt. Het glas was in mijn geval een prisma dat tussen de twee spiegels geplaatst was. Als de hoek van inval op dit grensvlak groter wordt dan een bepaalde hoek (de zogenaamde kritische hoek) zal al het licht worden gereflecteerd. Tijdens deze reflectie is er echter een component van het licht dat enigszins, over een heel kleine afstand, in de lucht boven het glasoppervlak doordringt. Het is mogelijk om alleen deze component te gebruiken voor metingen. De lucht achter het glas moet dan vervangen worden door een vloeistofstroom (de kritische hoek wordt in dat geval wel groter). In deze vloeistofstroom kunnen absorberende molekulen gebracht worden. Omdat het licht dat gebruikt wordt voor de metingen maar over zo'n korte afstand in de vloeistof doordringt, worden alleen die molekulen die aan het oppervlak plakken, of daar erg dicht bij in de buurt zijn, gemeten. Op deze manier kan dus onderscheid gemaakt worden tussen verschillende soorten molekulen. Als molekulen aan het oppervlak binden, wordt veel lichtabsorptie gemeten, terwijl de absorptie nihil is als ze niet binden aan het oppervlak. In dit geval worden slechts enkele molekulen, die in de buurt van het oppervlak zijn, waargenomen.

Het is voor de methode-ontwikkeling nodig om te onderzoeken of de absorberende stoffen in de vloeistofstroom, die over het prisma geleid werd, niet al te veel bleven plakken, zodat het prisma niet na iedere meting schoongemaakt moest worden. Dit bleek redelijk eenvoudig te kunnen worden beïnvloed door het aanpassen van de snelheid van de vloeistofstroom en het kiezen van een geschikte vloeistof. Daarna werden de specifieke interacties tussen bepaalde molekulen en het oppervlak bestudeerd. Op een "kaal"glasoppervlak kan gemeten worden welke molekulen gemakkelijk aan glas binden en welke niet, maar het is uitdagend om ook interacties aan andere oppervlakten dan glas te onderzoeken. Er zijn redelijk eenvoudige methodes om het glasoppervlak te bedekken met een laag van bepaalde molekulen. Eerst werd onderzocht in hoeverre deze bedekking volledig was. Het bleek dat één methode een prisma oplevert dat voor 100 % was bedekt met een enkele laag

molekulen, terwijl de bedekking in een andere methode niet meer dan 50 tot 75 % was. Vervolgens werd de interactie van een bepaald eiwit met de verschillende lagen getest. Op deze manier kon de goede gevoeligheid van cavity ring-down spectroscopie worden gebruikt voor oppervlakte-specifieke absorptiemetingen.

# Dankwoord

Onmisbaar in een proefschrift is natuurlijk het dankwoord. Ook ik heb tijdens mijn promotie-onderzoek gelukkig hulp gehad van een aantal mensen.

Op de eerste plaats wil ik graag mijn promotoren Cees Gooijer en Wim Ubachs, en mijn co-promotor Freek Ariese bedanken voor het creëren van een zeer interessante, multi-disciplinaire promotieplek en de vrijheid om mijn onderzoek op mijn eigen manier uit te voeren.

Erg belangrijk in iedere onderzoeksgroep is natuurlijk het ondersteunend personeel, en graag wil ik mijn favoriete technici Joost Buijs en Jacques Bouma bedanken. Joost Buijs heeft mij altijd goed geholpen met het schrijven en de installatie van computer-programma's. Ook wist hij precies bij welke leverancier ik mijn spullen het beste of snelste kon bestellen. Bij het opbouwen van mijn verschillende opstellingen heeft Jacques Bouma vooral meegeholpen met praktische zaken zoals de constructie van houders met de juiste vrijheidsgraden voor de uitlijning.

Voor uitleg op het gebied van LC, absorptiedetectoren, LC-pompen en dergelijke ben ik Pim Voogt natuurlijk dank verschuldigd. Vooral in het begin van mijn promotie heeft Arjan Wiskerke me goed op weg geholpen bij het bouwen van mijn eerste CRDS opstelling. Ook de werkplaatsmannen, met name Dick van Iperen en Klaas van Altena, hebben me altijd snel geholpen. Vaak konden mijn kleine klusjes wel even tussendoor, waarvoor mijn dank. De ontwerpen van Dick voor onder andere de liquid-only cavity en het prisma-flowcelletje, en de uitvoering van die ontwerpen door Klaas, hebben mijn onderzoek aanzienlijk vereenvoudigd.

Verder wil ik graag mijn collega's bedanken. Ik heb het genoegen gehad om bij twee vakgroepen te horen, ik heb dus veel mensen met verschillende achtergronden leren kennen. Het was altijd interessant om over mijn onderzoek te praten met zowel natuur- als scheikundigen en de verschillende invalshoeken met elkaar te vergelijken.

Aangezien ik scheikundige ben zal ik beginnen met het bedanken van mijn scheikunde collega's. Mensen van het eerste uur, waarvan ik me niet precies kan herinneren of ze voornamelijk tijdens mijn stage goede collega's en begeleiders waren of dat ze mij ook als aio hebben meegemaakt, zijn Arjen B., Aike, Evtim, Mirka, Eva en Junko. *Thanks also to our Italian maffia, Alois, Diego and later also Silvia.* Verder wil ik Joost de K., Arno, Wim R., Ivonne, Cecilia, Marleen en mijn enige student Hay-Yeng bedanken. *Many thanks to Kim and Gerardo in helping me with my efforts to set up a bio-assay.* De mensen van boven hebben me vooral geholpen met het creëren van een aangename werksfeer; Niels J., Ansgar, Mark, Jon, Linda, Jeroen K., Henk, René, Ben, Marek, Niels M., Felipe, Lygia, Ferry, Martin en iedereen die ik ben vergeten, bedankt!

*In the ALF group, I would like to thank the usual suspects: Edcel, Toncho, Ofelia, Sandro and Arjen. Thanks for all the nice times we had in and outside the lab, and your patience for explaining me some physics and what the heck the talks in the group-meetings were about.* Ook wil ik Kjeld en zijn (ex-)clubleden Stefan, Roel Z., Anne-Lisa, Amandine,

Dominik, Christoph; Eric-Jan, Rick, Kees de L., Wim V. en zijn coole jongens John, Tom, Rob en Roel R.; colleague-CRDS-user Dmitry, Ruth, and Ruud, en ook alle anderen die ik ben vergeten, bedanken.

Gedurende ongeveer driekwart jaar ging ik enkele dagen per week meten met een folded cavity aan de slag bij de Technische Universiteit van Eindhoven. Ik heb in de plasma and materials processing groep van Richard van de Sanden veel geleerd. Graag wil ik Richard v.d.S. en Andrew Pipino dan ook bedanken voor de mogelijkheid om bij hun in de groep te werken.

Ook ben ik dank verschuldigd aan Eric Louis en Erwin Zoethout van het FOM-instituut Rijnhuizen, die hun XPS-apparaat belangeloos beschikbaar hebben gesteld voor de analyse van verschillende opppervlaktes.

De onvoorwaardelijke steun van familie en vrienden was van onschatbare waarde en ze wisten me altijd op te beuren als ik mijn promotie-onderzoek even niet meer zag zitten. De meeste dank ben ik Lennard verschuldigd. Bedankt dat je er altijd voor me bent (en trouwens ook bedankt voor het ontwerpen van mijn cover).

# Curriculum Vitae

*7 January 1981*
Born in Terneuzen, The Netherlands.

*June 1999*
Diploma Atheneum, Reynaertcollege, Hulst, The Netherlands.

*September 1999 - January 2003*
Bachelor's degree Chemistry (Analytical Chemistry) (*cum laude*), Hogeschool West-Brabant, Etten-Leur, The Netherlands.

*January 2003 - June 2004*
Master's degree Chemistry (Analytical Sciences) (*cum laude*), Vrije Universiteit Amsterdam, The Netherlands.

Four months (spring 2004) traineeship in the group of V. Deckert, ISAS Institute for Analytical Sciences, Dortmund, Germany.
Topic: Atomic force measurements on single molecules of DNA immobilized on mica

Master thesis project in the group of ACAS Analytical Chemistry and Applied Spectroscopy, Vrije Universiteit Amsterdam, The Netherlands.
Topic: Development of a biocompatible gold or silver colloid for surface enhanced resonance Raman spectroscopy of cytochrome c

*July 2004 - June 2008*
PhD student in the group of ACAS (Analytical Chemistry and Applied Spectroscopy) and ALF (Atomic and Laser Physics), Laser Centre, Vrije Universiteit Amsterdam, The Netherlands.

Six months (fall 2006 until spring 2007) working visit in the group of PMP Plasma and Materials Processing, Eindhoven University of Technology, Eindhoven, The Netherlands.
Topic: EW-CRDS spectrosopy on methanol immobilized on the silica surface of a folded cavity

Oral presentations at various conferences: Cavity Ring-Down user meeting 2005 (Oxford, United Kingdom), International conference on Laser Probing 2006 (Vienna, Austria), Cavity Ring-Down user meeting 2007 (Greifswald, Germany), NWO Dutch Society of Scientific Research, Analytical Chemistry meeting 2007 (Lunteren, The Netherlands), LACSEA Laser Applications to Chemical, Safety and Environmental Analysis, Optical Society of America 2008 (St. Petersburgh, Florida, United States).